LANTHANIDE(III) COMPLEXES OF AROYLHYDRAZONES: DNA BINDING AND FLUORESCENCE STUDIES

Thesis submitted to the
University of Calicut for the award of

DOCTOR OF PHILOSOPHY IN CHEMISTRY

By

ANJANA T. M.

Under the Supervision of

Dr. SHEEJA S. R.
Professor of Chemistry

POST GRADUATE AND RESEARCH DEPARTMENT OF CHEMISTRY
GOVERNMENT COLLEGE MADAPPALLY, VADAKARA
DECEMBER 2025

DEPARTMENT OF CHEMISTRY
GOVT. COLLEGE MADAPPALLY, VADAKARA

CERTIFICATE

This is to certify that the thesis entitled "**Lanthanide(III) complexes of aroylhydrazones: DNA binding and fluorescence studies**" is an authentic record of precise research work carried out by **Anjana. T.M** under my guidance and supervision, for the award of the degree of Doctor of Philosophy in Chemistry under the faculty of Sciences, University of Calicut, Kerala and the same has not been submitted elsewhere for any degree or diploma.

The corrections/suggestions recommended by the adjudicators have been incorporated in the thesis and the content in the thesis and the soft copy are one and the same.

Madappally
08/12/2025

Dr. Sheeja. S. R.
(Supervising Teacher)
Professor
Department of Chemistry
Govt. College Madappally

DECLARATION

I, **Anjana T M,** hereby declare that the work presented in the thesis entitled "**Lanthanide(III) complexes of aroylhydrazones: DNA binding and fluorescence studies"** is based on the original work done by me under the guidance of **Dr. Sheeja S R**, Professor, Department of Chemistry, Government College Madappally, Vatakara, Kerala and has not been included in any other thesis submitted previously for the award of any degree. The contents of the thesis are undergone plagiarism check using iThenticate software at C.H.M.K. Library, University of Calicut, and the similarity index found within the permissible limit. I also declare that the thesis is free from AI generated contents.

Madappally
08/12/2025

Anjana.T M

Dr. Sheeja. S. R.
Professor
Department of Chemistry
Govt. College Madappally

Acknowledgement

Throughout the course of this thesis, I have been supported by many remarkable individuals whose presence made this journey possible. Countless people offered words of encouragement, invaluable assistance, and heartfelt friendship, lightening the challenges along the way. I am deeply grateful for the exceptional souls whose love, guidance, and steady support sustained me during this entire period. It is truly a pleasure to thank all those who have helped, inspired, and supported me during this period, and I cherish the memory of their kindness with deep appreciation and respect.

I would like to express my heartfelt gratitude to my supervisor, Prof. Dr. Sheeja S R, Department of Chemistry, Government College Madappally, University of Calicut, for her invaluable guidance, unwavering encouragement, and wholehearted support throughout the progress of my research work. Her exemplary professionalism, integrity and patience have been a constant source of motivation and direction at every stage of this work. It has been a blessing to have her as my guide, and I am profoundly grateful.

I am deeply indebted to Prof. Dr. M.R. Prathapachandra Kurup for his invaluable suggestions and immense knowledge throughout the entire course of this work. His insightful guidance, thoughtful feedback, and willingness to share his time generously have significantly enriched the quality of this work, and I am truly grateful for his mentorship.

I sincerely thank Mr. Shinu P M, Principal, and all the former principals who served during my research period at Govt. College Madappally, Vadakara, Kozhikode for their continuous encouragemnt and for providing the departmental facilities required to carry out and complete my research work

I gratefully acknowledge Dr. Subair. Naduparambath, Head of the Department of Chemistry, and also to the former Pricipal and HOD Dr. Preetha B for their generous support in providing the necessary research facilities and other resources throughout my Ph.D. program, which played a crucial role in the successful execution of my research.

I sincerely thank all the faculty members of the Department of Chemistry for their guidance, constructive feedback, and steadfast assistance throughout my doctoral studies. Their expertise and commitment to academic excellence have profoundly shaped my research journey. The encouragement, thoughtful discussions, and valuable insights I received from them have not only strengthened the quality of my work but have also contributed greatly to my intellectual growth and confidence as a researcher. I am truly grateful to have been part of such a supportive academic community.

I am deeply indebted to Dr. Manoj E Associate Professor, Department of Applied Chemistry Cochin University of Science and Technology for his invaluable guidance in the theoretical studies for this thesis. His profound knowledge, insightful advice, and expert direction greatly aided the progress of my research.

I would like to acknowledge all the non-teaching staff in the department for their invaluable assistance and thoughtful help.

I also wish to express my heartfelt thanks to Dr. Nithyaja B, Associate Professor of Physics, Govt. College Madappally, for providing guidance and access to the Physics research laboratory facilities, and to Dr. Sudheesh Kumar T K, Assistant Professor of Zoology, Govt. College Madappally, for their invaluable support and access to the Zoology research lab, which greatly contributed to my research.

I am especially grateful to Mrs. Bhagyasree G. S., research scholar in the Department of Physics, for her constant support, valuable suggestions, and companionship throughout my research. Her generosity in sharing knowledge, encouragement, and constructive feedback were invaluable in keeping me motivated and focused during challenging times. I also cherish the fun moments we shared, from lively discussions to our tea-time breaks, which made the research journey enjoyable and memorable.

It gives me great joy to express my sincere appreciation to Ms Vydhehi E K, research scholar in the Department of Chemistry, for being a constant source of motivation and companionship in the lab. During our light-hearted, joke-filled breaks, she made challenging days feel brighter, and her presence helped me stay focused and energized. I truly value how much she supported me emotionally and intellectually her presence made this journey far more meaningful and inspiring.

I deeply acknowledge the head of the institutions of SAIF- IIT Madras, CSIF-University of Calicut, STIC-Cochin University, CLIF-Kerala University and SAIF-MG University for doing my analysis, which facilitated in completion of the research work on time.

My heartfelt thanks go to my father, Mr. Asokan P M, and mother Mrs. Nalini T, for their constant love, prayers encouragement, and unwavering support. This accomplishment would not have been possible without them. I would also like to express my heartfelt gratitude to my brothers, Mr. Shijin T M and Mr. Shinoj T M, whose constant support has been a source of strength throughout this journey.

I sincerely thank my husband, Mr.Sujan C K, for his love, guidance and encouragement throughout my research journey. I am profoundly grateful to my son, Goutham Rishi, whose age has paralleled the span of my research journey, and who has been remarkably patient and understanding throughout, bringing joy and motivation to these years. A simple thank you is not enough to express my gratitude for his love, innocence, and quiet support, which have been a constant source of strength and inspiration during this journey.

I also express my sincere gratitude to my in-laws for the support and encouragement they have extended to me throughout this journey.

I would like to express my heartfelt gratitude to everyone who has offered their support, directly or indirectly, in the successful completion of my work.

Above all, I offer my humble thanks to God Almighty, the most merciful and beneficent, for His blessings that have guided me in completing this research successfully.

Anjana T M

Dedicated to
My son
Goutham Rishi

ABSTRACT

Schiff bases and their derivatives, particularly aroylhydrazones, have emerged as versatile ligands in coordination chemistry due to their ease of synthesis, structural flexibility, and strong metal-binding capabilities. Their multidentate nature and ability to exhibit keto–enol tautomerism enable diverse coordination geometries and significant functional applications. This thesis focuses on the synthesis, characterization, fluorescence, and DNA-binding studies of three aroylhydrazones: salicylaldehyde benzoylhydrazone (H_2salbh), salicylaldehyde nicotinoylhydrazone (H_2salnh), and indole-3-carbaldehyde benzoylhydrazone (Hindbh) and their Ce(III), Dy(III), and Gd(III) complexes, with and without L-histidine as the coligand.

The aroylhydrazones were successfully synthesized *via* condensation reactions and characterized by elemental analysis, ESI-MS, FT-IR, UV–vis, NMR, and single-crystal X-ray diffraction. The aroylhydrazones H_2salbh and H_2salnh act as tridentate (ONO) donors, while Hindbh behaves as a bidentate (NO) donor, forming stable, non-electrolytic complexes. The Ce(III), Dy(III), and Gd(III) complexes exhibited characteristic spectral features confirming metal–ligand interactions, with histidine coordination further stabilizing the complexes and modulating their photophysical properties.

The luminescence studies revealed significant enhancement upon metal coordination. The Ce(III) complexes displayed efficient $d \rightarrow f$ transitions with potential applications as blue-emitting materials in optoelectronic devices. The Dy(III) complexes showed strong fluorescence due to the suppression of photoinduced electron transfer

(PET) and activation of chelation-enhanced fluorescence (CHEF) mechanisms, indicating promise for bioimaging and luminescent probes. The Gd(III) complexes exhibited increased emission intensity and structural rigidity, suggesting their utility in sensing and multifunctional imaging platforms.

DNA-binding studies, investigated by UV–vis absorption spectroscopy, indicated that both aroylhydrazones and metal complexes interact with DNA primarily through external groove binding. Metal coordination enhanced binding affinity, particularly in Hindbh and its complexes (K_b ~10^5 M^{-1}), due to increased planarity and π-conjugation.

These findings highlight the crucial role of ligand design and metal ion selection in tuning photophysical and biological properties. Overall, this work demonstrates that aroylhydrazone-based lanthanide(III) complexes possess significant potential for applications in luminescent sensing, bioimaging, and therapeutic design, establishing a foundation for future exploration of multifunctional lanthanide-based materials in bioinorganic and photonic chemistry.

Keywords: Aroylhydrazones- Lanthanide(III) complexes- DNA binding -Photoluminescence- Bioimaging agents

സംഗ്രഹം

ലാന്തനൈഡ്(III) അരയോയിൽഹൈഡ്രാസോണുകളുടെ കോംപ്ലക്സുകൾ: ഡിഎൻഎ ബൈൻഡിംഗും ഫ്ലൂറസെൻസ് പഠനങ്ങളും

ഷിഫ് ബേസുകളും അവയുടെ ഡെറിവേറ്റീവുകളും, പ്രത്യേകിച്ച് അരോയിൽഹൈഡ്രസോണുകൾ, സംശ്ലേഷണത്തിലെ ലാളിത്യവും ഘടനാ വൈവിധ്യവും ശക്തമായ ലോഹബന്ധന ശേഷിയും കാരണം കോർഡിനേഷൻ രസതന്ത്രത്തിൽ പ്രധാനപ്പെട്ട ലിഗാൻഡുകളായി ഉയർന്നുവരുന്നു. അവയുടെ ബഹുദന്ത സ്വഭാവവും കീറ്റോ–ഇനോൾ ടോട്ടോമറിസം പ്രകടിപ്പിക്കാനുള്ള കഴിവും വ്യത്യസ്തമായ കോർഡിനേഷൻ ജ്യാമിതികളും വ്യാപകമായ പ്രവർത്തനപരമായ പ്രയോഗങ്ങൾക്കും അവയെ

സാദ്ധ്യമാക്കുന്നു. ഈ പഠനം മൂന്ന് അരോയിൽഹൈഡ്രസോണുകളുടെ H_2salbh, H_2salnh, Hindbh കൂടാതെ അവയുടെ Ce(III), Dy(III), Gd(III) കോംപ്ലക്സുകളുടെ (L-ഹിസ്റ്റിഡിൻ സാന്നിധ്യത്തോടെയും ഇല്ലാതെയും) സംശ്ലേഷണം, സ്വഭാവനിശ്ചയം, ഫ്ലൂറസൻസ്, DNA-ബന്ധന വിശകലനം എന്നിവയിൽ കേന്ദ്രീകരിക്കുന്നു.

അരോയിൽഹൈഡ്രസോണുകൾ കണ്ടൻസേഷൻ പ്രതിചരണങ്ങളിലൂടെ സംശ്ലേഷണം ചെയ്ത് മൂലകവിശകലനം, ESI-MS, FT-IR, UV–vis, NMR, സിംഗിൾ-ക്രിസ്റ്റൽ X-റേ ഡിഫ്രാക്ഷൻ തുടങ്ങിയ രീതികളിലൂടെ വിജയകരമായി സ്വഭാവനിശ്ചയം നടത്തി. H_2salbh, H_2salnh എന്നിവ ടൈഡന്റേറ്റ് (ONO) ലിഗാൻഡുകളായും Hindbh ബൈഡന്റേറ്റ് (NO) ലിഗാൻഡായും പ്രവർത്തിച്ച് സ്ഥിരതയുള്ള നോൺ-ഇലക്ട്രോളിറ്റിക് കോംപ്ലക്സുകൾ രൂപപ്പെടുത്തി. Ce(III), Dy(III), Gd(III) കോംപ്ലക്സുകൾ ലോഹ–ലിഗാൻഡ് സംവേദനത്തിന്റെ സവിശേഷ സ്പെക്ട്രൽ സൂചനകൾ പ്രകടിപ്പിച്ചു; ഹിസ്റ്റിഡിൻ കോർഡിനേഷൻ, കോംപ്ലെക്സുകളുടെ സ്ഥിരതയും ഫോട്ടോഫിസിക്കൽ ഗുണങ്ങളും മെച്ചപ്പെടുത്തി.

ല്യൂമിനസൻസ് പഠനങ്ങൾ ലോഹ കോർഡിനേഷൻ ഫ്ലൂറസൻസ് തീവ്രത ഗണ്യമായി വർദ്ധിപ്പിക്കുന്നതായി തെളിയിച്ചു. Ce(III) കോംപ്ലെക്സുകൾ $d \rightarrow f$

ട്രാൻസ്ഫർ കാരണം നീല വികിരണം പ്രദർശിപ്പിക്കുകയും ഓപ്റ്റോഇലക്ട്രോണിക് ഉപകരണങ്ങൾക്ക് അനുയോജ്യമാകുകയും ചെയ്തു. Dy(III) കോംപ്ലെക്സുകളിൽ PET ശമനവും CHEF മെക്കാനിസം സജീവമാകുന്നതുമൂലം ശക്തമായ ഫ്ലൂറസൻസ് ഉണ്ടാകുകയും ബയോഇമേജിംഗിനും ല്യൂമിനസന്റ് പ്രോബുകൾക്കും സാധ്യതകൾ ഉയർത്തിക്കാട്ടുകയും ചെയ്തു. Gd(III) കോംപ്ലെക്സുകൾ ഉയർന്ന എമിഷൻ തീവ്രതയും ഘടനാ ദൃഢതയും കാണിച്ചു. കൂടാതെ ഇവ സെൻസിംഗ്, മൾട്ടിമോഡൽ ഇമേജിംഗ് തുടങ്ങിയവയിൽ ഉപയോഗശേഷിയുള്ളവയാണെന്ന് സൂചിപ്പിച്ചു.

UV–vis ആബ്സോർപ്ഷൻ സ്പെക്ട്രോസ്കോപിയിലൂടെ നടത്തിയ DNA-ബന്ധന പഠനങ്ങൾ, ലിഗാൻഡുകളും കോംപ്ലെക്സുകളും പ്രധാനമായും ബാഹ്യ ഗ്രൂവ് ബൈൻഡിംഗ് വഴിയാണ് DNA-യുമായി ഇടപെടുന്നതെന്ന് തെളിയിച്ചു. ലോഹ കോർഡിനേഷൻ, ബന്ധന ആകർഷണശേഷി ഗണ്യമായി വർദ്ധിപ്പിച്ചു. മികച്ച പ്ലാനാരിറ്റിയും π-കോൺജുഗേഷനും കാരണം Hindbhയും അതിന്റെ കോംപ്ലെക്സുകളും ശക്തമായ ബന്ധനത്തിൽ ഏർപ്പെടുന്നതായി($K_b \sim 10^5\ M^{-1}$) കാണപ്പെട്ടു.

ഈ പഠനം ഫോട്ടോഫിസിക്കൽ, ജൈവ പ്രവർത്തനങ്ങൾ ക്രമീകരിക്കുന്നതിൽ ലിഗാൻഡ് രൂപകൽപ്പനയുടെയും ലോഹ അയൺ തിരഞ്ഞെടുപ്പിന്റെയും നിർണായകത വ്യക്തമായി അവതരിപ്പിക്കുന്നു. ചുരുക്കത്തിൽ, ഈ ഗവേഷണം അരോയിൽഹൈഡ്രസോൺ-അധിഷ്ഠിത ലാന്തനൈഡ്(III) കോംപ്ലെക്സുകൾ ല്യൂമിനസന്റ് സെൻസിംഗ്, ബയോഇമേജിംഗ്, ചികിത്സാ രൂപകൽപ്പന തുടങ്ങിയ മേഖലകളിൽ വലിയ സാദ്ധ്യത വഹിക്കുന്നതായി കാണിച്ചുതരുന്നു. ബയോഇനോർഗാനിക്, ഫോട്ടോണിക് രസതന്ത്രങ്ങളിൽ ഭാവിയിലേക്കുള്ള ബഹുധാരണ വസ്തുക്കളിലേക്ക് വഴിതെളിക്കുന്നു.

സൂചകപദങ്ങൾ: അരോയിൽ ഹൈഡ്രസോണുകൾ – ലാന്തനൈഡ്(III) കോംപ്ലക്സുകൾ – DNA ബന്ധനം – ഫോട്ടോല്യൂമിനസെൻസ് – ബയോഇമേജിംഗ് ഏജന്റുകൾ

PREFACE

Aroylhydrazones represent a versatile class of organic compounds formed through the condensation of aromatic acid hydrazides with aldehydes or ketones. They act as effective chelating agents for transition metals, lanthanides, and main-group elements. Their significance arises from their structural flexibility, ease of synthesis, and stability against hydrolysis, as well as their ability to exhibit keto–enol tautomerism and E/Z isomerism, which enable multiple coordination modes. The presence of an additional carbonyl donor site in aroylhydrazones enhances their chelation diversity, coordination geometries, and applicability across various fields of chemistry. The lone pair of electrons on the sp^2-hybridized nitrogen atom plays a crucial role in governing their chemical reactivity and biological activity. Owing to these features, aroylhydrazones readily form stable coordination complexes with both transition and inner transition metal ions. These complexes display a wide range of properties and applications, including photoluminescence, DNA binding, catalysis, and diverse biological activities.

This thesis explores the fluorescence and DNA binding properties of aroylhydrazones and their Ce(III), Dy(III) and Gd(III) complexes, providing insights into their photoluminescence and biological potential. The thesis is organised into nine Chapters, providing a detailed account of the synthesis, characterization,

fluorescence and DNA-binding studies, with the summary and recommendations presented in Chapter 8 and 9.

Chapter 1 provides a comprehensive introduction to the chemistry of aroylhydrazones and their coordination complexes with lanthanide ions, specifically cerium(III), dysprosium(III), and gadolinium(III). It begins with a foundational overview of coordination chemistry, tracing its historical development and highlighting the significance of Schiff bases and aroylhydrazones in metal complexation. The Chapter outlines the synthesis, structural characteristics, and versatile applications of aroylhydrazones and their lanthanide complexes, focusing on their photoluminescent and DNA-binding properties. It further explores the unique features of Ce(III), Dy(III), and Gd(III) ions, emphasizing their luminescent and biomedical relevance, and provides a critical outlook on recent advancements in their use for sensing, imaging, and therapeutic purposes, thereby establishing the scientific context of the study.

Chapter 2 systematically details the synthesis and characterization of three aroylhydrazones salicylaldehyde benzoylhydrazone (H_2salbh), salicylaldehyde nicotinoylhydrazone (H_2salnh), and indole-3-carbaldehyde benzoylhydrazone (Hindbh) prepared *via* condensation reactions. These aroylhydrazones were chosen for their multidentate chelating potential and diverse structural features. Comprehensive characterization using elemental analysis, ESI-MS, FT-IR, UV–vis, NMR, and single-crystal X-ray diffraction confirmed their successful formation, molecular stoichiometry, and

structural integrity. FT-IR spectroscopy verified aroylhydrazone formation through characteristic N—H, C=N, C=O, and O–H stretching vibrations, while ^{1}H NMR spectroscopy confirmed azomethine protons. Single-crystal X-ray diffraction of Hindbh further elucidated its structure, revealing that these aroylhydrazones predominantly exist in the keto form.

In Chapter 3, six Ce(III) complexes incorporating these aroylhydrazones, with and without L-histidine as a coligand, are synthesized and characterized. Elemental analysis confirmed 1:1 metal-to-ligand ratios, and molar conductance measurements indicated non-electrolytic behavior. FT-IR studies revealed coordination *via* oxygen and nitrogen donor atoms, while new bands confirmed Ce–O and Ce–N bond formation. Mass spectrometry supported the proposed structures, and UV–vis studies identified intraligand charge-transfer and ligand-to-metal charge-transfer transitions, along with $4f \rightarrow 5d$ transitions in H_2salbh and H_2salnh complexes, which were red-shifted upon histidine coordination. Structurally, H_2salbh and H_2salnh acted as tridentate ONO ligands, while Hindbh coordinated bidentately, with histidine enhancing the coordination sphere.

The synthesis and characterisation of six Dy(III) complexes using the same aroylhydrazones, with and without L-histidine are explained in Chapter 4. Elemental analysis and molar conductance studies confirmed non-electrolytic behaviour and validated the proposed compositions. FT-IR and UV–vis spectroscopy, along with mass spectrometry, confirmed coordination through oxygen and

nitrogen atoms and successful formation of the complexes. The aroylhydrazones maintained their bidentate or tridentate coordination modes, while L-histidine improved the overall coordination geometry, demonstrating the ligand's adaptability in constructing stable lanthanide complexes with potential functional applications.

In Chapter 5, six Gd(III) complexes are also prepared and characterized. FT-IR spectroscopy confirmed metal coordination *via* azomethine nitrogen and carbonyl oxygen, supported by M–O and M–N bands. UV–vis spectra displayed intraligand charge-transfer transitions indicative of ligand-metal interactions, while MALDI-TOF mass spectrometry validated the molecular structures. Molar conductance confirmed non-electrolytic behaviour, and histidine coordination further stabilized the complexes. H_2salbh and H_2salnh remained tridentate ligands, while Hindbh coordinated bidentately, highlighting the ligands' versatility in stabilizing Gd(III) complexes.

The luminescent properties of all synthesized Ce(III), Dy(III), and Gd(III) complexes were explored in Chapter 6, revealing significant enhancement upon complexation. Ce(III) complexes of H_2salbh and H_2salnh exhibited efficient $d \rightarrow f$ transitions, with nanosecond photoluminescence lifetimes, and histidine further improved quantum yields, indicating potential as blue-emitting OLED materials. Dy(III) complexes showed strong fluorescence enhancement due to suppression of PET and activation of CHEF mechanisms, with one complex proving effective for bioimaging. Gd(III) complexes displayed increased emission intensity through

structural rigidity and enhanced radiative decay pathways, demonstrating the importance of ligand design in tuning luminescent properties for sensing, imaging, and optoelectronic applications.

The interaction between Schiff bases and DNA plays a crucial role in the design and synthesis of new pharmaceutical compounds. Chapter 7 explores the DNA-binding capabilities of the aroylhydrazones and their Ce(III), Dy(III), and Gd(III) complexes are investigated using UV–vis spectroscopy. Incremental addition of the aroyl hydrazones and metal complexes induced hyperchromism, suggesting external groove-binding. Metal coordination enhanced binding affinity, with Hindbh and its complexes exhibiting the highest binding constants (K_b ~10^5 M^{-1}), attributed to the planarity and extended π-conjugation of the indole ring. H_2salnh complexes showed moderate binding, while H_2salbh complexes displayed lower affinity. These findings underscore the influence of ligand structure and metal coordination on DNA interaction and highlight the potential of Hindbh-based lanthanide complexes as scaffolds for DNA-targeted therapeutic and bioinorganic applications.

The last two chapters of this thesis deal with the general conclusions and recommendations of the study.

CONTENTS

	Page No.
CHAPTER 1	**1-43**
INTRODUCTION	
1.1. Introduction	1
1.2. Schiff bases	1
1.3. Hydrazones	3
1.4. Aroylhydrazones	6
1.5. Applications of metal complexes of aroylhydrazones	7
1.5.1. Applications in biology and medicine	7
1.5.2. Applications in photoluminescence	15
1.6. Scope and objectives of the present study	19
1.7. Various metals used in the present study	21
1.7.1. Cerium	21
1.7.2. Dysprosium	23
1.7.3. Gadolinium	26
1.8. Physical measurements	29
1.8.1. Partial elemental analysis	30
1.8.2. Conductivity Measurements	30
1.8.3. Magnetic Susceptibility Measurements	30
1.8.4. Infrared Spectroscopy	31
1.8.5. Electronic spectroscopy	31
1.8.6. Nuclear Magnetic Resonance (NMR) spectroscopy	32
1.8.7. Mass spectrometry	32
1.8.8. Fluorescence spectroscopy	32
1.8.9. Single crystal XRD	33
1.8.10. DNA binding studies	33
References	34

CHAPTER: 2 **45-65**

SYNTHESIS AND SPECTRAL CHARACTERIZATION OF THE AROYLHYDRAZONES: SALICYLALDEHYDE BENZOYLHYDRAZONE, SALICYLALDEHYDE NICOTINOYLHYDRAZONE AND INDOLE-3-CARBALDEHYDE BENZOYLHYDRAZONE

2.1. Introduction 45

2.2. Materials and Methods 46

2.2.1. Synthesis of aroylhydrazones 46

2.2.1.1. Synthesis of salicylaldehyde benzoylhydrazone (H_2salbh) 46

2.2.1.2. Synthesis of salicylaldehyde nicotinoylhydrazone (H_2salnh) 47

2.2.1.3. Synthesis of indole-3-carbaldehyde benzoylhydrazone (Hindbh) 47

2.3. Results and Discussion 48

2.3.1. Characterizations of aroylhydrazones 48

2.3.1.1. Partial elemental analysis 48

2.3.1.2. Mass spectrometry 50

2.3.1.3. FT-IR spectroscopy 51

2.3.1.4. Electronic spectroscopy 53

2.3.1.5. Crystal structure of Hindbh 55

2.3.1.6. NMR spectroscopy 58

2.4. Conclusion 60

References 62

CHAPTER: 3 **67-90**

SYNTHESIS AND CHARACTERIZATION OF A SERIES OF CERIUM(III) COMPLEXES DERIVED FROM SALICYLALDEHYDE BENZOYLHYDRAZONE, SALICYLALDEHYDE NICOTINOYLHYDRAZONE AND INDOLE-3-CARBALDEHYDE BENZOYLHYDRAZONE

3.1. Introduction 67

3.2. Experimental 68

3.2.1. Materials 68

3.2.2. Synthesis of ligands 68

3.2.3. Synthesis of Ce(III) complexes 69

3.2.3.1. Synthesis of [Ce(Hsalbh)$(NO_3)_2$] (1) 69
3.2.3.2. Synthesis of [Ce(Hsalnh)$(NO_3)_2$] (2) 69
3.2.3.3. Synthesis of [Ce(Hindbh)$(NO_3)_3$] (3) 70
3.2.3.4. Synthesis of [Ce(Hsalbh)his(NO_3)] (4) 70
3.2.3.5. Synthesis of [Ce(Hsalnh)his(NO_3)] (5) 71
3.2.3.6. Synthesis of [Ce(Hindbh)(his)$(NO_3)_2$] (6) 71
3.3. Results and Discussion 73
3.3.1. Partial Elemental analysis 73
3.3.2. Conductivity measurements 75
3.3.3. Mass Spectrometry 75
3.3.4. FT-IR Spectroscopy 79
3.3.5. Electronic Spectroscopy 83
3.4. Conclusion 85
References 88
CHAPTER: 4 **91-110**
SYNTHESIS AND CHARACTERIZATION OF A SERIES OF DYSPROSIUM(III) COMPLEXES DERIVED FROM SALICYLALDEHYDE BENZOYLHYDRAZONE, SALICYLALDEHYDE NICOTINOYLHYDRAZONE AND INDOLE-3-CARBALDEHYDE BENZOYLHYDRAZONE
4.1. Introduction 91
4.2. Experimental 91
4.2.1. Materials 91
4.2.2. Synthesis of ligands 92
4.2.3. Synthesis of Dy(III) complexes 92
4.2.3.1. Synthesis of [Dy(Hsalbh)$(OAc)_2CH_3OH(H_2O)_2$] (7) 92
4.2.3.2. Synthesis of [Dy(Hsalnh)$(OAc)_2(H_2O)_3$] (8) 92
4.2.3.3. Synthesis of [Dy(Hindbh$(OAc)_3(H2O)_3$] (9) 93
4.2.3.4. Synthesis of [Dy(Hsalbh)$(his)_2(H_2O)$] (10) 93
4.2.3.5. Synthesis of Dy(Hsalnh)his$(OAc)(H_2O)_2$] (11) 94
4.2.3.6. Synthesis of [Dy(Hindbh)$(his)_2(OAc)H_2O$] (12) 94
4.3. Results and Discussion 96
4.3.1. Partial Elemental analysis 96

4.3.2. Conductivity measurements 97
4.3.3. Mass Spectrometry 97
4.3.4. FT-IR Spectroscopy 100
4.3.5. Electronic Spectroscopy 104
4.4. Conclusion 106
References 108
CHPTER:5 **109-128**
SYNTHESIS AND CHARACTERIZATION OF A SERIES OF GADOLINIUM(III) COMPLEXES DERIVED FROM SALICYLALDEHYDE BENZOYLHYDRAZONE AND SALICYLALDEHYDE NICOTINOYL HYDRAZONE
5.1. Introduction 111
5.2. Experimental 112
5.2.1. Materials 112
5.2.2. Synthesis of ligands 112
5.2.3. Synthesis of Gd(III) complexes 112
5.2.3.1. Synthesis of [Gd(Hsalbh)$_2$(OAc)(H$_2$O)] (13) 112
5.2.3.2. Synthesis of [Gd(Hsalnh)$_2$(OAc)(H$_2$O)] (14) 113
5.2.3.3. Synthesis of [Gd(Hindbh(OAc)$_3$(H$_2$O)$_3$] (15) 113
5.2.3.4. Synthesis of [Gd(Hsalbh)$_2$his] (16) 114
5.2.3.5. Synthesis of [Gd(H$_2$salnh)$_2$his] (17) 114
5.2.3.6. Synthesis of [Gd(Hindbh)(his)$_2$(OAc)H$_2$O] (18) 114
5.3. Results and Discussion 117
5.3.1. Partial Elemental analysis 117
5.3.2. Conductivity measurements 119
5.3.3. Mass Spectrometry 119
5.3.4. FT-IR Spectroscopy 120
5.3.5. Electronic Spectroscopy 123
5.4. Conclusion 125
References 126
CHAPTER: 6 **129-164**
PHOTOLUMINESCENCE STUDIES OF COMPLEXES OF AROYLHYDRAZONES
6.1. Introduction 129

6.1.1. Mechanisms of lanthanide luminescence 129
6.1.1.1. Interconfigurational $4f^n$ - $4f^n5d^1$ transitions 130
6.1.1.2. Charge-transfer transitions 130
6.1.1.3. Intraconfigurational *f-f* transitions 131
6.1.2. Application of Photoluminescence: Lanthanide complexes as fluorescent probes 133
6.1.3. Fluorescence quantum yield 134
6.1.4. Fluorescence lifetime (τ) 135
6.2. Fluorescence studies 135
6.2.1. Experimental 135
6.2.2. Results and discussion 136
6.2.2.1. Photoluminescence studies of aroylhydrazones 136
6.2.2.1.1. Fluorescence studies 136
6.2.2.1.2. Fluorescence lifetime decay studies and quantum yields 137
6.2.2.2. Photoluminescence studies of Ce(III) complexes 139
6.2.2.2.1. Fluorescence studies 139
6.2.2.2.2. Fluorescence lifetime decay studies and quantum yields 143
6.2.2.3. Photoluminescence studies of Dy(III) complexes 145
6.2.2.3.1. Fluorescence studies 145
6.2.2.3.2. Fluorescence lifetime decay studies and quantum yields 148
6.2.2.4. Photoluminescence studies of Gd(III) complexes 151
6.2.2.4.1. Fluorescence studies 151
6.2.2.4.2. Fluorescence lifetime decay studies and quantum yields 154
6.2.2.5. Bioimaging 157
6.3. Conclusion 159
References 161

CHAPTER: 7 **165-185**
DNA BINDING STUDIES OF COMPLEXES OF AROYLHYDRAZONES
7.1. Introduction 165
7.2. DNA binding studies 167
7.2.1. Modes of binding 167
7.2.1.1. Covalent binding 168
7.2.1.2. Non covalent binding 168
7.2.1.2.1. Intercalation 168
7.2.1.2.2. Groove binding 169
7.2.1.2.3. Electrostatic binding 169
7.2.2. Experimental 169
7.2.2.1. Absorption spectroscopic study 169
7.3. Results and discussion 170
7.3.1. DNA Binding study of aroylhydrazones 171
7.3.2. DNA Binding study of Ce(III) complexes 173
7.3.3. DNA Binding study of Dy(III) complexes 175
7.3.4. DNA Binding study of Gd(III) complexes 178
7.4. Conclusion 179
References 181
CHAPTER 8 GENERAL CONCLUSIONS **187-192**
CHAPTER 9 RECOMMENDATIONS **193**

LIST OF TABLES

Table No.	*Title*	*Page No.*
2.1.	The Compositional Details of Aroylhydrazones	49
2.2.	FT-IR Spectral Data of Aroylhydrazones	53
2.3.	UV-visible Spectral Data of Aroylhydrazones in DMF (10^{-5} M)	54
2.4.	Crystal Data and Structure Refinement for Hindbh	57
2.5.	Selected Bond Lengths [Å] and Angles [º] For Hindbh	58
3.1.	The Compositional Details of the Synthesized Ce(III) Complexes	74
3.2.	The Molar Conductances of The Ce(III) Complexes.	75
3.3.	Infrared Spectral Data of The Ce(III) Complexes	82
3.4.	UV-visible Spectral Data of Ce(III) Complexes in DMF (10^{-5} M)	84
4.1.	The Compositional Details of the Synthesized Dy(III) Complexes	97
4.2.	The Molar Conductance of the Dy(III) Complexes	98
4.3.	Infrared Spectral Data of the Dy(III) Complexes	102
4.4.	UV-visible Spectral Data of Dy(III) Complexes in DMF (10^{-5} M)	105
5.1.	The Compositional Details of the Synthesized Gd(III) Complexes	118
5.2.	The Molar Conductance of the Gd(III) Complexes	119
5.3.	Infrared Spectral Data of the Gd(III) Complexes	122
5.4.	UV-visible Spectral Data of Gd(III) Complexes in DMF (10^{-5} M)	124
6.1.	Photoluminescence Parameters of Hydrazones in DMF Solutions	139

6.2.	Photoluminescence Parameters of the Ce(III) Complexes in DMF Solutions	145
6.3.	Photoluminescence Parameters of the Dy(III) Complexes in DMF Solutions	151
6.4.	Photoluminescence Parameters of the Gd(III) Complexes in DMF Solutions	156
7.1.	The DNA Binding Constants of Aroylhydrazones	173
7.2.	The DNA Binding Constants of Ce(III) Complexes	175
7.3.	The DNA Binding Constants of Dy(III) Complexes	177
7.4.	The DNA Binding Constants of Gd(III) Complexes	179

LIST OF FIGURES

Figure No.	*Title*	*Page No.*
1.1.	General Coordination Mode of Aroylhydrazones	6
2.1.	ESI-MS Spectrum of H_2salbh	50
2.2.	ESI-MS Spectrum of H_2salnh	51
2.3.	FT-IR Spectrum of H_2salbh	52
2.4.	FT-IR Spectrum of H_2salnh	52
2.5.	FT-IR Spectrum of Hindbh	53
2.6.	UV-visible Spectrum of H_2salbh	54
2.7.	UV-visible Spectrum of H_2salnh	55
2.8.	UV-visible Spectrum of Hindbh	55
2.9.	Structure and Labeling Diagram for Hindbh	56
2.10.	^{1}H NMR Spectrum of H_2salbh	59
2.11.	^{1}H NMR Spectrum of H_2salnh	59
2.12.	^{1}H NMR Spectrum of Hindbh	59
3.1.	Mass Spectrum of 1	76
3.2.	Mass Spectrum of 2	77
3.3.	Mass Spectrum of 3	77
3.4.	Mass Spectrum of 4	78
3.5.	Mass Spectrum of 5	78
3.6.	Mass Spectrum of 6	79
3.7.	IR Spectrum of 1	82
3.8.	IR Spectrum of 2	82
3.9.	IR Spectrum of 3	83
3.10.	IR Spectrum of 4	83
3.11.	IR Spectrum of 5	83
3.12.	IR Spectrum of 6	83
3.13.	UV-vis Spectrum of 1	85
3.14.	UV-vis Spectrum of 2	85
3.15.	UV-vis Spectrum of 4	85

3.16.	UV-vis Spectrum of 5	85
4.1.	Mass Spectrum of 8	99
4.2.	Mass Spectrum of 10	99
4.3.	Mass Spectrum of 11	100
4.4.	IR Spectrum of 7	103
4.5.	IR Spectrum of 8	103
4.6.	IR Spectrum of 9	103
4.7.	IR Spectrum of 10	103
4.8.	IR Spectrum of 11	103
4.9.	IR Spectrum of 12	103
4.10.	UV-vis Spectrum of 7	105
4.11.	UV-vis Spectrum of 8	105
4.12.	UV-vis Spectrum of 9	106
4.13.	UV-vis Spectrum of 10	106
5.1.	IR Spectrum of 13	122
5.2.	IR Spectrum of 14	122
5.3.	IR Spectrum of 16	123
5.4.	IR Spectrum of 17	123
5.5.	UV-vis Spectrum of 13	124
5.6.	UV-vis Spectrum of 14	124
5.7.	UV-vis Spectrum of 16	124
5.8.	UV-vis Spectrum of 17	124
6.1.	(A) Emission Spectra of H_2salbh and H_2salnh in DMF Solution (10-5 M) at Room Temperature with Excitation at 330 nm. (B) Emission Spectra of Hindbh in DMF Solution (10-5 M) at Room Temperature with Excitation at 330 nm.	137
6.2.	(A). Emission Spectra of H_2salbh and 1 in DMF Solution (10-5 M) at Room Temperature with Excitation at 330 nm. (B) Emission Spectra of H_2salnh and 2 in DMF Solution (10-5 M) at Room Temperature with Excitation at 330 nm, (C) Emission Spectra of Hindbh and 3 in DMF Solution (10-5) at Room Temperature with Excitation at 330 nm.	140
6.3.	(A) Emission Spectra of H_2salbh, 1 and 4 in DMF Solution (10^{-5} M) at Room Temperature with Excitation at 330 Nm. (B) Emission Spectra of H_2salnh, 2 and 5 in DMF Solution (10^{-5} M) at Room Temperature with Excitation at 330 nm. (C) Emission Spectra of Hindbh, 3 and 6 in DMF solution (10^{-5}) at Room Temperature with Excitation at 330 nm.	142

6.4.	The Comparative Fluorescence Decay Measurements of the Hydrazones and their Cerium(III) Complexes.	144
6.5.	(A). Normalised Fluorescence Emission Spectra of H_2salbh, 7 and 10 in Dmf Solution (10^{-5} M) at Room Temperature with Excitation at 330 nm. (B) Normalised Fluorescence Emission Spectra of H_2salnh, 8 and 11 in DMF Solution (10^{-5} M) at Room Temperature with Excitation at 330 nm.	147
6.6.	(A) Fluorescence Emission Spectra of H_2salbh, 7 and 10 in DMF Solution (10^{-5} M) at Room Temperature with Excitation at 330 nm. (B) Fluorescence Emission Spectra of H_2salnh, 8 and 11 in DMF Solution (10^{-5} M) at Room Temperature with Excitation at 330 nm.	147
6.7.	The Comparative Fluorescence Decay Measurements of The Hydrazones and their Dy(III) Complexes.	149
6.8.	(A). Normalised Fluorescence Emission Spectra of H_2salbh, 13 and 16 in DMF Solution (10^{-5} M) at Room Temperature with Excitation at 330 nm. (B) Normalised Fluorescence Emission Spectra of H_2salnh, 14 and 17 in DMF Solution (10^{-5} M) at Room Temperature with Excitation at 330 nm. (C) Normalised Fluorescence Emission Spectra of Hindbh, 15 and 18 in DMF Solution (10^{-5} M) at Room Temperature with Excitation at 330 nm.	152
6.9.	(A) Fluorescence Emission Spectra of H_2salbh, 13 and 16 in DMF Solution (10^{-5} M) at Room Temperature with Excitation at 330 nm. (B) Fluorescence Emission Spectra of H_2salnh, 14 and 17 in DMF Solution (10^{-5} M) at Room Temperature with Excitation 330 nm (C) Normalised Fluorescence Emission Spectra of Hindbh, 15 and 18 in DMF Solution (10^{-5} M) at Room Temperature with Excitation at 330 nm.	154
6.10.	The Comparative Fluorescence Decay Measurements of the Hydrazones and their Gd(III) Complexes.	155
6.11.	Cell Imaging in HeLa Cells. A and B: Bright and Fluorescence Images of HeLa Cells (Control) Alone.	158
6.12.	C, D and E: Fluorescence Images of the HeLa Cells Treated with 25, 50 and 100 µg /mL of Compound 8.	158
7.1.	Electronic Absorption Spectra of CT-DNA with Different Concentrations (25, 50, 100 µg/ mL) of the Aroylhydrazones.	172

7.2.	Electronic Absorption Spectra of CT-DNA with Different Concentrations (25, 50, 100 µg/ mL) of the Ce(III) Complexes.	174
7.3.	Electronic Absorption Spectra of CT-DNA with Different Concentrations (25, 50, 100 µg/ mL) Dy(III) Complexes.	176
7.4.	Electronic Absorption Spectra of CT-DNA with Different Concentrations (25, 50, 100 µg/ mL) Gd(III) Complexes.	178

LIST OF SCHEMES

Scheme No.	*Title*	*Page No.*
1.1.	Synthesis of Schiff Base	2
1.2	General Formation of Hydrazone.	4
1.3	General Formation of Aroylhydrazone	6
2.1	Synthesis of H_2salbh	47
2.2	Synthesis of H_2salnh	47
2.3	Synthesis of Hindbh	48
3.1	Synthesis of Cerium(III) Complexes	72
4.1	Synthesis of Dysprosium(III) Complexes	95
5.1	Synthesis of Gadolinium(III) Complexes	115

CHAPTER 1

INTRODUCTION

1.1. Introduction

Coordination chemistry is one of the important branches of chemistry. The contributions of the famous scientists, such as Alfred Werner, Linus Pauling and John C Slater, are significant for the development of coordination chemistry. A large number of coordination compounds were synthesized so far, due to their versatile applications in different fields such as industry, medicine and energy technology. Thus, in the past decades, it developed as an important research area and many reports were published on their outstanding applications.

In coordination compounds, the central metal ion is surrounded by the non-metal species, which is known as ligands. The metal ion along with the ligands imparts various properties to the coordination compounds. According to the number of ligands and the nature of the metal ion, these compounds adopt different geometries. If more than one donor atom is present in the ligand, chelate compounds will be formed. Thus, different coordination compounds will have different chemical and biological properties, according to the nature of the metal ion, nature of the ligand and geometry of the compound [1].

1.2. Schiff bases

Schiff bases are important class of organic compounds, distinguished by their ease of synthesis and ability to form stable metal complexes. In 1864, the German chemist Hugo Schiff synthesized the first Schiff base and now, large number of Schiff bases were reported.

They are imines formed by the condensation of primary amines with carbonyl compounds. The general structure of Schiff bases can be expressed as $R^1R^2C=NR^3$, where R's are alkyl or aryl groups [2]. Synthesis of the Schiff base is given in Scheme 1.1.

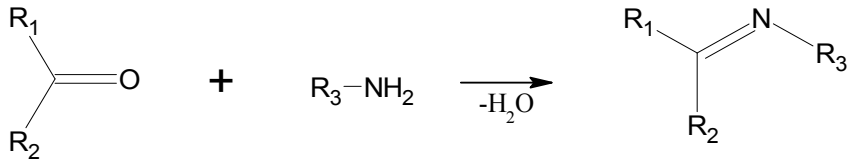

Scheme 1.1. Synthesis of Schiff base

The characteristic functional group in Schiff bases is the imine (C=N) group, which can form coordinate bond with metal ion during complexation. As the number of coordination sites in the ligand increases, they can form more stable complexes with metal ions [3]. A variety of Schiff bases can be synthesized by modifying the structures of precursors. This enables to synthesize ligands with two or more donor atoms, which can form chelates. Chelation increases stability due to chelate effect. Such Schiff bases can form a large number of complexes with a wide range of transition and inner-transition metal ions [4].

The diverse applications of Schiff bases and their complexes make them a prominent ligand in coordination chemistry. As per the previous reports, they have antibacterial, antiviral, antifungal, anti-inflammatory, anticancer and antioxidant properties. On complexation with metal ions, they will have more target specificity and pharmacokinetic profiles. Their lanthanide complexes were found to

exhibit selective antimicrobial applications and they show different extent of interaction with different bacterial stains. Both the transition and inner-transition metal complexes were found to exhibit enhanced bioactivity and stability. Also, the complexation was found to enhance the scope of these compounds in various domains of science [5].

The Schiff bases are also important as molecular sensors and as catalysts in various organic and industrial processes. Their metal complexes were found to be useful in organic catalysis, oxygen transport systems and corrosion inhibition, particularly in acidic environment [6]. Furthermore, they have distinctive optical and electrochemical properties. Such physicochemical features make them prominent in industrial applications such as photoluminescent materials, antioxidants and bactericides [7].

1.3. Hydrazones

Hydrazones are important class of Schiff bases, which can serve as multidentate ligands and thus, they can form very stable complexes with metal ions, by chelation. These complexes will be of diverse geometries and reactivities, which can be utilized for a variety of applications [8].

Due to the higher stability and hydrolytic resistance, hydrazones are one of the prominent ligands in coordination chemistry. Another peculiarity of this ligand is that both nucleophilic and electrophilic centres are present in the same compound. The important chemical unit in the hydrazones is C=N–N and here, the carbon atom

has electrophilic nature, which may be attacked by nucleophilic reagents. At the same time, the nitrogen atom is an electron rich centre and it interacts with electrophilic reagents. This feature is widely utilized in organic synthesis and catalysis [9].

Hydrazones are synthesized by the condensation reactions of hydrazides or their derivatives with the carbonyl compounds. The reaction scheme is given in Scheme 1.2. The synthetic route is straightforward and usually, the products are obtained in high yield. Also, the purification steps are not so complex that the synthesis is economical. Thus, hydrazones are popular ligands in coordination chemistry. In the backbone of hydrazone structure, the nitrogen and oxygen atoms serve as donor atoms and they can form chelate rings which stabilize the metal centres, during complexation [10].

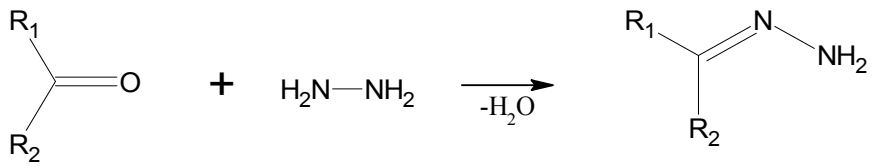

Scheme 1.2. General formation of hydrazone.

The complexes of hydrazones display promising biological properties. These complexes exhibit activity against a broad range of pathogens, and their antimicrobial, antitubercular, anticancer and antioxidant effects have already been reported. Also, it was observed that the bioactivity of hydrazones is enhanced upon coordination with metal ions. On coordination, the hydrazones show improved cellular

uptake, change in redox potential and the interaction with the biomolecular targets was observed to be facilitated [11].

The significant and attractive features of hydrazones as ligands are the ease of synthesis, multifunctional reactivity and strong coordinating ability. Thus, they are in the forefront position in coordination chemistry due to their adaptability and performance for complexation.

The applications of hydrazones and their complexes have been widely reported so far, which include in diverse disciplines such as catalysis, analytical chemistry, materials science and medicinal chemistry. Their ability to form stable chelate complexes with a wide range of metal ions and suitability for constructing functional materials with tailored physicochemical and electronic properties make them a demanding ligand in coordination chemistry [12]. Due to their diverse bioactivity, hydrazones and their complexes are reported to show antimicrobial, antiviral, anticancer, antitubercular, antioxidant and enzyme-inhibitory properties. They are versatile scaffolds in drug discovery and biomedical research. Also, their fluorescent properties were also reported and they can be used as fluorescent sensors. The azomethine nitrogen and carbonyl oxygen are the main donor sites in hydrazones and the number of donor sites can be increased by selecting the hydrazide and carbonyl compound suitably. Thus, the geometry and the electronic environment around the metal centre can be modified. This flexibility is key to tuning properties such as lipophilicity, redox behaviour, reactivity, and stability [13,14].

1.4. Aroylhydrazones

Aroylhydrazones are formed through the condensation of aryl or heteroaryl aldehydes or ketones with hydrazine or hydrazide derivatives. They contain the functional –CH=N–NH–C(O)– group, which offers multiple potential donor atoms for metal coordination. Depending on their substitution pattern, these ligands can act as bidentate or tridentate donors. In cases where side chains with additional donor atoms are absent, they typically coordinate through the imine nitrogen and the carbonyl oxygen, forming stable chelates with metal centres [15]. General formation and coordination mode of aroylhydrazones is given in Scheme 1.3 and in Fig. 1.1 respectively.

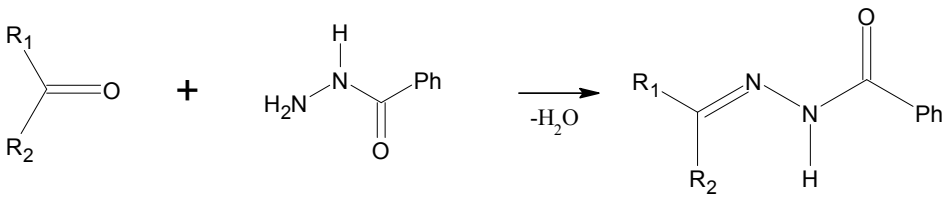

Scheme 1.3. General formation of aroylhydrazone

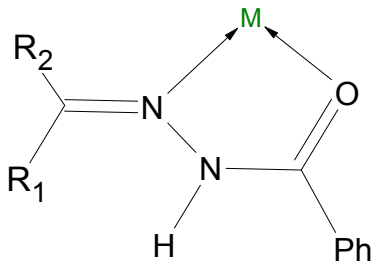

Fig. 1.1. General coordination mode of aroylhydrazones

The presence of aromatic or heteroaromatic rings attached to the hydrazone backbone can significantly influence the structural and electronic properties of the aroylhydrazone. During the synthesis of

hydrazones, if aroylhydrazide is used, then aroylhydrazones are obtained as product. As mentioned above, the change in the substituents, on the hydrazones, will modify their solubility, lipophilicity and biological properties. Aroylhydrazones can form strong complexes with various metal ions and they exhibit diverse geometries and electronic properties [9].

The complexes of aroylhydrazones are highly interesting area to scientists due to their potential in catalysis, materials science, and bioinorganic chemistry. The coordination modes of the hydrazones can be tuned by changing the substituents on them, and thus, metal complexes of different geometry can be synthesized. The coordination geometry influence the biological properties of the complexes. The metal-to-ligand ratio, ligand denticity, nature of the metal ion and the p^H of the medium are some important factors that decide the coordination environment and thereby, geometry of the complex. Thus, metal complexes can be synthesized for targeted functions and this makes them versatile systems for applications in various fields such as pharmaceuticals, analytical chemistry and materials science [16-18].

1.5. Applications of metal complexes of aroylhydrazones

1.5.1. Applications in biology and medicine

Metal complexes of hydrazone-based ligands are well known to exhibit a broad range of biological activities, including antimicrobial, anticancer, antitubercular, and enzyme-inhibiting effects. These wide ranges of applications arise from the azomethine functionalities present in the aroylhydrazones.

Recently numerous scientific investigations advance in the synthesis and biological evaluation of aroylhydrazone-metal complexes especially in the field of cancer diagnosis and therapy. Mohan *et al.* recently synthesized novel (η^6-benzene) ruthenium(II) aroylhydrazone complexes. The cytotoxic activity against MCF-7 breast cancer cells of these complexes were greatly enhanced when compared to the standard chemotherapeutic agent, cisplatin. Fluorescence staining assays confirmed that the observed cell death was predominantly mediated through apoptosis. This study accounts the potential of the ruthenium complexes as effective anticancer agents [19].

In the field of antimicrobial research, Kuriakose and Kurup reported the synthesis of a tridentate ONO donor aroylhydrazone and its *cis*-MoO_2 complex, both showing notable antibacterial activity, particularly against *Escherichia coli*. This highlights the potential application of these complexes in developing new antimicrobial agents [18]. In addition, Hegde and co-workers synthesized Co(II), Ni(II), Cu(II), and Zn(II) complexes of a quinolone-based aroylhydrazone ligand. They evaluated the antimicrobial and antitubercular activities and found that these complexes exhibit potent efficacy against both Gram-positive and Gram-negative bacteria. Also, it is interesting to note that the antitubercular activity of Cu(II) complexes were comparable to streptomycin, highlighting their promise as effective therapeutic agents against infectious diseases [20]. A similar work was carried out by, Sawkmie and colleagues. They synthesized bidentate NO fluorenyl benzohydrazone and its Ru(II), Rh(III), and Ir(III)

complexes. The complexes formed were stable five-membered chelates and exhibited strong antibacterial and anticancer activities. The cytotoxicity of some of the compounds were comparable to cisplatin., positioning them as dual-functional therapeutic agents [21].

Hydrazone derivatives have also found to exhibit promising antiparasitic activity. Following this, Hassan *et al.* synthesized a series of indole-hydrazone derivatives. Among these compounds, the structure of benzoic acid hydrazide derivative was confirmed by single crystal X-ray crystallography and found that it exist in the stable E-anti configuration. Furthermore, this compound exhibited significant polarity and potent anti-Toxoplasma activity and showed a considerable reduction percent of cyst burden in infected mouse brains by 49%, underscoring its potential as an antiparasitic agent [22].

In the field of oncology, Han and colleagues developed a series of thieno[3,2-d]pyrimidine derivatives that containing aroylhydrazone or aryl-hydrazide groups. These derivatives act as dual PI3K/mTOR inhibitors suggesting their potential as cancer therapeutic agets. These compounds show good inhibition against colorectal, prostate, lung, and breast cancers. Their structure-activity relationship (SAR) analysis revealed that molecules combining an aryl hydrazide at C-6 with a 2-aminopyrimidine group at C-2 showed the most potent antiproliferative activity, and one optimized compound demonstrated strong dual-target inhibition and cell-cycle modulation. These findings highlight this scaffold as a valuable platform for developing targeted anticancer therapies capable of promoting apoptosis [23].

A similar work was done by Karabeliov *et al.* and they synthesized a series of novel 1,3,4-oxadiazole and aroylhydrazone derivatives. They evaluated the effects of these new derivatives on isolated rat brain synaptosomes. Several compounds effectively protected against 6-OHDA-induced oxidative stress by preserving synaptosomal viability and reduced glutathione levels against toxic agent. Additionally, all the compounds displayed a good predicted ADME profiles, establishing these derivatives as a promising candidates for neuroprotective therapeutics [24].

Studies show structural modification of aroylhydrazones has also lead to enhanced biological activity. For example, Hrušková and co-authors synthesized ten analogs of methyl- and ethyl-substituted salicylaldehyde isonicotinoylhydrazone (SIH)-derivatives with modified hydrazide scaffolds. These modifications significantly improved plasma stability and highly selective antiproliferative activity against MCF-7 and HL-60 cell lines. Notably, the lipophilic derivatives showed a considerable antiproliferative effect and protected cardiomyoblasts against oxidative stress with a five-fold higher selectivity compared to the parent compound SIH, suggesting its dual therapeutic benefits [25]. A further structural-modification strategy was explored by Żołnowska *et al.,* who synthesized benzenesulfonamide–aroylhydrazone conjugates, which potently inhibited cancer-relevant carbonic anhydrase isozymes. One of the synthesized compound demonstrated high cytotoxicity and selectivity toward MCF-7 breast cancer cells. while triggering MAPK/ERK-mediated cell-cycle arrest and mitochondrial apoptosis, establishing

these conjugates as promising candidates for anticancer therapeutics [26].

In further exploration of metal-hydrazone complexes, Al Banna and colleagues reported Ni(II) complexes with *in-situ* generated N,O-bidentate aroylhydrazone Schiff base ligands. Structural characterization and molecular docking studies showed the potential inhibition towards cancer-related proteins (PDB ID:2P85). Also, pharmacokinetic and toxicological studies suggest their relatively safe drug administrative properties [27].

The role of metal coordination in enhancing biological activity has also been extensively explored. Fousiamol and Kurup synthesized a new NNO-donor aroylhydrazone ligand and its one bis-coordinated and two box dimer copper(II) complexes. Structural and spectral studies confirmed distinct geometries, and the complexes were found to exhibit good antibacterial and cytotoxic activities, underscoring the potential of copper(II) hydrazone complexes for antimicrobial and anticancer applications [28].

Li and colleagues extended this approach to iron complexes and synthesized two o-vanillin–based Fe(III) Schiff-base aroylhydrazone complexes with six-coordinate octahedral configuration. Both complexes induce morphological changes and aggregation of DNA and bovine serum albumin (BSA) and even DNA damaged in the presence of the complex with reducing agent ascorbic acid, emphasizing the broader biological significance of Fe(III) hydrazone systems [29]. Recently, Dash *et al*. synthesized and

characterized a series of oxidovanadium(V) complexes with aroylhydrazone ligands incorporating heterocycles such as furan, thiophene, and pyridine. These complexes exhibited minor groove DNA binding, highest photo-induced DNA cleavage activity of ~65%. Additionally the compounds also exhibited cytotoxic activity against HeLa cancer cells, indicating strong potential for therapeutic applications [30].

A similar work was done by Monikaa and team. They synthesized dinuclear arene Ru(II) benzilbis(furoylhydrazone) complexes exhibiting a piano-stool structure confirmed by single-crystal X-ray analysis. These complexes displayed cancerous cell growth resistance property against A549 and HeLa cell lines. One of the synthesized complexes exhibited a two- fold higher activity in inhibition of all the cancer cells than cisplatin. Further, fluorescent staining methods confirmed apoptosis induction, attributed to electron-releasing substituents that enhanced hydrophobicity and cellular uptake, providing insight into their mode of action [31].

Further investigations into metal coordination chemistry by Yueqin Li and colleagues, led to the synthesis of Ni(II) and Co(II) complexes of an asymmetrical aroylhydrazone. Both complexes exhibit distorted octahedral geometry confirmed by X-ray crystallography. The DNA and protein-binding affinity, potential for free radical scavenging and cytotoxicity of the complexes were determined. Furthermore they exhibited strong cytotoxicity against HeLa and A549 cancer cell lines [32].

Copper(II) complexes have also garnered significant attention for their cytotoxic and DNA-binding properties. Ramachandran and team focused on aroylhydrazone-based copper complexes, demonstrating strong DNA-binding capabilities through intercalation and efficient plasmid DNA cleavage in the presence of ascorbic acid. These copper complexes exhibited significantly enhanced cytotoxicity against various human cancer cell lines compared to the free ligands and cisplatin [33]. Similarly, Deng and co-workers reported that, among a series of copper(II)-aroylhydrazone complexes, the 1:1:1 Cu(II)/ligand/co-ligand complexes demonstrated higher cytotoxicity against various human cancer cell lines, including cisplatin-resistant A549cisR cells, compared to traditional 1:1 Cu(II)/ligand complexes. Mechanistic studies showed that the 1:1:1 mixed-ligand complex [Cu(L2)(Py)NO_3] induced DNA damage, resulting in mitochondria-mediated apoptotic cell death. [34].

The cytotoxic potential and therapeutic interventions of aroylhydrazones and their metal complexes has been further demonstrated by Johnson *et al*., who investigated pyridoxal and salicylaldehyde hydrazones. The hydrazones effectively suppressed DNA synthesis in human and rodent cell lines, and the copper(II) complex SBH showed enhanced inhibitory activity compared to the free ligand. Notably, these compounds exhibited low toxicity in mice and selective effects toward different cell types, supporting their potential in for proliferative disorders [35].

Lin Pan and co-authors also synthesized a series of new copper(II) with tridentate aroylhydrazone ligands. These complexes exhibit strong inhibitory activity against *Helicobacter pylori* urease, with low micromolar IC_{50} values. This positions these complexes as promising candidates, for therapeutic intervention in urease-related diseases [36].

Other researchers have also added noteworthy contributions to the field. For instance, Mathews and colleagues synthesized a new ONO-donor aroylhydrazone ligand and its two cobalt(III) complexes. The complexes exhibited enhanced antibacterial and antifungal activity relative to the free ligand, indicating their potential against a broad spectrum of pathogenic microorganisms [37].

Hou *et al*. synthesized three aroylhydrazone-Cu(II) complexes and assessed their *in vitro* anticancer proprties against a panel of cell lines. An MTT assay revealed that these Cu(II) complexes exhibited enhanced anticancer activity toward several tumor cell types than cisplatin. Among them, a mixed-ligand Cu(II) complex showed higher anticancer activity, including significant inhibition in a 3D tumor spheroid model. Flow cytometry, fluorescence imaging, and western blot analysis revealed that this complex induced reactive oxygen species-mediated apoptotic cell death. This highlights its potential for anticancer therapy [38].

Further exploration by Sahu *et al*. led to the synthesis of five new anionic aqueous dioxidovanadium(V) complexes with the aroylhydrazone ligands incorporating different alkali metals. These complexes were characterized by various physicochemical methods

and showed stable solution-phase behaviour. The biological behavior of the complexes was evaluated by DNA and protein binding studies and confirmed their strong interaction with biomolecules. Importantly, the complexes exhibited highest activity against colon cancer (HT-29), outperforming cisplatin in some cases. The study also highlighted the crucial role of hydrophobicity in the cytotoxicity, alongside antimigration effects observed in wound-healing assays [39].

Additionally, palladium(II) complexes have also shown promising applications in therapeutic and imaging. Vignesh *et al*. designed a novel class of palladium(II) complexes of the general formula [Pd(L)(PPh_3)Cl], where L is a pyrene-based aroylhydrazone ligand. One of the complexes, featuring a unique monodentate coordination of the ligand, demonstrated strong interactions with DNA and bovine serum albumin, along with superior selectivity towards cancer cells. Additionally, its efficient cellular uptake was confirmed with fluorescence imaging, suggesting significant potential for simultaneous cancer therapy and bioimaging [40].

1.5.2. Applications in photoluminescence

Nowadays aroylhydrazone-based compounds have become increasingly important due to their strong fluorescence and wide-ranging biological applications. Wang *et al*. designed a diarylethene derivative with an aroylhydrazone unit as a dual responsive sensor for Cu^{2+} detection. The colorimetric and fluorimetric dual sensing of Cu^{2+} was achieved. The sensor was used for the fabrication of test strips that can be used as the standard cards for detecting Cu^{2+}, highlighting

its potential for practical, applied on-site Cu^{2+} sensing applications [41].

Expanding the scope of luminescent materials, Borbone *et al*. synthesized a series of cadmium(II) complexes with conjugated O,N,O ligands and coordinated pyridine and polyvinylpyridine based polymers. All the compounds exhibited bright luminescence in the solid state. Cadmium(II)-aroylhydrazone complexes and metallopolymers exhibited strong, color-tunable solid-state luminescence. Grafting onto poly(4-vinylpyridine) significantly enhanced photoluminescence quantum yields, positioning these materials as promising candidates for optoelectronic devices [42].

In biological sensing, Moumita Chakraborty and co-authors developed a Cu(II) complex of a benzoylhydrazone-based Schiff base ligand with high selectivity and sensitivity toward sulfide ions (S^{2-}) in aqueous buffer. The complex exhibited a low detection limit (6.9×10^{-7} M) and strong binding constant, with sensing attributed to displacement of the fluorescent ligand by sulfide ions, making it promising for environmental and biological S^{2-} detection [43].

Similarly, Dwivedi *et al*. (2020) reported an aroylhydrazone-based fluorescent probe with a large Stokes shift for selective Cu^{2+} detection in pure aqueous media through static fluorescence quenching. The probe forms a 1:2 complex with Cu^{2+} *via* intramolecular charge transfer (ICT), enabling visible color change and high sensitivity without self-quenching. It was successfully applied for

in vivo Cu^{2+} imaging in Drosophila, confirming its biocompatibility and suitability for biological sensing [44].

Zhang *et al*. (2021) designed a tripodal aroylhydrazone-based fluorescent sensor useful for the selective detection of Hg^{2+} and Br^- ions in solution and living cells. The sensor demonstrated high binding affinity and low detection limits (4.95×10^{-8} M for Hg^{2+}). This is attributed to its tripodal structure of aroylhydrazone enhancing stronger binding force for guest ions. Importantly, it was effectively applied for *in vivo* fluorescence imaging of Hg^{2+} and Br^- in living cells [45].

In solid-state fluorescence research, Diana and team (2019) synthesized two tridentate pyridinyl-hydrazone zinc(II) complexes. Both complexes exhibited intense blue fluorescence in solid state due to AIE effects. These complexes showed photoluminescence quantum yields ranging from to 20-30%, making them very promising as fluorophore dopants for blue-emissive layers for optoelectronic devices. Their study emphasized the role of molecular design in enhancing emission properties for device integration [46].

Transition metal aroylhydrazone complexes have further revealed dual benefits bright fluorescence coupled with antimicrobial activity. Dongare and Aswar synthesied a new aroylhydrazone and its metal complexes with Cr(III), Fe(III), Mn(II), Co(II), Ni(II), and Cu(II). These complexes adopted octahedral geometry and exhibited strong fluorescence at around 527–533 nm. The *in vitro* antimicrobial potency of ligand and its metal complexes were also studied.

Molecular docking studies suggested good binding affinity with bacterial and fungal enzymes, indicating pharmaceutical potential [47].

Zhao et al. (2022) designed and synthesized a salicylaldehyde benzoyl hydrazone CySBH based near-infrared (NIR) fluorescent probe, for selective detection of Cu^{2+}. The probe exhibits a distinct fluorescence quenching upon coordination with Cu^{2+}, allowing for real-time tracking of copper ions. CySBH demonstrated rapid recognition of Cu^{2+} with excellent selectivity over other metal ions. The authors further showed that the probe has low cytotoxicity, allowing visualization of Cu^{2+} in two different cell lines through fluorescence imaging. Importantly, CySBH can also be applied for *in vivo* monitoring of Cu^{2+}, due to its NIR emission, highlighting its potential for studying copper-related biological processes and disease diagnostics [48].

On the sensing front, Akther Rupaa *et al*. synthesized a novel hydrazide–hydrazone compound, 5-bromo-2-hydroxy-N′-[(1E)-1-(thiophen-2-yl)ethylidene]benzohydrazide (L). Fluorescence studies demonstrated a ratiometric and turn-on fluorescence response specifically toward Fe^{3+} ions, while demonstrating a colorimetric response in the presence of Cu^{2+} ions. Job plot analysis confirmed a 2:1 binding stoichiometry between L and both metal ions, indicating strong and specific complex formation. These results suggest that L functions effectively as a dual sensor, combining sensitive fluorescence detection of Fe^{3+} with colorimetric detection of Cu^{2+},

making it a promising candidate for metal ion sensing applications [49].

Recently, Patra *et al*. reported five fluorescent ONO donor-based diorganotin(IV) aroylhydrazone complexes. All the compounds exhibited high luminescent properties with a quantum yield of 17–53%. Fluorescence quenching studies demonstrated their effective binding to bovine serum albumin *via* static quenching. Cellular uptake and live cell confocal microscopy confirmed mitochondrial localization in cancer cells. Biologically, these complexes showed promising anticancer activity by inducing apoptotic cell death and increasing reactive oxygen species (ROS) levels, linking their fluorescence to both imaging and therapeutic applications [50].

1.6. Scope and objectives of the present study

Aroylhydrazones are prominent ligand in coordination chemistry with significant applications in various areas such as biological activities, non-linear optics, sensors and catalysis. Salicylaldehyde benzoylhydrazone and its derivatives were reported to exhibit strong anticancer effects by inhibiting DNA synthesis, with structural modifications enhancing their therapeutic potential. Also, salicylaldehyde nicotinoylhydrazone protects cells from oxidative stress and enhances the safety and efficiency of chemotherapy drugs. Additionally, indole carbaldehyde benzoylhydrazone demonstrates promising activity against chronic Toxoplasma infection, reducing parasite cysts and highlighting its potential as a novel therapeutic agent.

The biological activity and the stability of the Schiff base-complexes were found to be enhanced by incorporating amino acid as coligand. One of the essential amino acid, L-Histidine, contains an imidazole ring with three potential donor atoms, the amino nitrogen, the imidazole nitrogen and the carboxylate oxygen. Its natural detoxifying properties, particularly in reducing environmental radiation hazards, are also to be mentioned.

The metal complexes of aroylhydrazones as principal ligand and L-histidine as coligand were prepared. The presence of multiple donor sites with the ligands and the presence of L-histidine enhance the stability and biological activity of the compounds.

Based on these considerations, we synthesized Ce(III), Dy(III), and Gd(III) complexes of these aroylhydrazones and systematically studied their fluorescence characteristics along with their DNA-binding properties.

The objectives of the present work include

- ✓ To synthesize aroylhydrazones.
- ✓ To synthesize lanthanide (Ce(III), Dy(III), Gd(III)) complexes of the aroylhydrazones, with and without incorporating L-histidine as a coligand.
- ✓ To characterize the compounds using various analytical tools.
- ✓ To study their luminescence and DNA binding properties.

1.7. Various metals used in the present study

1.7.1. Cerium

The lanthanide element, cerium, was discovered by Berzelius and Hisinger in 1803. It is one of the most abundant rare earth elements in the Earth's crust, ranking 25th overall and exceeding the abundance of copper. It is commonly found in minerals like bastnaesite and monazite, often co-occurring with calcium due to their similar ionic radii (Ce^{3+}: 1.01 Å; Ca^{2+}: 1.00 Å). Because of this similarity, calcium can be substituted with cerium in biological systems without disrupting structural or physiological processes, allowing it to integrate into calcium-binding sites, especially in mineralized tissues like bone [51].

However, cerium has been associated with soft tissue calcification, potentially through interference with calcium–pyrophosphate interactions. The favourable features of cerium, such as low toxicity, biocompatibility, and redox activity, have aroused interest in its use in biomedical applications. For example, Taha *et al*. synthesized a Ce(III) Schiff base complex that exhibited pronounced anticancer, antiviral, antioxidant, and antifungal effects. This was supported by molecular docking studies that confirmed strong binding interactions with relevant biological targets [52]. Similarly, Saad *et al*. reported a Ce(III) Schiff base complex with improved antimicrobial activity compared to the free ligand, demonstrating activity against various bacterial and fungal strains, most notably Fusarium oxysporum [53].

In addition to their biological applications, cerium(III) complexes have been recognized for their distinctive photophysical characteristics. Yin *et al*. (2015) synthesized luminescent Ce(III) complexes that display visible $4f \rightarrow 5d$ electronic transitions with emission peaks between 518 and 553 nm and excited-state lifetimes ranging from 24 to 67 ns. These complexes exhibit strong metalloradical reducing power in their excited states, which enables photochemical halogen atom abstraction from sp^3 and sp^2 carbon–halogen bonds (X = Cl, Br, I). Additionally, the halogen abstraction reactions can be catalytically sustained through photosensitizers that promote salt metathesis and reduction, demonstrating the potential of these complexes in catalytic photoredox processes [54].

Qiao *et al*. investigated Ce(III) complexes with guanidinate, amide, and aryloxide ligands, revealing that higher guanidinate substitution levels suppress nonradiative decay and reduce Stokes shifts, thereby improving emission efficiency. This work helped in developing a predictive model for designing tunable, high-performance luminophores [55]. Additionally, Wang *et al*. reported a deep-blue OLED based on a Ce(III) complex, which exhibited a short excited-state lifetime of 42 ns and an external quantum efficiency (EQE) of 12.4%. These performance metrics surpass those of many conventional phosphorescent and thermally activated delayed fluorescence (TADF) emitters, emphasising the potential of Ce(III) for high-speed, high-efficiency optoelectronic devices [56].

In corrosion science, Wang *et al*. introduced a Ce(III)-based Schiff base complex that achieved more than 90% corrosion inhibition efficiency for 2024 aluminum alloy in concentrated HCl. This was attributed to the formation of a compact, stable, and parallel-oriented protective film, as observed by spectroscopic and molecular dynamics studies [57].

All these findings provide testimony to the versatility of cerium(III) complexes, which combine biological compatibility, photochemical reactivity, and advanced optical performance and reaffirm them as promising candidates across biomedical, catalytic, and materials science applications.

1.7.2. Dysprosium

Dysprosium (Dy), a heavy rare-earth element with atomic number 66 and atomic weight 162.5 u, was first discovered by Boisbaudran in 1886. It exhibits a metallic silver luster and is typically found combined with other lanthanides in minerals such as fergusonite and euxenite, rather than in its elemental form. It is commonly processed as dysprosium oxide (Dy_2O_3), a white powder and find extensive applications in optical materials, glass additives, and magnetic resonance imaging (MRI) contrast agents. The electronic configuration of Dy is [Xe]$4f^{10}6s^2$, and its trivalent ion, Dy^{3+}, displays notable luminescent properties arising from intra-4*f* electronic transitions. Specifically, Dy^{3+} emits intense blue light around 480 nm ($^4F_{9/2} \rightarrow {}^6H_{15/2}$), attributed to magnetic dipole transitions, and yellow light near 573 nm ($^4F_{9/2} \rightarrow {}^6H_{13/2}$), resulting from electric dipole

transitions. The relative intensity of these emissions depends strongly on the host lattice symmetry and ligand environment, allowing tunable emission colors ranging from blue through yellow to near-white light. Upon ultraviolet excitation, typically at 365 nm, Dy^{3+} ions also emit sharp lines including red near 670 nm ($^4F_{9/2} \rightarrow {}^6H_{11/2}$), contributing to cool or near-white light generation. These spectral characteristics make Dy^{3+} an excellent activator for white light-emitting phosphors, widely employed in white light-emitting diodes (LEDs), owing to their high quantum efficiency, spectral tunability, long excited-state lifetimes, and facile fabrication [58,59].

Based on these intrinsic properties, extensive research has focused on synthesizing Dy(III)-based complexes to harness and enhance their luminescent and functional capabilities. For example, Yi Yin *et al*. reported a triple helical-like Dy(III) complex that exhibits strong, selective fluorescence turn-on/off sensing of Al(III) ions and 4,5-dimethyl-2-nitroaniline (DMNA), with high sensitivity and anti-interference performance. The photoinduced electron transfer (PET) mechanism is the underlying principle of the fluorescence response, and the inner filter effect (IFE) also influences emission in the presence of DMNA. This work shows the potential of Dy(III)-based complexes in selective fluorescence sensing of metal ions and nitroaromatic compounds [60]. Similarly, Randa M. Al-As'ad and colleagues synthesized Dy(III) complexes with Schiff base ligands that exhibited intense visible-region fluorescence. Their photoluminescence studies revealed bright emissions, with X-ray crystallography and density functional theory (DFT) calculations confirming that the

coordination environment plays a pivotal role in luminescent behaviour, supporting their suitability as light-emitting materials [61]. Berezhnytska *et al*. explored a series of Dy(III) *β*-diketonate and heteroligand complexes, demonstrating that both the chemical nature of substituents and the morphology of powdered samples significantly influence emission intensity. These findings highlight the critical role of ligand design and material dispersion in optimizing fluorescence in Dy(III)-based luminescent materials [62].

Malik *et al*. synthesized Dy(III) complexes containing mono- and bidentate ligands that achieved efficient near-white light emission through balanced blue (~480 nm) and yellow (~575 nm) bands, arising from the dominant $^{4}F9_{9/2} \rightarrow {}^{6}H_{13/2}$ transition. This enabled tunable Commission Internationale de l'Éclairage (CIE) color coordinates and highlighted the importance of ligand architecture in improving Dy(III) fluorescence for white-light emitting devices and laser applications [63]. Complementing these photonic studies, Ali Tilehkan and Majid Arvand investigated a Dy(III) complex with 1,10-phenanthroline-5,6-dione, which exhibited strong fluorescence and a high DNA-binding constant (K_b=3×10^5 M^{-1}). Fluorescence resonance energy transfer (FRET) experiments confirmed close proximity between the complex and DNA, while electrochemical and spectroscopic studies indicated groove-binding stabilized by hydrogen bonding and van der Waals interactions, accentuating its potential for biomedical applications [64]. Nishita Dua, Monika Punia, and Priti Boora synthesized five Dy(III) complexes incorporating *β*-diketone and various auxiliary ligands that displayed characteristic blue (~484 nm) and yellow (~575 nm)

emissions, with monoexponential photoluminescence decay behaviour indicative of single luminescent centres. The calculated CIE coordinates and correlated color temperature (CCT) values confirmed the emission in the cool white-light region and proved their suitability in white OLED and lighting applications [65].

Apart from luminescence, Dy^{3+} ions possess significant biomedical relevance owing to their paramagnetic nature, facilitating use as MRI contrast agents. When incorporated into biocompatible materials like hydroxyapatite, they serve as suitable candidates for luminescent bioimaging. Moreover, the radioactive isotope Dy-165 finds use in therapeutic applications such as non-invasive treatment of joint diseases. Additionally, Dy-doped zinc oxide nanostructures have shown enhanced luminescence and modified electrical properties, making them valuable in photocatalysis, gas sensing, and semiconductor technologies [66].

Dy(III) has a myriad of favourable features, such as the versatile luminescent, sensing, and biological properties of Dy(III) complexes, tunable emission profiles and robust stability, which establish dysprosium as a promising element for advanced applications in photonics, optoelectronics, biosensing, and medical diagnostics.

1.7.3. Gadolinium

The spectral analysis of the mineral samarskite by the Swiss chemist Jean Charles Galissard de Marignac Gadolinium led to the discovery of the element Gadolinium in 1880. The element is named

after gadolinite, a mineral itself named in honor of the Finnish chemist Johan Gadolin, recognized for his early work in rare earth chemistry. Gadolinium is a silver-white metal that remains solid at room temperature and has notable paramagnetic properties.

The electronic configuration of neutral gadolinium is [Xe] $4f^7 5d^1 6s^2$. In its most stable oxidation state, Gd^{3+}, the configuration becomes $4f^7$. This half-filled *f*-orbital arrangement, with seven unpaired electrons, is electronically stable and results in a high magnetic moment. Gadolinium is widely used as a contrast agent in magnetic resonance imaging (MRI) [67].

Based upon these fundamental properties, Sheikh *et al*. reported the synthesis and characterization of fluorescent gadolinium(III)-oligopeptide complexes and developed their carbon nanotube (CNT) composite for potential anticancer applications. The study demonstrated dual functionality. The complexes exhibited white and green light emission under confocal microscopy along with significant *in vitro* cytotoxicity against HeLa cells, with IC_{50} values as low as 10 nM for the CNT composite. Transmission electron microscopy further confirmed cellular uptake of the CNT-gadolinium complex, indicating its use in an effective targeted delivery system [68].

In quest of the multifunctional potential of gadolinium complexes, Vijayaraj *et al*. synthesized a series of 2,2′-bipyridyl-based hetero-binuclear Gd(III)–Cu(II) complexes and characterized them using spectroscopic and electrochemical methods. These complexes

demonstrated multiple features, including DNA binding, catalytic oxidation of 1,2-benzenediol, and fluorescence activity with varying excited-state lifetimes. Strikingly, they exhibited significant magnetic behaviour attributed to ferromagnetic coupling. Some complexes also showed efficient DNA cleavage *via* singlet oxygen-mediated oxidative damage to plasmid DNA, indicating potential applications in biochemical and medicinal fields [69].

Wang *et al*. described the synthesis of a Gd(III)-based trinuclear cluster bridged by μ-O-hydrazone ligands *via* the solvothermal method incorporating multidentate Schiff base and β-diketonate ligands. This Gd_3 cluster exhibited pronounced magnetocaloric effects, achieving a maximum magnetic entropy change of 20.60 $JK^{-1}kg^{-1}$ at 2 K under an applied magnetic field of 7 T, indicating the potential of Gd(III) clusters in cryogenic magnetic refrigeration technologies [70].

In terms of analytical applications, Ganjali *et al*. developed a novel gadolinium-selective membrane sensor based on a new S–N Schiff's base incorporated into a poly(vinyl chloride) matrix. The sensor exhibited a wide linear detection range from 1.0×10^{-1} to 1.0×10^{-5} M, with a Nernstian slope of 19.8 ± 0.3 mV/decade. It showed high selectivity against various metal ions, including other lanthanides and heavy metals, fast response, good stability over nine weeks, and was successfully employed in the potentiometric titration of Gd(III) and determination in biological samples such as urine [71].

Kaczmarek *et al*. synthesized a novel gadolinium(III) nitrate complex *via* template condensation with a Schiff base ligand. Single-

crystal X-ray diffraction indicated a nine-coordinated Gd(III) centre with a distorted tricapped trigonal prism geometry coordinated exclusively by oxygen donors. Uncoordinated methanol molecules linked these complexes into infinite chains *via* hydrogen bonding. Spectroscopic studies showed low fluorescence quantum yields, varying with solvent, confirming detailed structural and photophysical properties [72].

Recently, Shi *et al*. developed a facile synthesis method for gadolinium(III)-chelated carbon quantum dots (CQD–DTPA–Gd) designed as dual-modal probes for fluorescence and magnetic resonance imaging. The Gd^{3+} ions were chelated onto the surface of DTPA-functionalized CQDs without changing core optical properties. The resulting nanoparticles exhibited high water solubility, excellent cell permeability, and minimal cytotoxicity. Enhanced longitudinal relaxivity (56.72 $mM^{-1}s^{-1}$) highlighted their potential as efficient and safe bioimaging agents [73].

All these studies emphasise the versatility of gadolinium complexes, utilising their unique electronic and magnetic properties for applications ranging from targeted cancer therapy and DNA interaction to magnetic refrigeration, selective sensing, and advanced biomedical imaging.

1.8. Physical measurements

The physicochemical methods adopted during the present study are discussed below.

1.8.1. Partial elemental analysis

The elemental composition (C, H and N) of the synthesized aroylhydrazones and their metal complexes was determined using a Vario EL III CHNS elemental analyzer. These microanalyses were conducted by the Thermo Scientific FLASH 2000 HT analyzer at the CSIF, University of Calicut, India. Prior to analysis, all samples were properly dried in order to ensure accuracy in evaluating their purity and chemical composition.

1.8.2. Conductivity Measurements

The electrolytic nature of the synthesized metal complexes was assessed by measuring their molar conductivities (λ_m) in N,N-dimethylformamide (DMF) solutions at a concentration of 10^{-3} M. The measurements were carried out at room temperature (298 K) using a Digital TDS/ conductivity meter. In order to get accurate results, the instrument was calibrated with a standard 0.1 N KCl prior to data collection. All conductivity measurements were carried out at the Department of Chemistry, Government College, Madappally, Kozhikode, Kerala, India.

1.8.3. Magnetic Susceptibility Measurements

The magnetic susceptibility measurements of the synthesized complexes were measured using powdered samples at room temperature (298 K) using a Sherwood Scientific Magnetic Susceptibility Balance. All measurements were obtained from the Central Instrumentation and Research Laboratory (CIRL), Govt. College for Women, Thiruvananthapuram, Kerala, India.

1.8.4. Infrared Spectroscopy

Infrared spectroscopy is an analytical technique used for identifying functional groups and distinct bonds in coordination compounds. The characteristic absorption bands provide information about various vibrational modes, and shifts in these bands upon complexation are indicative of the interactions between metal ions and donor atoms of the aroylhydrazones. These spectral changes provide strong evidence for the formation of coordination bonds.

In this study, the IR spectra of the synthesized ligands and their corresponding metal complexes were recorded in the 4000–400 cm^{-1} region using the KBr pellet. IR spectra were recorded on Agilent Cary 620 FT-IR Imaging system coupled with Cary 660 FT-IR Spectrometer, in the spectral range 4000 to 400 cm^{-1} at the CSIF, University of Calicut, India**.**

1.8.5. Electronic spectroscopy

Electronic spectroscopy is a useful technique for investigating the electronic structure and geometry in coordination complexes, as it involves electronic transitions between energy levels that correspond to wavelengths in the ultraviolet and visible regions.

The UV–visible absorption spectra of the compounds were recorded using quartz cuvettes of 1 cm path length using DMF as the solvent. The spectral measurements were obtained from a LAMBDA 650 UV–visible spectrophotometer (PerkinElmer) at the Inter University Instrumentation Centre (IUIC), Mahatma Gandhi University, Kottayam, and also on a SYSTRONICS 117 UV–visible

spectrophotometer at the Department of Chemistry, Government College, Madappally, University of Calicut, Kerala, India.

1.8.6. Nuclear Magnetic Resonance (NMR) spectroscopy

Nuclear Magnetic Resonance (NMR) spectroscopy makes use of the magnetic properties of atomic nuclei, such as hydrogen, to provide information about the structure and chemical environment of molecules. The ^{1}H NMR spectra of the synthesized aroylhydrazones were recorded using a Bruker AV III 500 MHz NMR at SAIF, IIT Madras, India.

1.8.7. Mass spectrometry

Mass spectrometry is a precise analytical technique used to determine a compound's molecular weight, elemental composition, and structural features by examining the mass-to-charge (*m/z*) ratios of ions formed from them.

Mass spectra of the aroylhydrazones were obtained using a Liquid Chromatograph - Quadrupolar Time of Flight - High Resolution Mass Spectrometer (LC-QTOF-HRMS) at SAIF, IIT Madras, India and the mass spectra of the complexes were obtained using a MALDI time-of-flight Bruker Autoflex max LRF mass spectrometer at STIC, CUSAT, India.

1.8.8. Fluorescence spectroscopy

Fluorescence spectroscopy is a non-destructive and highly sensitive method that examines the light emitted by a sample when its electrons, excited by incoming photons, relax back to their ground state, providing insights into the sample's energy levels.

The fluorescence spectra were determined on a Horiba fluorolog fluoroscence spectrometer with excitation wavelength at 330 nm, scan from 350 to 640 nm with a 150 nm/sec of scan speed at the SAIF, M.G University, Kottayam, India, and Fluorescence Quantum yield was measured using Quanta-φ Integrating sphere attached to Fluorolog-3 spectrofluorometer at the CLIF, University of Kerala, India.

The bioimaging study was carried out at the Biovent Innovations, StartUp under KUBIIC, Thiruvananthapuram, India.

1.8.9. Single crystal XRD

Single-crystal X-ray diffraction data of the aroylhydrazone (Hindbh) were collected using a Bruker D8 VENTURE SC-XRD system, employing Mo Kα radiation (λ = 0.71073 Å) at SAIF, IIT Madras, India. Data collection and cell refinement were performed with APEX3, processing and intensity integration were done using SAINT, absorption corrections applied *via* SADABS, and the structure solved and refined by full-matrix least-squares on F^2 using SHELXTL, with hydrogen atoms positioned in calculated geometries.

1.8.10. DNA binding studies

DNA binding studies were carried out on a double beam Shimadzu UV-visible 1900i spectrophotometer at CRMAS Thiruvananthapuram, India.

References

1. Bernhardt, P.V. and Lawrance, G.A., 2025. *Introduction to coordination chemistry*. John Wiley & Sons.

2. Kargar, H., Fallah-Mehrjardi, M. and Munawar, K.S., 2024. Metal complexes incorporating tridentate ONO pyridyl hydrazone Schiff base ligands: Crystal structure, characterization and applications. *Coordination Chemistry Reviews*, *501*, p. 215587.

3. Fallah-Mehrjardi, M., Kargar, H. and Munawar, K.S., 2024. Tridentate ONO hydrazone Schiff base complexes in organic transformations: Catalytic and mechanistic studies. *Inorganica Chimica Acta*, *560*, p. 121835.

4. Keikha, A.O., Shahraki, S., Dehghanian, E. and Mansouri-Torshizi, H., 2025. Effect of the central metal ion on some pharmacological properties of new Schiff base complexes: Anticancer, antioxidant, kinetic/thermodynamic and computational studies. *Spectrochimica Acta Part A: Molecular and Biomolecular Spectroscopy*, *325*, p. 125034.

5. Sogukomerogullari, H.G., Başaran, E., Kepekçi, R.A., Türkmenoğlu, B., Sarıoğlu, A.O. and Köse, M., 2025. Novel europium(III), terbium(III) and gadolinium(III) Schiff base complexes: Synthesis, structural, photoluminescence, antimicrobial, antioxidant and molecular docking studies. *Polyhedron*, *265*, p. 117275.

6. Cao, J., Jia, Z., Chen, W., Song, Y., Yu, Z., Dong, Y. and Ren, Y., 2025. Synthesis, crystal structures, fluorescence properties, theoretical calculations and substitution effect of mono zinc(II) Schiff base complexes. *Inorganica Chimica Acta*, 577, p. 122494.

7. Turan, N., Seymen, H., Gündüz, B., Buldurun, K. and Çolak, N., 2024. Synthesis, characterization of Schiff base and its metal complexes and investigation of their electronic and photonic properties. *Optical Materials*, *148*, p. 114802.

8. Zhu, J.H., He, X., Wu, Y., Huang, H., Yang, D., Li, J., Gu, M., Wang, L., Li, M., Chen, X. and Peng, X., 2025. Cyclometalated Iridium(III) Schiff Base Complexes for Chemiluminogenic Bioprobes. *Angewandte Chemie*, *137*(16), p.e202419856.

9. Reshma, P.R., Tom, L., Dhanya, N.P., Hussan, K.S., Raphael, V.P., Bhagyesh, V.B. and Joseph, B., 2025. Two novel aroyl hydrazones from 4-methoxybenzhydrazide: Comprehensive study including synthesis, X-ray crystallography, DFT analysis, antibacterial activity and molecular docking. *Journal of Molecular Structure*, 1335, p. 141866.

10. Ashraf, T., Maryam, A., Hussain, R., Rani, S., Ali, B., Imran, M., Ashraf, S., Rahim, U. and Sumrra, S.H., 2025. Synthesis, characterization, natural bond orbital and nonlinear optical exploration of Cu(II), Co(II) and Ni(II) complexes derived from hydrazone Schiff base ligands. *Journal of Molecular Structure*, 1323, p. 140804.

11. Çınarlı, M., Ataol, Ç.Y., Zeyrek, C.T., Öğütcü, H., Açık, L. and Batı, H., 2025. Design, synthesis, characterization, theoretical calculations, molecular docking studies and biological evaluation of new Fe(II) and Cu(II) complexes of 2-acetylpyridine derivative sulfonyl hydrazone Schiff base. *Journal of Molecular Structure*, 1321, p. 140112.

12. Gayathri, S., Viswanathamurthi, P., Malecki, J.G., Bhavadharini, A. and Senthilkumar, K., 2025. Copper(I) complexes with heteroaromatic hydrazone ligands: Synthesis, crystal structure and catalytic insights for tetrazole synthesis. *Inorganica Chimica Acta*, 575, p. 122418.

13. Dilek, Ö., Dükel, M., Zarzour, F., Atay, Ç.K. and Tilki, T., 2025. Structure–activity optimization of deferasirox-derived aroyl hydrazones: Synthesis, DFT characterization and mechanistic insights into selective anticancer activity against colon and breast cancer. *Bioorganic Chemistry*, 165, p. 109061.

14. Zülfikaroğlu, A., Çelikoğlu, E. and Çiğil, A.B., 2025. Synthesis and characterization of acrylate-functionalized Cu(II) hydrazone complexes: Antimicrobial performance in UV-cured polyurethane coatings. *Materials Today Communications*, 77, p. 113880.

15. Nishana, L., Sakthivel, A. and Kurup, M.R.P., 2023. Syntheses, structural characterizations and catalytic activities of manganese(II) aroylhydrazone complexes. *Journal of Molecular Structure*, 1281, p. 135128.

16. Kadyan, K., Singh, R., Sindhu, J., Kumar, P., Devi, M., Lal, S., Kumar, A., Singh, D. and Kumar, H., 2025. Exploring the structural versatility and dynamic behavior of acyl/aroyl hydrazones: A comprehensive review. *Topics in Current Chemistry*, 383(2), pp. 1–67.

17. Bashir, M., Dar, A.A. and Yousuf, I., 2023. Syntheses, structural characterization and cytotoxicity assessment of novel Mn(II) and Zn(II) complexes of aroyl-hydrazone Schiff base ligand. *ACS Omega*, 8(3), pp. 3026–3042.

18. Kuriakose, D. and Kurup, M.P., 2020. Synthesis, spectral, structural and antibacterial studies of ONO donor aroylhydrazone and its Mo(VI) complex. *Journal of Molecular Structure*, 1213, p. 128188.

19. Mohan, N., Muthumari, S. and Ramesh, R., 2016. Synthesis, structure and anticancer activity of (η^6-benzene)ruthenium(II) complexes containing aroylhydrazone ligands. *Journal of Organometallic Chemistry*, 807, pp. 45–51.

20. Hegde, G.S., Bhat, S.S., Netalkar, S.P., Hegde, P.L., Kotian, A., Butcher, R.J. and Revankar, V.K., 2021. The Co(II), Ni(II), Cu(II) and Zn(II) complexes of aroylhydrazone of quinolone core: syntheses, characterization and evaluation of antimicrobial and antitubercular activity. *Inorganica Chimica Acta*, *522*, p.120352.

21. Sawkmie, M., Bhattacharyya, M., Banothu, V., Kaminsky, W., Gannon, P.M., Majaw, S. and Kollipara, M.R., 2023. Ruthenium, rhodium, and iridium complexes featuring fluorenyl benzohydrazone derivatives: Synthesis and preliminary investigation of their anticancer and antibacterial activity. *Journal of Molecular Structure*, *1291*, p.135994.

22. Hassan, E.M., Soliman, S.M., Moneer, E.A., Hagar, M., Barakat, A., Haukka, M. and Rasheed, H., 2023. Synthesis, X-ray structure, Hirshfeld, DFT Conformational, cytotoxic, and Anti-toxoplasma studies of New Indole-Hydrazone derivatives. *International Journal of Molecular Sciences*, *24*(17), p.13251.

23. Han, Y., Tian, Y., Wang, R., Fu, S., Jiang, J., Dong, J., Qin, M., Hou, Y. and Zhao, Y., 2020. Design, synthesis and biological evaluation of thieno [3,2-d] pyrimidine derivatives containing aroyl hydrazone or aryl hydrazide moieties for PI3K and mTOR dual inhibition. *Bioorganic Chemistry*, *104*, p.104197.

24. Karabeliov, V.R., Kondeva-Burdina, M.S., Vassilev, N.G., Yovkova, E.K. and Angelova, V.T., 2022. Neuroprotective evaluation of novel substituted 1,3,4-oxadiazole and aroylhydrazone derivatives. *Bioorganic & Medicinal Chemistry Letters*, *59*, p.128516.

25. Hrušková, K., Potůčková, E., Hergeselova, T., Liptakova, L., Hašková, P., Mingas, P., Kovaříková, P., Šimůnek, T. and Vávrová, K., 2016. Aroylhydrazone iron chelators: Tuning antioxidant and antiproliferative properties by hydrazide modifications. *European Journal of Medicinal Chemistry*, 120, pp. 97–110.

26. Żołnowska, B., Sławiński, J., Chojnacki, J., Petreni, A., Supuran, C.T. and Kawiak, A., 2024. Novel benzenesulfonamide-aroylhydrazone conjugates as carbonic anhydrase inhibitors that induce MAPK/ERK-mediated cell cycle arrest and mitochondrial-associated apoptosis in MCF-7 breast cancer cells. *Bioorganic & Medicinal Chemistry*, *114*, p.117958.

27. Al Banna, M.H., Uzzaman, M., Saleh, M.A., Zangrando, E., Howlader, M.B.H., Ansary, M.R.H., Miyatake, R. and Sheikh, M.C., 2024. Ni(II) complexes with in-situ generated N, O-bidentate aroylhydrazone Schiff base ligands: One-pot synthesis, characterization, crystal structure, and in-silico studies. *Journal of Molecular Structure*, *1295*, p.136698.

28. Fousiamol, M.M., Sithambaresan, M., Damodaran, K.K. and Kurup, M.P., 2020. Syntheses, spectral aspects and biological studies of bromide and azide bridged box dimer copper(II) complexes of an NNO donor aroylhydrazone. *Inorganica Chimica Acta*, *501*, p.119301.

29. Li, Y., Qian, C., Li, Y., Yang, Y., Lin, D., Liu, X. and Chen, C., 2021. Syntheses, crystal structures of two Fe(III) Schiff base complexes with chelating o-vanillin aroylhydrazone and exploration of their bio-relevant activities. *Journal of Inorganic Biochemistry*, *218*, p.111405.

30. Dash, S.P., Panda, A.K., Pasayat, S., Dinda, R., Biswas, A., Tiekink, E.R., Mukhopadhyay, S., Bhutia, S.K., Kaminsky, W. and Sinn, E., 2015. Oxidovanadium(V) complexes of aroylhydrazones incorporating heterocycles: Synthesis, characterization and study of DNA binding, photo-induced DNA cleavage and cytotoxic activities. *RSC Advances*, 5(64), pp. 51852–51867.

31. Monika, S. and Ramesh, R., 2023. New dinuclear arene Ru(II) benzilbis(furoylhydrazone) complexes: synthesis, structure, and anticancer activity. *New Journal of Chemistry*, *47*(33), pp.15622-15630.

32. Li, Y., Yang, Z., Zhou, M., Li, Y., He, J., Wang, X. and Lin, Z., 2017. Ni(II) and Co(II) complexes of an asymmetrical aroylhydrazone: Synthesis, molecular structures, DNA binding, protein interaction, radical scavenging and cytotoxic activity. *RSC Advances*, 7(66), pp. 41527–41539.

33. Ramachandran, E., Gandin, V., Bertani, R., Sgarbossa, P., Natarajan, K., Bhuvanesh, N.S., Venzo, A., Zoleo, A., Glisenti, A., Dolmella, A. and Albinati, A., 2018. Synthesis, characterization and cytotoxic activity of novel copper(II) complexes with aroylhydrazone derivatives. *Journal of Inorganic Biochemistry*, 182, pp. 18–28.

34. Mo, Q., Deng, J., Liu, Y., Huang, G., Li, Z., Yu, P., Gou, Y. and Yang, F., 2018. Mixed-ligand Cu(II) hydrazone complexes designed to enhance anticancer activity. *European Journal of Medicinal Chemistry*, 156, pp. 368–380.

35. Johnson, D.K., Murphy, T.B., Rose, N.J., Goodwin, W.H. and Pickart, L., 1982. Cytotoxic chelators and chelates 1. Inhibition of DNA synthesis in cultured rodent and human cells by aroylhydrazones and by a copper(II) complex of salicylaldehyde benzoyl hydrazone. *Inorganica Chimica Acta*, *67*, pp.159-165.

36. Pan, L., Wang, C., Yan, K., Zhao, K., Sheng, G., Zhu, H., Zhao, X., Qu, D., Niu, F. and You, Z., 2016. Synthesis, structures and *Helicobacter pylori* urease inhibitory activity of copper(II) complexes with tridentate aroylhydrazone ligands. *Journal of Inorganic Biochemistry*, 159, pp. 22–28.

37. Mathews, N.A., Jose, A. and Kurup, M.P., 2019. Synthesis and characterization of a new aroylhydrazone ligand and its cobalt(III) complexes: X-ray crystallography and in vitro antibacterial and antifungal activities. *Journal of Molecular Structure*, 1178, pp. 544–553.

38. Hou, L., Jia, X., Wu, Y., Li, J., Yao, D., Gou, Y. and Huang, G., 2021. Aroylhydrazone Cu(II) complexes: Syntheses, crystal structures and anticancer properties. *Journal of Molecular Structure*, 1239, p. 130469.

39. Sahu, G., Banerjee, A., Samanta, R., Mohanty, M., Lima, S., Tiekink, E.R. and Dinda, R., 2021. Water-soluble dioxidovanadium(V) complexes of aroylhydrazones: DNA/BSA interactions, hydrophobicity and cell-selective anticancer potential. *Inorganic Chemistry*, 60(20), pp. 15291–15309.

40. Vignesh, A., Binoy, A., Thurakkal, L., Bhuvanesh, N.S., Sadhukhan, S. and Porel, M., 2024. Pyrene aroylhydrazone-based Pd(II) complexes for DNA/protein binding, cellular imaging and in vitro anticancer activity via ROS production. *Journal of Molecular Structure*, 1295, p. 136693.

41. Wang, L., Li, Y., Zheng, C., Liao, G. and Pu, S., 2021. An aroylhydrazone-containing diarylethene derivative derived chemosensor for colorimetric and fluorimetric dual sensing of Cu^{2+}. *Journal of Photochemistry and Photobiology A: Chemistry*, 409, p. 113128.

42. Borbone, F., Caruso, U., Concilio, S., Nabha, S., Piotto, S., Shikler, R., Tuzi, A. and Panunzi, B., 2017. From cadmium(II)-aroylhydrazone complexes to metallopolymers with enhanced photoluminescence: A structural and DFT study. *Inorganica Chimica Acta*, 458, pp. 129–137.

43. Chakraborty, M., Mondal, A., Ghosh, A., Mahapatra, A., Mondal, T.K. and Chattopadhyay, S.K., 2025. Synthesis, crystal structure and sulphide ion sensing study of a Cu(II) complex of aroylhydrazone. *Polyhedron*, 265, p. 117294.

44. Dwivedi, R., Singh, S., Chauhan, B.S., Srikrishna, S., Panday, A.K., Choudhury, L.H. and Singh, V.P., 2020. Aroylhydrazone with large Stokes shift as a fluorescent probe for detection of Cu^{2+} in pure aqueous medium and in vivo studies. *Journal of Photochemistry and Photobiology A: Chemistry*, 395, p. 112501.

45. Zhang, Z.H., Zhang, Y.M., Kan, X.T., Yang, Q.Y., Li, Y.J., Wei, T.B., Yao, H. and Lin, Q., 2021. Tripodal aroylhydrazone-based AIE fluorescent sensor for relay detection of Hg^{2+} and Br^{-} in living cells. *Dyes and Pigments*, 191, p. 109389.

46. Diana, R., Panunzi, B., Tuzi, A. and Caruso, U., 2019. Two tridentate pyridinyl-hydrazone zinc(II) complexes as fluorophores for blue-emitting layers. *Journal of Molecular Structure*, 1197, pp. 672–680.

47. Dongare, G. and Aswar, A., 2024. New aroyl heterocyclic (E)-N′-((2-hydroxynaphthalen-1-yl)methylene)-4-oxopiperidine-1-carbohydrazide and its metal complexes: Synthesis, spectroscopic, thermal, DFT, molecular docking and antimicrobial studies. *Research on Chemical Intermediates*, 50(2), pp. 745–788.

48. Zhao, J., Wang, Y.Y., Chen, W.L., Hao, G.S., Sun, J.P., Shi, Q.F., Tian, F. and Ma, R.T., 2022. A salicylaldehyde benzoyl hydrazone based near-infrared probe for copper(II) and its bioimaging applications. *RSC advances*, *12*(5), pp.3073-3080.

49. Rupa, S.A., Patwary, M.A.M., Ghann, W.E., Abdullahi, A., Uddin, A.R., Mahmud, M.M., Haque, M.A., Uddin, J. and Kazi, M., 2023. Synthesis of a novel hydrazone-based compound applied as a fluorescence turn-on chemosensor for iron(III) and a colorimetric sensor for copper(II): Antimicrobial, DFT and molecular docking studies. *RSC Advances*, 13(34), pp. 23819–23828.

50. Patra, S.A., Sahu, G., Pattanayak, P.D., Sasamori, T. and Dinda, R., 2022. Mitochondria-targeted luminescent organotin(IV) complexes: Synthesis, photophysical characterization and live cell imaging. *Inorganic Chemistry*, 61(42), pp. 16914–16928.

51. Jakupec, M.A., Unfried, P. and Keppler, B.K., 2005. Pharmacological properties of cerium compounds. *Reviews of Physiology, Biochemistry and Pharmacology*, pp. 101–111.

52. Taha, R.H., Saleh, A.M., Abbass, L.M., El-Fakharany, E.M., Almutlq, N.J., Hussein, M.F. and Moustafa, S.M., 2025. Impact of Fe(III) and Ce(III) ions on pharmacological properties of a novel Schiff base ligand: Anticancer, antiviral, antioxidant, antifungal investigations and computational insights. *Journal of Molecular Liquids*, 427, p. 127382.

53. Saad, H.E., El-Reash, G.M.A., Gaber, M., Hashem, M.A., El-Reash, Y.G.A., Elamin, N.Y., Elamin, M.R. and El-Sayed, Y.S., 2024. A novel isatin Schiff base cerium complex: Synthesis, characterization, antimicrobial activity and molecular docking studies. *BMC Genomics*, 25(1), p. 162.

54. Yin, H., Carroll, P.J., Anna, J.M. and Schelter, E.J., 2015. Luminescent Ce(III) complexes as stoichiometric and catalytic photoreductants for halogen atom abstraction reactions. *Journal of the American Chemical Society*, 137(29), pp. 9234–9237.

55. Qiao, Y., Sergentu, D.C., Yin, H., Zabula, A.V., Cheisson, T., McSkimming, A., Manor, B.C., Carroll, P.J., Anna, J.M., Autschbach, J. and Schelter, E.J., 2018. Understanding and controlling the emission brightness and color of molecular cerium luminophores. *Journal of the American Chemical Society*, 140(13), pp. 4588–4595.

56. Wang, L., Zhao, Z., Zhan, G., Fang, H., Yang, H., Huang, T., Zhang, Y., Jiang, N., Duan, L., Liu, Z. and Bian, Z., 2020. Deep-blue organic light-emitting diodes based on a doublet *d–f* transition cerium(III) complex with 100% exciton utilization efficiency. *Light: Science & Applications*, 9(1), p. 157.

57. Wang, X., Liu, Y., Li, Z., Li, Z., Ren, A., Wang, S. and Wu, B., 2025. A Schiff base–Ce^{3+} complex as a high-efficiency corrosion inhibitor for 2024 aluminum alloy in high-temperature concentrated HCl. *Surface and Interface Analysis*, 57(10), pp. 763–774.

58. Kumar, R. and Mishra, S.K., 2022. Luminescence and photodetection characteristics of rare earth–doped zinc oxide nanostructures. In: *Ceramic Science and Engineering*. Elsevier, pp. 263–294.

59. Gupta, I., Singh, S., Bhagwan, S. and Singh, D., 2021. Rare earth (RE)-doped phosphors and their emerging applications: A review. *Ceramics International*, 47(14), pp. 19282–19303.

60. Yin, Y., Luo, R., Wang, W., Wang, R., Jiang, N., Chen, P., Yu, H.J., Bi, S.Y. and Shao, F., 2024. A dysprosium(III)-based triple helical-like complex as a turn-on/off fluorescence sensor for Al(III) and 4,5-dimethyl-2-nitroaniline. *Dalton Transactions*, 53(12), pp. 5544–5552.

61. Al-As'ad, R.M., Abu-Yamin, A.A., Korb, M., Al Khalyfeh, K., Elayan, I.A., Almatarneh, M.H., Juwhari, H.K., Amarne, H., Taher, D., Ishtaiwi, Z. and Lang, H., 2023. Synthesis, characterization, crystal structure and DFT calculations of a dysprosium(III) (E)-ethyl-4-(2-hydroxybenzylideneamino)benzoate complex. *Journal of Molecular Structure*, 1280, p. 135061.

62. Berezhnytska, O.S., Savchenko, I.O., Horbenko, A.E., Rohovtsov, O.O., Rusakova, N.V. and Trunova, O.K., 2023. Synthesis and luminescence properties of Dy(III) complexes and metallopolymers: Influence of substituent nature on emission. *Journal of Molecular Structure*, 1293, p. 136148.

63. Malik, S., Jakhar, K., Singh, D., Hooda, A., Redhu, S., Dalal, S., Aggarwal, V., Kumar, S., Malik, R.S. and Kumar, P., 2024. Optimizing white light emission in Dy(III) complexes: Impact of energy transfer from mono- and bidentate ligands on luminescence. *RSC Advances*, 14(31), pp. 22642–22655.

64. Tilehkan, A. and Arvand, M., 2025. Dysprosium complex with 1,10-phenanthroline-5,6-dione: Synthesis, structure, DNA-binding profile and in vitro cytotoxic evaluation against HT29 cancer cell lines. *Polyhedron*, 267, p. 117367.

65. Dua, N., Punia, M. and Doon, P.B., 2025. Structural and photometric study of cool white light-emitting Dy(III) complexes sensitized with *β*-diketone for lighting applications. *Journal of Fluorescence*, 35(6), pp. 4849–4860.

66. Nasiri-Tabrizi, B., Basirun, W.J., Yeong, C.H. and Thein, W.M., 2023. Development of the third generation of bioceramics: Doping hydroxyapatite with *s*-, *p*-, *d*- and *f*-block cations and their potential applications in bone regeneration and void filling. *Ceramics International*, 49(5), pp. 7142–7179.

67. Voncken, J.H.L., 2016. *The rare earth elements: An introduction*. Cham: Springer International Publishing.

68. Sheikh, A.H., Khalid, A., Khan, F. and Begum, A., 2019. Fluorescent gadolinium(III)–oligopeptide complexes and carbon nanotube composite as dual modality anticancer agents. *ChemistrySelect*, 4(1), pp. 228–235.

69. Vijayaraj, A., Prabu, R., Suresh, R., Kumari, R.S., Kaviyarasan, V., Narayanan, V., Tamizhdurai, P., Mangesh, V.L., Alasmary, F.A., Rajaji, U. and Govindasamy, M., 2023. DNA binding, cleavage, catalytic and magnetic activity of 2,2′-bipyridyl-based heterobinuclear Gd(III), Cu(II) complexes and their electrochemical and fluorescence studies. *Arabian Journal of Chemistry*, 16(5), p. 104656.

70. Wang, W.M., Gao, Y., Yue, R.X., Qiao, N., Wang, D.T., Shi, Y., Zhang, H. and Cui, J.Z., 2020. Construction of a family of Ln_3 clusters using multidentate Schiff base and *β*-diketonate ligands: Fluorescence properties, magnetocaloric effect and slow magnetic relaxation. *New Journal of Chemistry*, 44(22), pp. 9230–9237.

71. Ganjali, M.R., Emami, M., Rezapour, M., Shamsipur, M., Maddah, B., Salavati-Niasari, M., Hosseini, M. and Talebpoui, Z., 2003. Novel gadolinium poly(vinyl chloride) membrane sensor based on a new S–N Schiff base. *Analytica Chimica Acta*, 495(1–2), pp. 51–59.

72. Kaczmarek, M.T., Jastrząb, R., Kubicki, M., Gierszewski, M. and Sikorski, M., 2015. Supramolecular polymer of a Schiff base gadolinium complex: Synthesis, crystal structure and spectroscopic properties. *Inorganica Chimica Acta*, 430, pp. 108–113.

73. Shi, Y., Pan, Y., Zhong, J., Yang, J., Zheng, J., Cheng, J., Song, R. and Yi, C., 2015. Facile synthesis of gadolinium(III) chelate-functionalized carbon quantum dots for fluorescence and magnetic resonance dual-modal bioimaging. *Carbon*, 93, pp. 742–750.

CHAPTER 2

SYNTHESIS AND SPECTRAL CHARACTERIZATION OF THE AROYLHYDRAZONES: SALICYLALDEHYDE BENZOYLHYDRAZONE, SALICYLALDEHYDE NICOTINOYLHYDRAZONE AND INDOLE-3-CARBALDEHYDE BENZOYLHYDRAZONE

2.1. Introduction

Hydrazones are a promising class of organic compounds formed by the condensation of a ketone or aldehyde with hydrazine or its derivatives in acidic conditions. The presence of the (—CO—NH—N=CH—) group imparts exceptional properties to the aroylhydrazones [1-3]. They are extensively studied in various fields of science. In aroylhydrazones, the donor sites present are the amide oxygen, imine nitrogen, and the oxygen atom in the carbonyl compounds. The architectural beauty of the aroylhydrazones routes from this multiple donor sites. The ease of synthesis, strong coordination ability, and outstanding structural versatility are some of the key features that attract researchers to the synthesis of aroylhydrazones. They form fascinating compounds with transition as well as inner transition metal ions. In recent years, the complexes of inner transition metal ions have gained considerable attention among researchers owing to their wide variety of potential applications [4-8].

Aroylhydrazones have a prominent role in the field of photoluminescence. They are endowed by the efficiency of harvesting the light energy, and they transfer it to the corresponding trivalent metal ions. The ability of aroylhydrazones, to act as chelating antennas, sensitizes the luminescence of lanthanide ions. Additionally, they possess a strong ability to shield lanthanide ions from solvent molecules that lead to non-radiative transitions and thereby quench fluorescence [9-11].

Aroylhydrazones are also known for their numerous biological applications including anticancer, antibacterial, antimicrobial, antifungal, anticonvulsant, antimalarial, and anti-inflammatory properties [12-14]. One of the major biological activities of aroylhydrazones is DNA binding [15]. DNA is the primary intracellular pharmacological target of anticancer drugs. Aroylhydrazones have strong efficiency to bind with the DNA molecules. The conjugated pi systems, along with the rigid molecular structure of aroylhydrazones, are the key factors that are leading to stronger interactions with DNA molecules [16-19].

Based on these considerations, we have synthesized three aroylhydrazones salicylaldehyde benzoylhydrazone, salicylaldehyde nicotinoylhydrazone and indole-3-carbaldehyde benzoylhydrazone.

2.2. Materials and Methods

Benzhydrazide, nicotinic hydrazide, indole-3-carbaldehyde and salicylaldehyde were purchased from Sigma Aldrich and were used without further purification. The solvents, methanol, acetic acid and N,N-dimethylformamide (DMF), were procured from Merck. All the chemicals utilized were of analar grade and were used as received.

2.2.1. Synthesis of aroylhydrazones

2.2.1.1. Synthesis of salicylaldehyde benzoylhydrazone (H_2salbh)

To the methanolic solution (10 mL) of benzhydrazide (0.136 g, 1 mmol), salicylaldehyde (0.122 g, 1 mmol) in methanol (10 mL) was added, followed by two drops of acetic acid and refluxed for 3 h. Dark

yellow crystals of H_2salbh were separated and filtered off, washed with methanol, and then dried in air. The corresponding synthesis procedure is presented in Scheme 2.1. Yield: (0.2402 g) 76.3%. Melting point: 172°C. Elemental Anal. Found (Calcd) %: C: 69.41 (69.99); H: 4.82 (5.03); N: 11.91 (11.66) for $C_{14}H_{12}N_2O_2$. ^{1}H NMR (CH_3OD, ppm): δ 8.54 (1H, s).

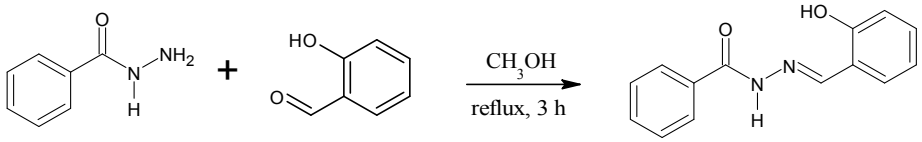

Scheme 2.1. Synthesis of H_2salbh

2.2.1.2. Synthesis of salicylaldehyde nicotinoylhydrazone (H_2salnh)

The method of synthesis of H_2salnh was similar to that of H_2salbh, except that benzhydrazide was replaced by nicotinic hydrazide (0.137 g, 1 mmol). Pale yellow crystals of H_2salnh were washed with methanol, followed by ether and then dried in air. The corresponding synthesis procedure is presented in Scheme 2.2. Yield: (0.2402 g) 82.3%. Melting point: 163°C. Elemental Anal. Found (Calcd) %: C: 65.15 (64.72); H: 4.12 (4.60); N: 17.33 (17.42) for $C_{13}H_{11}N_3O_2$.^{1}H NMR (CH_3OD, ppm): δ 8.56 (1H, s).

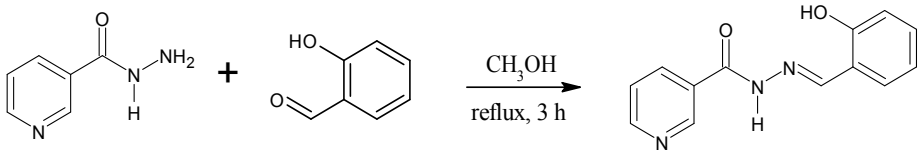

Scheme 2.2. Synthesis of H_2salnh

2.2.1.3. Synthesis of indole-3-carbaldehyde benzoylhydrazone (Hindbh)

A solution of benzhydrazide (0.136 g, 1 mmol) in methanol (10 mL) was mixed with indole-3-carbaldehyde (0.145 g, 1 mmol)

dissolved in methanol (10 mL). To the resulting mixture, two drops of glacial acetic acid were added. The reaction mixture was refluxed in water bath for 3 hours. Pale yellow crystals of Hindbh were separated and filtered off, washed with methanol, and dried in air. The corresponding synthesis procedure is illustrated in Scheme 2.3. Yield: (0.2633 g) 86.5%. Melting point: 192°C. Elemental Anal. Found (Calcd) %: C: 72.99 (73.51); H: 4.98 (5.25); N: 15.96 (16.03) for $C_{16}H_{13}N_3O$. ^{1}H NMR (CH_3OD, ppm): δ 8.60 (1H, s).

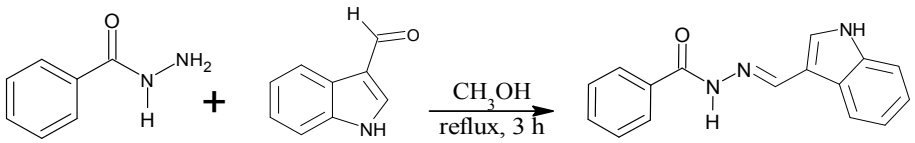

Scheme 2.3. Synthesis of Hindbh

2.3. Results and Discussion

2.3.1. Characterizations of aroylhydrazones

The aroylhydrazones, H_2salbh, H_2salnh and Hindbh were characterized by partial elemental analysis, ESI-MS, FT-IR, UV-vis and ^{1}H NMR spectroscopy. The molecular structure of Hindbh was obtained from single-crystal XRD studies.

2.3.1.1. Partial elemental analysis

The elemental analysis (C, H, and N) and analytical data of aroylhydrazones are shown in Table 2.1. They closely match the empirical formula.

Table 2.1. The compositional details of aroylhydrazones

Compound	Empirical formula	Formula Weight (g/mol)	Colour (Yield %)	Melting point (°C)	Found (Calcd %)		
					C	H	N
H_2salbh	$C_{14}H_{12}N_2O_2$	240.25	Dark yellow (76.3)	172	69.41 (69.99)	4.82 (5.03)	11.91 (11.66)
H_2salnh	$C_{13}H_{11}N_3O_2$	241.24	Pale yellow (82.3)	163	65.15 (64.72)	4.12 (4.60)	17.33 (17.42)
Hindbh	$C_{16}H_{13}N_3O$	263.29	Pale yellow (86.5)	192	72.99 (73.51)	4.98 (5.25)	15.96 (16.03)

2.3.1.2. Mass spectrometry

Mass spectra of the aroylhydrazones were examined using LC-QTOF-HRMS, a highly reliable analytical technique for the structural elucidation of unknown compounds [20-22]. Here, the chromatographic techniques are coupled with mass spectrometry.

The expected molecular ion peaks of the two aroylhydrazones were obtained at *m/z* 241.100 $[M+1]^+$ for H_2salbh, and *m/z* 242.05 $[M+1]^+$ for H_2salnh. This confirms the structure and purity of the synthesized aroylhydrazones. The mass spectra of the aroylhydrazones are given in Figs. 2.1 and 2.2.

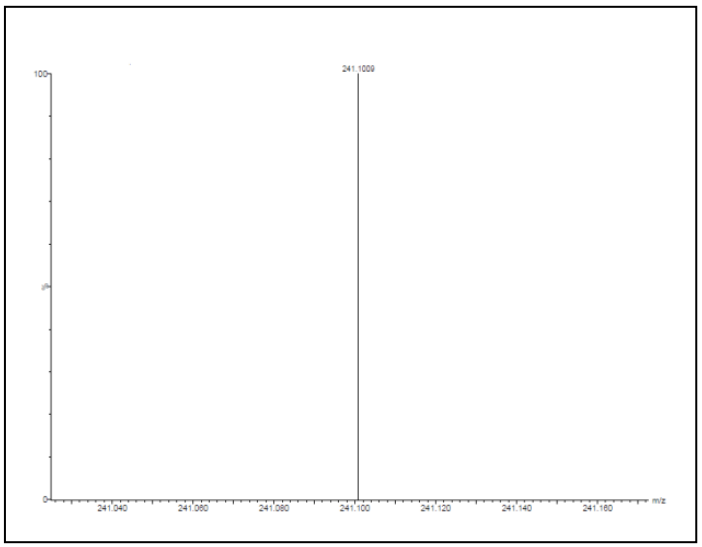

Fig. 2.1. ESI-MS spectrum of H_2salbh

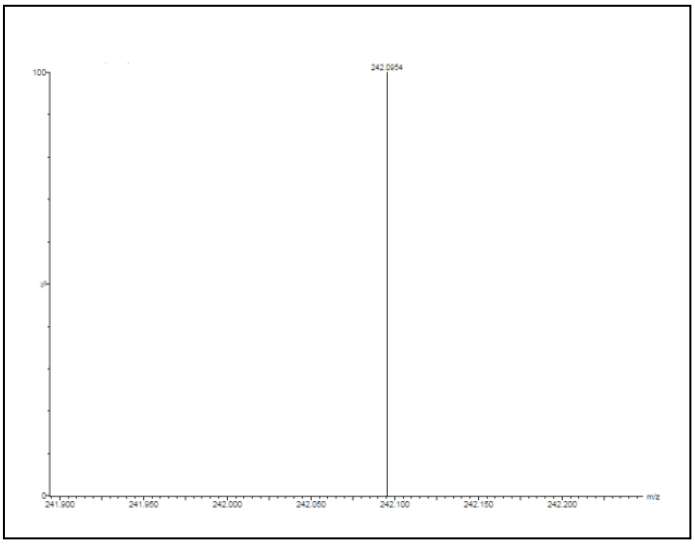

Fig. 2.2. ESI-MS spectrum of H_2salnh

2.3.1.3. FT-IR spectroscopy

The FT-IR spectroscopy is a powerful tool to identify the functional groups present in an organic compound. The characteristic IR bands of the aroylhydrazones, H_2salbh, H_2salnh, and Hindbh, displayed a strong band in the region 3270, 3194, and 3231 cm^{-1}, attributing to the stretching vibrations of the ν(N–H) group. The bands corresponding to the azomethine (C=N) group formed by the condensation of hydrazide and aldehyde are also verified by the IR spectroscopy [23]. For H_2salbh, the ν(C=N) band was seen at 1622 cm^{-1}, for H_2salnh at 1585 cm^{-1}, and for Hindbh at 1596 cm^{-1}. A broad stretching vibration band of the phenolic O–H group is observed at 3505 and 3501 cm^{-1} in H_2salbh and H_2salnh, respectively [24]. In contrast, this band is absent in the IR spectrum of Hindbh, consistent with the absence of a phenolic hydroxyl group in its molecular framework. Furthermore, another prominent band was observed at

1677 and 1700 cm^{-1} for H_2salbh and H_2salnh, respectively, while Hindbh showed this band at 1635 cm^{-1}. This can be attributed to the ν(C=O) stretching vibrational frequencies. IR spectra of the aroylhydrazones are shown in Figs. 2.3 to 2.5. Also, the stretching frequencies of some important functionalities of the aroylhydrazones are listed in Table 2.2.

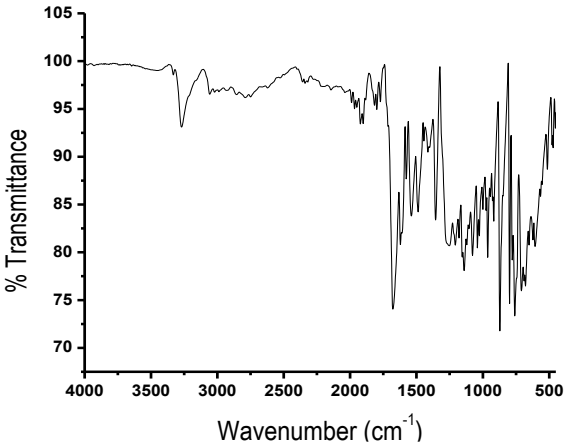

Fig. 2.3. FT-IR spectrum of H_2salbh

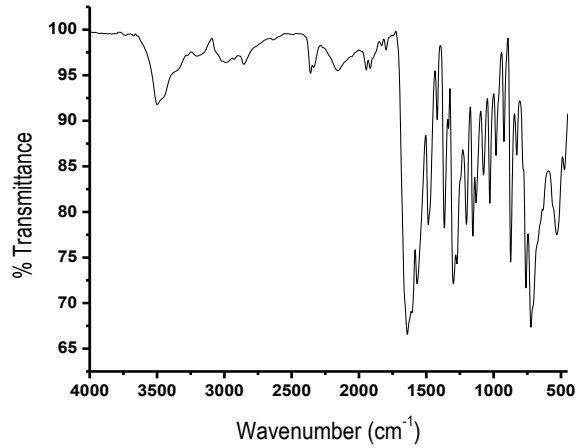

Fig. 2.4. FT-IR spectrum of H_2salnh

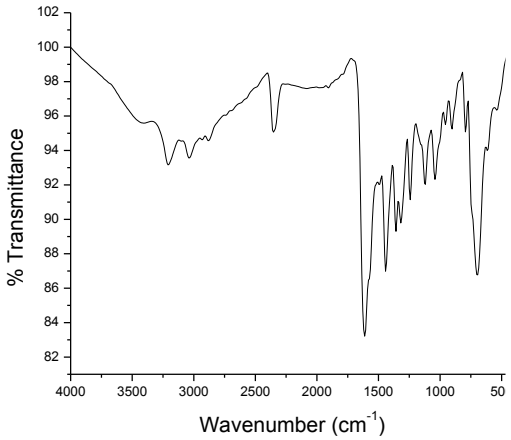

Fig. 2.5. FT-IR spectrum of Hindbh

Table 2.2. FT-IR spectral data of aroylhydrazones

Compound	*ν*(O–H) cm^{-1}	*ν*(N–H) cm^{-1}	*ν*(C=O) cm^{-1}	*ν*(C=N) cm^{-1}
H_2salbh	3505	3270	1677	1622
H_2salnh	3501	3194	1700	1585
Hindbh	------	3231	1635	1596

2.3.1.4. Electronic spectroscopy

The UV-vis absorption spectra of the hydrazones, H_2salbh, H_2salnh and Hindbh were recorded in DMF (10^{-5} M) solution in the range of 200 to 800 nm. The UV-vis spectra of H_2salbh and H_2salnh resembled each other, probably due to their structural similarity. The hydrazone, H_2salbh, exhibited three absorption bands at 299, 310 and 330 nm. Similarly, the UV-vis spectrum of H_2salnh also comprises three absorption bands at 300, 310 and 332 nm [25]. Likewise, the hydrazone, Hindbh, displayed absorption bands at 302, 315, and 330

nm. The high energy bands observed at 299 to 310 nm region, clearly represent the $\pi \rightarrow \pi^*$ transitions in the aroylhydrazones. Furthermore, the low energy bands seen at 332 and 337 nm are due to the $n \rightarrow \pi^*$ transitions. These intra-ligand transitions of the $\pi \rightarrow \pi^*$ type arise from the aromatic ring, and $n \rightarrow \pi^*$ transitions from the azomethine and keto groups [20]. The spectral assignments of the aroylhydrazones are given in Table 2.3, and their corresponding spectra are presented in Figs. 2.6 to 2.8.

Table 2.3. UV-visible spectral data of aroylhydrazones in DMF (10^{-5} M)

Compound	Electronic spectral bands, λ_{max} (nm)	Assignment
H_2salbh	299, 310, 337	$\pi \rightarrow \pi^*$, $n \rightarrow \pi^*$
H_2salnh	300, 310, 332	$\pi \rightarrow \pi^*$, $n \rightarrow \pi^*$
Hindbh	302, 315, 330	$\pi \rightarrow \pi^*$, $n \rightarrow \pi^*$

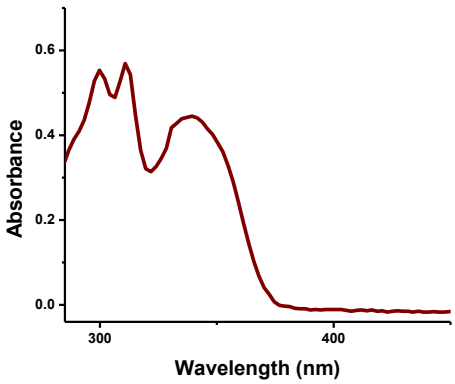

Fig. 2.6. UV-visible spectrum of H_2salbh

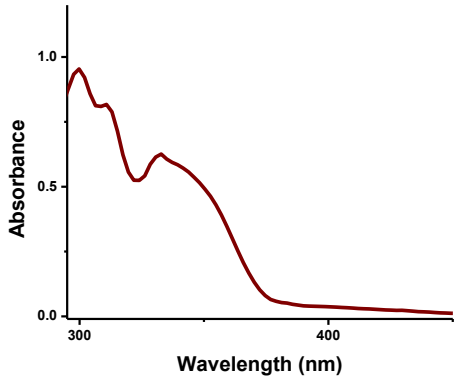

Fig. 2.7. UV-visible spectrum of H_2salnh

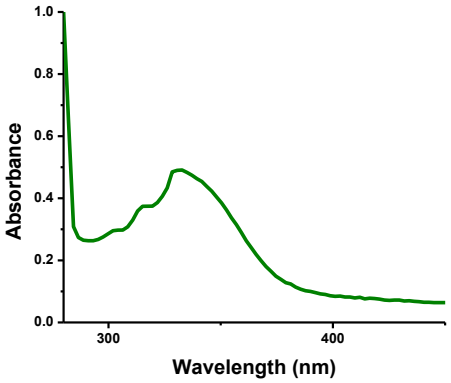

Fig. 2.8. UV-visible spectrum of Hindbh

2.3.1.5. Crystal structure of Hindbh

Single crystals of the aroylhydrazone, Hindbh, suitable for X-ray diffraction studies were isolated from mother liquor itself. The compound crystallizes in the orthorhombic crystal system with space group *Pbca*, consistent with the structure reported previously in the literature [26]. The unit cell parameters are a = 17.464(5) Å, b = 7.738(2) Å, c = 20.167(5) Å, with $\alpha = \beta = \gamma = 90°$, confirming the orthorhombic symmetry. The asymmetric unit contains one molecule, with Z = 8 in the unit cell. The molecular formula $C_{16}H_{13}N_3O$

corresponds to a formula weight of 263.29 g/mol, and the calculated density is 1.283 g/cm^3. The molecular structure of $C_{16}H_{13}N_3O$ is shown in Fig. 2.9 and selected geometric parameters are listed in Table 2.4.

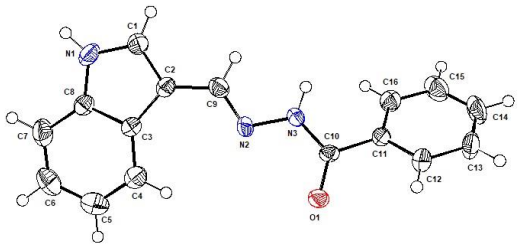

Fig. 2.9. Structure and labeling diagram for Hindbh

The compound features a hydrazone functional group, formed by the condensation of benzhydrazide and indole-3-carbaldehyde, as evidenced by characteristic bond distances. The N(1)–C(1) and N(1)–C(8) bond lengths are 1.355(5) Å and 1.372(5) Å, respectively, consistent with typical C–N single bond distances. The N(2)–N(3) bond length of 1.390(4) Å and the N(3)–C(10) bond length of 1.332(5) Å, along with the adjacent C(10)–O(1) bond of 1.246(5) Å, confirm the presence of a –CONH– linkage.

The aromatic rings in the structure are largely planar with torsion angles close to 0° or 180°, suggesting extended π-conjugation across the system. For example, the torsion angle N(1)–C(1)–C(2)–C(9) is 177.6(4)°, and C(6)–C(7)–C(8)–N(1) is 177.5(5)°, indicating that the fused ring system and substituents are mostly coplanar. The molecular packing is stabilized by intermolecular hydrogen bonding interactions. Two significant hydrogen bonds are observed: N(1)–H(1A)...O(1) and N(3)–H(3)...O(1). An analysis of the bond lengths

and angles (Table 2.5) confirms the aromatic and amide character of the molecule. The internal bond angles at the nitrogen centres, such as C(1)–N(1)–C(8) at 109.2(4)°, and N(2)–N(3)–C(10) at 122.1(3)°, are consistent with sp^2 hybridization, typical for conjugated amide systems.

Table 2.4. Crystal data and structure refinement for Hindbh

Empirical formula	$C_{16}H_{13}N_3O$
Formula weight	263.29
Temperature	298(2) K
Wavelength	0.71073 Å
Crystal system, space group	Orthorhombic, *Pbca*
Unit cell dimensions	*a* = 17.464(5) Å alpha = 90 deg. *b* = 7.738(2) Å beta = 90 deg. *c* = 20.167(5) Å gamma = 90 deg.
Volume	2725.3(13) A^3
Z, Calculated density	8, 1.283 Mg/m^3
Absorption coefficient	0.083 mm^{-1}
F(000)	1104
Crystal size	0.302 x 0.115 x 0.032 mm
Theta range for data collection	3.518 to 20.837 deg.
Limiting indices	-17<=*h*<=17 -7<=*k*<=7 -20<=*l*<=20
Reflections collected / unique	36750 / 1425 [R(int) = 0.2055]
Completeness to theta = 20.837	99.7 %
Absorption correction	Semi-empirical from equivalents
Max. and min. transmission	0.7446 and 0.4958
Refinement method	Full-matrix least-squares on F^2
Data / restraints / parameters	1425 / 0 / 182
Goodness-of-fit on F^2	1.248
Final R indices [I>2sigma(I)]	R1 = 0.0691, wR2 = 0.1479
R indices (all data)	R1 = 0.0880, wR2 = 0.1564
Extinction coefficient	0.012(2)
Largest diff. peak and hole	0.212 and -0.206 $e.A^{-3}$

Table 2.5. Selected bond lengths [Å] and angles [º] for Hindbh

Bond lengths		**Bond angles**	
C(1)-C(2)	1.372(6)	N(1)-C(1)-C(2)	110.6(4)
C(2)-C(9)	1.433(6)	N(1)-C(8)-C(7)	130.5(4)
C(2)-C(3)	1.438(6)	N(2)-C(9)-C(2)	123.9(4)
C(3)-C(8)	1.411(6)	O(1)-C(10)-N(3)	123.5(4)
C(8)-N(1)	1.372(5)	N(3)-C(10)-C(11)	115.2(3)
C(9)-N(2)	1.280(5)	C(1)-N(1)-C(8)	109.2(4)
C(10)-O(1)	1.246(5)	C(9)-N(2)-N(3)	112.9(3)
C(10)-N(3)	1.332(5)	C(10)-N(3)-N(2)	122.1(3)
N(2)-N(3)	1.390(4)	N(2)-N(3)-H(3)	118.9

2.3.1.6. NMR spectroscopy

To further confirm the structure of aroylhydrazones, NMR spectral studies were carried out. The ^{1}H NMR spectra of the aroylhydrazones were measured in CH_3OD with tetramethylsilane (TMS) as the internal standard. The presence of a singlet at δ 8.54 ppm in H_2salbh, 8.56 ppm in H_2salnh, and 8.60 ppm in Hindbh in the downfield region of the spectrum can be attributed to the azomethine (–C=N–) protons. This observation clearly confirms the formation of aroylhydrazones through the condensation of the aldehyde moiety and the corresponding hydrazide [27]. The signals corresponding to the NH and phenolic OH protons of the aroylhydrazones were not observed, likely due to rapid exchange with the solvent. Furthermore, the appearance of the characteristic NMR signals of both hydrazones at nearly the same position of the spectrum may be due to the structural similarity of both hydrazones. The remaining doublets and multiplets observed in the region 6.9-7.6 ppm are due to the aromatic protons [28]. The ^{1}H NMR spectra of aroylhydrazones are presented in Figs. 2.10 to 2.12.

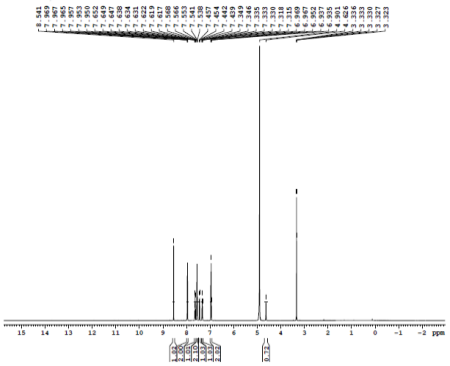

Fig. 2.10. ^{1}H NMR spectrum of H_2salbh

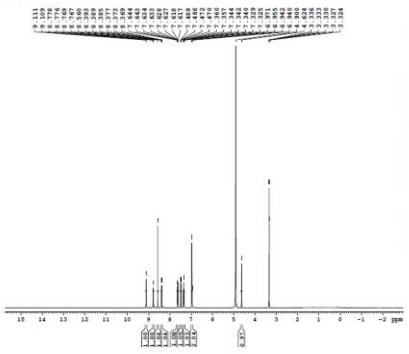

Fig. 2.11. ^{1}H NMR spectrum of H_2salnh

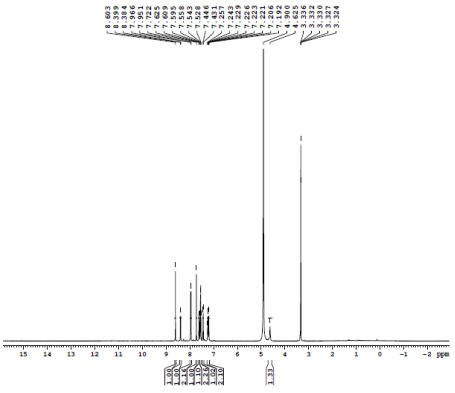

Fig. 2.12. ^{1}H NMR spectrum of Hindbh

2.4. Conclusion

The synthesis, experimental methods, and characterization of the aroylhydrazones, salicylaldeyde benzoylhydrazone (H_2salbh), salicylaldeyde nicotinoylhydrazone (H_2salnh), and indole-3-carbaldehyde benzoylhydrazone (Hindbh) are emphasized in chapter 2. The aroylhydrazones syntheised were characterized by partial elemental analysis, mass spectrometry and spectroscopic techniques such as, FT-IR, UV-vis and ^{1}H NMR spectroscopy. The molecular structure of Hindbh was obtained from single-crystal XRD studies.

Partial elemental analysis data are consistent with the theoretical values, confirming the purity and stoichiometry of the synthesized compounds. The ESI mass spectra exhibited the expected $[M+1]^+$ molecular ion peaks, providing further evidence of the molecular identity of the ligands. FT-IR spectral analysis showed absorption bands for ν(N–H), ν(C=N), ν(C=O), and ν(O–H) stretching vibrations, supporting the formation of the hydrazone framework. Notably, the absence of the phenolic O–H stretching band in the IR spectrum of Hindbh is consistent with its structural composition lacking a phenolic group.

UV-visible spectroscopic studies carried out in DMF demonstrated typical $\pi\rightarrow\pi^*$ and $n\rightarrow\pi^*$ transitions, arising from the aromatic and heteroatomic functional groups present in the ligands. The similarity in spectral features among the compounds can be attributed to their comparable structural motifs. The $\pi\rightarrow\pi^*$ transitions were observed in the higher energy region (299–315 nm), while the

lower energy bands (330–337 nm) were attributed to $n \rightarrow \pi^*$ transitions associated with the azomethine and carbonyl functionalities. These transitions are indicative of the extended conjugation present in the aroylhydrazone system.

The ^{1}H NMR spectral data further substantiated the formation of the hydrazone linkages, with characteristic singlets observed for the azomethine protons. The similarity in the chemical shifts among the hydrazones reflects their structural resemblance and confirms the expected proton environments. The structural information of the aroylhydrazones were obtained from these studies. Furthermore, these studies reveal that the aroylhydrazones mainly ocur in the keto form rather than the enol form.

References

1. Rajmohan, G., Shanmugam, R., Elangovan, A., Sankaranarayanan, R.K., Ravindran, G., Dineshkumar, P. and Arivazhagan, G., 2022. Synthesis, characterization and topological properties of new hydrazone derivatives. *Journal of Molecular Structure*, 1251, p. 132028.

2. Chakraborty, M., Mondal, A., Ghosh, A., Mahapatra, A., Mondal, T.K. and Chattopadhyay, S.K., 2025. Synthesis, crystal structure and sulphide ion sensing study of a Cu(II) complex of aroylhydrazone. *Polyhedron*, 265, p. 117294.

3. Bashir, M., Dar, A.A. and Yousuf, I., 2023. Syntheses, structural characterization and cytotoxicity assessment of novel Mn(II) and Zn(II) complexes of an aroylhydrazone Schiff base ligand. *ACS Omega*, 8(3), pp. 3026–3042.

4. Nishana, L., Sakthivel, A. and Kurup, M.R.P., 2023. Syntheses, structural characterizations and catalytic activities of manganese(II) aroylhydrazone complexes. *Journal of Molecular Structure*, 1281, p. 135128.

5. Özbek, F.E.Ö., Uğurlu, G., Kalay, E., Necefoğlu, H. and Hökelek, T., 2021. Theoretical and experimental assessment of structural, spectroscopic, electronic and nonlinear optical properties of two aroylhydrazone derivatives. *Journal of Molecular Structure*, 1223, p. 128982.

6. Aravindakshan, A.A., Mohan, N., Kurup, M.P., Erkan, S., Kaya, S. and Manoj, E., 2024. Mononuclear and binuclear dioxidomolybdenum(VI) chelates derived from a tridentate ONO donor aroylhydrazone: Spectral, structural, DFT and in silico biological investigations. *Polyhedron*, 256, p. 116998.

7. Hou, L., Jia, X., Wu, Y., Li, J., Yao, D., Gou, Y. and Huang, G., 2021. Aroylhydrazone Cu(II) complexes: Syntheses, crystal structures and anticancer properties. *Journal of Molecular Structure*, 1239, p. 130469.

8. Sheeja, S.R., Mangalam, N.A., Sithambaresan, M., Kurup, M.P., Kaya, S. and Serdaroğlu, G., 2021. Spectral studies and quantum chemical ab initio calculations for copper(II) complexes of two

heterocyclic aroylhydrazones. *Journal of Molecular Structure*, 1245, p. 131001.

9. Al Riyami, N.A. and Al-Rasbi, N.K., 2024. Factors that influence the energy transfer pathways in luminescent lanthanide Schiff base complexes. *Inorganica Chimica Acta*, 572, p. 122324.

10. Masuya-Suzuki, A., Goto, S., Nakamura, R., Karashimada, R., Kubota, Y., Tsunashima, R. and Iki, N., 2022. Emergence of the super antenna effect in mixed crystals of ytterbium and lutetium complexes showing near-infrared luminescence. *RSC Advances*, 12(47), pp. 30598–30604.

11. Duan, Y.Y., Wu, D.F., Chen, H.H., Wang, Y.J., Li, L., Gao, H.L. and Cui, J.Z., 2022. New dinuclear lanthanide complexes derived from Schiff base ligand and *β*-diketonate co-ligand: Synthesis, crystal structures, luminescent and magnetic properties. *Polyhedron*, 225, p. 116070.

12. Maniyampara, P.K., Bhagiyalakshmi, M., Kurup, M.P., Manoj, E. and Damodaran, K.K., 2024. Bromo substituted aroylhydrazones: Synthesis, crystal structures, Hirshfeld surface analysis, 3D energy frameworks, DNA/BSA binding and antimicrobial activity. *Journal of Molecular Structure*, 1318, p. 139214.

13. Nair, Y., Joy, F., Vinod, T.P., Vineetha, M.C., Kurup, M.P., Kaya, S., Serdaroğlu, G. and Erkan, S., 2024. Spectroscopic, crystal structure and DFT-assisted studies of some nickel(II) chelates of a heterocyclic-based NNO donor aroylhydrazone: In vitro DNA binding and docking studies. *Molecular Diversity*, 28(2), pp. 509–530.

14. Zahirović, A., Fetahović, S., Feizi-Dehnayebi, M., Bešta-Gajević, R., Dizdar, M., Ostojić, J. and Roca, S., 2024. Substituent effect in salicylaldehyde 2-furoic acid hydrazones: Theoretical and experimental insights into DNA/BSA affinity modulation, antimicrobial and antioxidant activity. *Journal of Molecular Structure*, 1312, p. 138628.

15. Tabassum, S., Asim, A., Arjmand, F., Afzal, M. and Bagchi, V., 2012. Synthesis and characterization of copper(II) and zinc(II)-based potential chemotherapeutic compounds: their biological evaluation viz. DNA binding profile, cleavage and

antimicrobial activity. *European journal of medicinal chemistry*, *58*, pp.308-316.

16. Kanchanadevi, S., Fronczek, F.R. and Mahalingam, V., 2021. Ruthenium(III) hydrazone complexes with triphenylphosphine/triphenylarsine co-ligands: Synthesis, DNA/BSA binding, antioxidative and cytotoxic activity. *Inorganica Chimica Acta*, 526, p. 120532.

17. Fayad, E., Katouah, H.A., Abuzahrah, S.S., Ali, O.A.A., Alqahtani, A.S., Al-Salmi, F.A., Alshaya, D.S., Almaaty, A.H.A., Elsaid, F.G., Farouk, N.A. and Sophy, M.A.E., 2025. Novel 2-aroyl-1-acetylhydrazine derivatives: Assessment of biological activity as therapeutic agents. *Journal of Molecular Structure*, 1322, p. 140185.

18. Mahadevi, P., Sumathi, S., Dasgupta, S. and Noor, A., 2024. Bioactive benzhydrazone-derived Schiff base and its metal(II) complexes: Synthesis, characterisation, cytotoxicity, DNA binding/cleavage, antimicrobial and antioxidant activity. *Inorganic Chemistry Communications*, 167, p. 112800.

19. Stražić, D., Benković, T., Gembarovski, D., Kontrec, D. and Galić, N., 2014. Comprehensive ESI-MS and MS/MS analysis of aromatic hydrazones derived from nicotinic acid hydrazide. *International Journal of Mass Spectrometry*, 371, pp. 54–64.

20. Anjana, T.M., Manoj, E., Naseera, C.M., Liyakhath, F.M., Thayyullathil, A., Naduparambath, S., Sheeja, S.R. and Kurup, M.P., 2025. Photophysical properties, DFT calculations and DNA binding studies of a series of deep blue emitting cerium(III) complexes. *Journal of Molecular Structure*, *1327*, p. 141186.

21. Yasuhara, A., Tanaka, Y., Makishima, M., Suzuki, S. and Shibamoto, T., 2011. LC-MS analysis of low molecular weight carbonyl compounds as 2,4-dinitrophenylhydrazones using negative-ion electrospray ionization mass spectrometry. *Journal of Chromatography Separation Techniques*, 2(108), p. 2.

22. Pouralimardan, O., Chamayou, A.C., Janiak, C. and Hosseini-Monfared, H., 2007. Hydrazone Schiff base–manganese(II) complexes: Synthesis, crystal structure and catalytic reactivity. *Inorganica Chimica Acta*, 360, pp. 1599–1608.

23. Kuriakose, M., Kurup, M.P. and Suresh, E., 2007. Spectral characterization and crystal structure of 2-benzoylpyridine nicotinoylhydrazone. *Spectrochimica Acta Part A: Molecular and Biomolecular Spectroscopy*, 66(2), pp. 353–358.

24. Silverstein, R.M. and Bassler, G.C., 1962. Spectrometric identification of organic compounds. *Journal of Chemical Education*, 39(11), p. 546.

25. Singh, Y., Patel, R.N., Patel, S.K., Jadeja, R.N., Patel, A.K., Patel, N., Roy, H., Bhagriya, P., Singh, R., Butcher, R.J. and Jasinski, J.P., 2020. Supramolecular assemblies of new pseudohalide end-to-end bridged copper(II) complex and structural variety of penta- and hexa-coordinated metal(II) complexes with hydrazido-based ligand. *Inorganica Chimica Acta*, 503, p. 119371.

26. Hassan, E.M., Soliman, S.M., Moneer, E.A., Hagar, M., Barakat, A., Haukka, M. and Rasheed, H., 2023. Synthesis, X-ray structure, Hirshfeld, DFT conformational, cytotoxic and anti-toxoplasma studies of new indole-hydrazone derivatives. *International Journal of Molecular Sciences*, 24(17), p. 13251.

27. Wang, L., Guo, D.G., Wang, Y.Y. and Zheng, C.Z., 2014. 4-Hydroxy-3-methoxy-benzaldehyde series aroylhydrazones: Synthesis, thermostability and antimicrobial activities. *RSC Advances*, 4(102), pp. 58895–58901.

28. Thankamony, M., Sindhu Kumari, B., Rijulal, G. and Mohanan, K., 2009. Lanthanum(III) chloride complexes with heterocyclic Schiff bases: Synthesis, spectroscopic characterization and thermal studies. *Journal of thermal analysis and calorimetry*, *95*(1), pp.259-266.

CHAPTER 3

SYNTHESIS AND CHARACTERIZATION OF A SERIES OF CERIUM(III) COMPLEXES DERIVED FROM SALICYLALDEHYDE BENZOYLHYDRAZONE, SALICYLALDEHYDE NICOTINOYLHYDRAZONE AND INDOLE-3-CARBALDEHYDE BENZOYLHYDRAZONE

3.1. Introduction

Cerium is the most abundant and important lanthanide ion on earth, with the highest stability with air. The cerium(III) complexes have exciting photophysical properties and have a significant role in the field of optics and are excellent candidates for the fabrication of optical sensors, light emitting diodes, and laser diodes. They are well known for their emission in the UV to green region. The spin allowed 4*f*–5*d* transitions, short emission lifetime, and strong fluorescence emission are the prominent features inherent in cerium(III) complexes [1-3]. Besides these features, the cerium(III) complexes are also known for their cytotoxicity and anticancer activity. Moreover, Ce^{3+} ions are capable of replacing the calcium-dependent reactions involved in the biological system due to their similarity in ionic radii with Ca^{2+}. By utilizing this feature, Ce^{3+} based antithrombic drugs were developed in the past decades [2-5]. Recently, Sheta and coworkers synthesized a cerium-Schiff base complex useful as a kidney biomarker for selective detection of human creatinine [2,6].

The photoluminescence efficiency and biological activity of lanthanide complexes mainly depend on the coordinated organic ligands. Aroylhydrazones are one of the most important classes of organic ligands, with outstanding chelating ability with transition and inner transition metal ions [2]. They greatly enhance the photoluminescence properties by effectively transferring the absorbed energy to the excited states of lanthanide ions. Their structural flexibility, stability, and the ease of preparation make them remarkable

in the field of coordination chemistry. Compared to transition metal complexes, the rare earth metal complexes are of greater importance due to their unique magnetic and photoluminescent properties [2,7].

The biological activity and stability of Schiff base complexes can be improved by incorporating amino acids into it. L-Histidine is one of the essential bioactive amino acids containing an imidazole ring with three sites available for coordination, namely the amino nitrogen, the imidazole nitrogen, and the carboxylate oxygen. Also, L-histidine is a well-known natural detoxifier that can reduce the radiation hazards in the environment [2,8,9]. This chapter includes the synthesis and spectral characterization of a series of cerium(III) complexes containing salicylaldehyde benzoylhydrazone, salicylaldehyde nicotinoylhydrazone, indole-3-carbaldehyde benzoylhydrazone and the coligand L-histidine.

3.2. Experimental

3.2.1. Materials

All reagents and solvents were of analytical grade. $Ce(NO_3)_3 \cdot 6H_2O$ and L-Histidine were obtained from Sigma Aldrich. Solvents such as N,N-dimethylformamide (DMF), methanol, acetic acid, and ether were purchased from commercial suppliers and employed as received without further purification.

3.2.2. Synthesis of ligands

Chapter 2 explains the method of preparation and characterization of the aroylhydrazones H_2salbh, H_2salnh and Hindbh.

3.2.3. Synthesis of Ce(III) complexes

Cerium(III) complexes were synthesized using the aroylhydrazones H_2salbh, H_2salnh and Hindbh as the primary ligands and L-histidine as the coligand (Scheme 3.1).

3.2.3.1. Synthesis of [Ce(Hsalbh)(NO$_3$)$_2$] (1)

To the methanolic solution of H_2salbh (0.240 g, 1 mmol), methanolic solution of $Ce(NO_3)_3 \cdot 6H_2O$ (0.434 g, 1 mmol) was added. The solution was refluxed in water bath for 4 hours. After cooling, the grey colored precipitate of **1** was filtered off, washed with methanol, followed by ether and then, air dried. Yield: (0.0503 g) 66.3%. λ_m(DMF): 6 ohm^{-1}cm^{2}mol^{-1}. μ: 2.4 B.M. Elemental Anal. Found (Calcd) %: C: 33.24 (33.40); H: 2.18 (2.20); N: 10.81 (11.13) for [Ce(Hsalbh)$(NO_3)_2$]. MALDI-TOF-MS *m/z* 617.73 $[M+5H_2O+1Na+H]^+$, (Calcd 616.44).

3.2.3.2. Synthesis of [Ce(Hsalnh)(NO$_3$)$_2$] (2)

$Ce(NO_3)_3 \cdot 6H_2O$ (0.434 g, 1 mmol) was dissolved in methanol (20 mL) to which a methanolic solution of H_2salnh (0.241 g, 1 mmol) was added. The reaction mixture was then refluxed for 4 hours. Then, the pale yellow-colored precipitate was washed with methanol followed by ether, and air dried. Yield: (0.5043 g) 68.7%. λ_m(DMF): 9 ohm^{-1}cm^{2}mol^{-1}. μ: 2.2 B.M. Elemental Anal. Found (Calcd) %: C: 31.41 (30.96); H: 2.51 (2.00); N: 14.34 (13.89) for [Ce(Hsalnh)$(NO_3)_2$]. MALDI-TOF-MS *m/z* 617.86 $[M+5H_2O+Na]^+$, (Calcd 617.42).

3.2.3.3. Synthesis of [Ce(Hindbh)(NO$_3$)$_3$] (3)

Hindbh (0.263 g, 1 mmol) dissolved in methanol was mixed with a methanolic solution of $Ce(NO_3)_3 \cdot 6H_2O$ (0.434 g, 1 mmol), and the resulting mixture was refluxed in a water bath for 4 hours. Upon cooling to room temperature, a pale yellow precipitate of complex **3** was formed. It was filtered, washed successively with methanol and diethyl ether, and then air-dried.Yield: (0.5894 g). 59.2%. λ_m(DMF): 7 ohm^{-1}cm^{2}mol^{-1}. μ: 2.1 B.M. Elemental Anal.Found (Calcd) %: C: 32.60 (32.24); H: 2.22 (2.68); N: 14.26 (14.11) for [Ce(Hindbh)(NO$_3$)$_3$]. MALDI-TOF-MS *m/z* 717.3 $[M+7H_2O+2H]^+$, (Calcd 717.5).

3.2.3.4. Synthesis of [Ce(Hsalbh)his(NO$_3$)] (4)

To the methanolic solution of H$_2$salbh (0.240 g, 1 mmol), a methanolic solution of $Ce(NO_3)_3 \cdot 6H_2O$ (0.434 g, 1 mmol) and a methanolic solution of L-histidine (0.155 g, 1 mmol) were added. The reaction mixture was refluxed in a water bath for 4 hours. The resulting dark brown precipitate was washed with methanol, ether, and then, air dried. Yield: (0.5955 g) 65.3%. λ_m(DMF): 15 ohm^{-1}cm^{2}mol^{-1}. μ: 2.3 B.M. Elemental Anal. Found (Calcd) %: C: 40.88 (40.34); H: 3.29 (3.22); N: 14.07 (14.11) for [Ce(Hsalbh)his(NO$_3$)]. MALDI-TOF-MS *m/z* 617.917 $[M+Na]^+$, (Calcd 618.50).

3.2.3.5. Synthesis of [Ce(Hsalnh)his(NO$_3$)] (5)

Complex **5** was synthesized by a method similar to that of complex **4**, using H_2salnh (0.241g, 1 mmol) instead of H_2salbh. Dark brown coloured precipitate was washed with methanol, followed by ether, and air dried. Yield: (0.5965 g) 64.4%. λ_m(DMF): 12 ohm^{-1}cm^{2}mol^{-1}. μ: 2.4 B.M. Elemental Anal. Found (Calcd) %: C: 38.12 (38.26); H: 3.21 (3.04); N: 15.84 (16.44) for [Ce(Hsalnh)his(NO_3)]. MALDI-TOF-MS *m/z* 742.173 [M +H_2O+4CH_3OH]$^+$, (Calcd 742.68).

3.2.3.6. Synthesis of [Ce(Hindbh)(his)(NO$_3$)$_2$] (6)

A methanolic solution of Hindbh (0.263 g, 1 mmol) was mixed with methanolic solutions of $Ce(NO_3)_3{\cdot}6H_2O$ (0.434 g, 1 mmol) and L-histidine (0.155 g, 1 mmol). The solution was refluxed in a water bath for 4 hours. Upon cooling, a pale yellow precipitate was formed, which was filtered off, washed sequentially with methanol and diethyl ether, and then air-dried. Yield: (0.6816 g) 52.4%. λ_m(DMF): 10 ohm^{-1}cm^{2}mol^{-1}. μ: 2.1 B.M. Elemental Anal. Found (Calcd) %: C: 38.48 (38.77); H: 3.45 (3.11); N: 16.70 (16.44) for [Ce(Hindbh)(his)(NO_3)$_2$]. MALDI-TOF-MS *m/z* 927.4 [M +7H_2O+3CH_3OH+Na]$^+$, (Calcd 926.7).

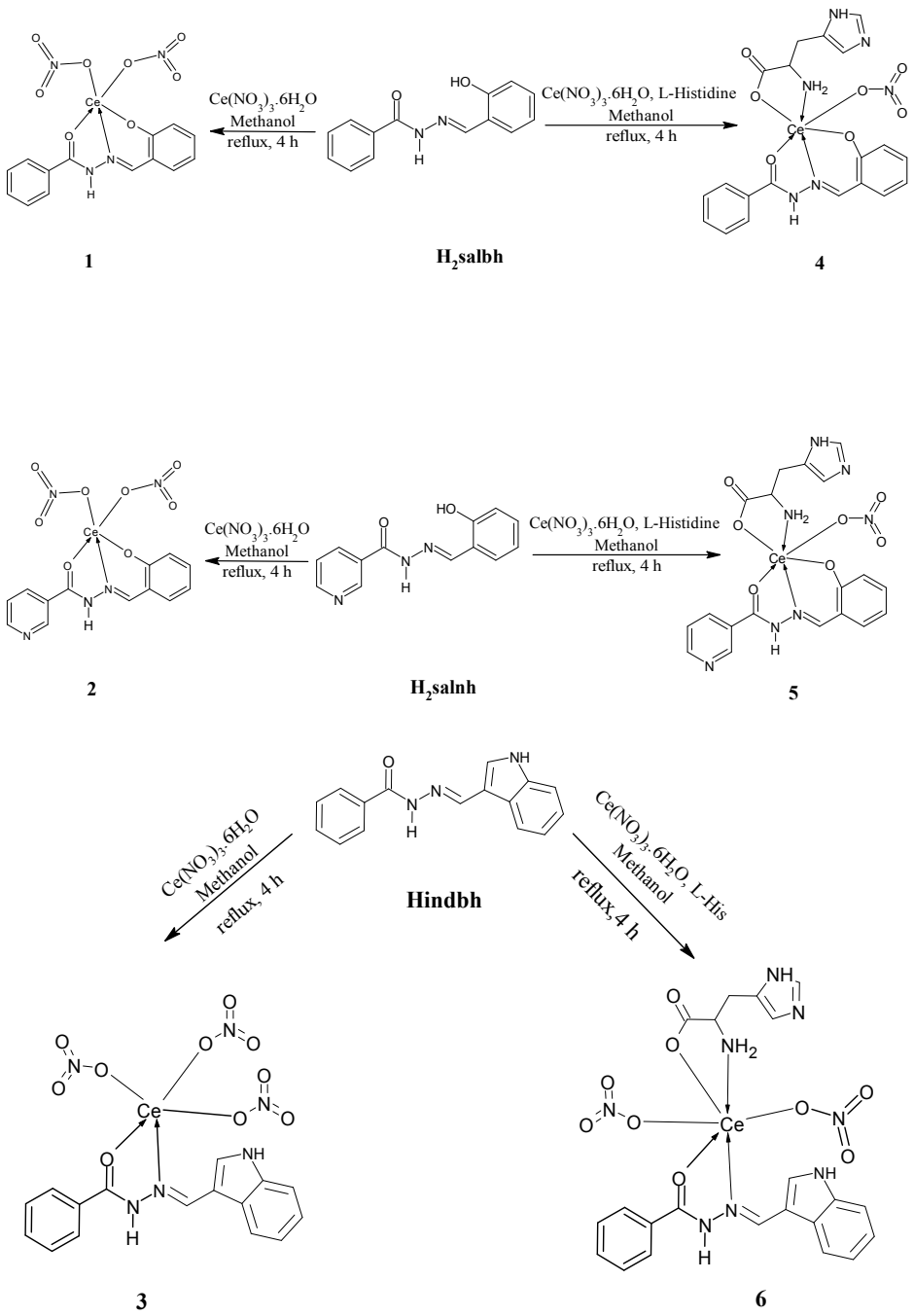

Scheme 3.1. Synthesis of cerium(III) complexes

3.3. Results and Discussion

The cerium(III) complexes of aroylhydrazones were successfully synthesized and characterized by partial elemental analysis, molar conductance, magnetic moment, ESI-MS, FT-IR and electronic spectroscopy. In the cerium(III) complexes **1**, **2**, **4** and **5**, the aroylhydrazones H_2salbh and H_2salnh, act as a tridentate ONO donor, coordinating through the carbonyl oxygen, phenolic oxygen and azomethine nitrogen. In contrast, in complexes **3** and **6**, Hindbh act as a bidentate donor, coordinating through azomethine nitrogen and carbonyl oxygen atom. All the cerium(III) complexes exhibit distint colour and are stable in air. They show good solubility in dipolar aprotic solvents like DMF and DMSO.

3.3.1. Partial Elemental analysis

The elemental analysis (C, H, and N) of the Ce(III) complexes of aroylhydrazones are listed in Table 3.1. The calculated values are in good agreement with the analytical data, and were used to confirm the formulae of the complexes. Also, the elemental analyses data obtained for the Ce(III) complexes explain that the aroylhydrazone and Ce(III) combine in a 1:1 molar ratio to form the complexes [2].

Table 3.1. The compositional details of the synthesized Ce(III) complexes

Compound	Empirical formula	Formula Weight (g/mol)	Colour (Yield %)	Found (Calcd %)		
				C	H	N
1	$C_{14}H_{11}CeN_4O_8$	503.3	Grey 66.3	33.24 (33.40)	2.18 (2.20)	10.81 (11.13)
2	$C_{13}H_{10}CeN_5O_8$	504.3	Pale Yellow 68.7	31.41 (30.96)	2.51 (2.00)	14.34 (13.89)
3	$C_{16}H_{13}CeN_6O_{10}$	589.4	Pale Yellow 59.2	32.60 (32.24)	2.22 (2.68)	14.26 (14.11)
4	$C_{20}H_{19}CeN_6O_7$	595.5	Dark brown 65.3	40.88 (40.34)	3.29 (3.22)	14.07 (14.11)
5	$C_{19}H_{18}CeN_7O_7$	596.5	Dark brown 64.4	38.12 (38.26)	3.21 (3.04)	15.84 (16.44)
6	$C_{22}H_{21}CeN_8O_9$	681.6	Pale Yellow 52.4	38.48 (38.77)	3.45 (3.11)	16.70 (16.44)

3.3.2. Conductivity measurements

The electrolytic nature of the Ce(III) complexes was evaluated by measuring their molar conductance in DMF at room temperature. The values ranged from 9 to 15 $ohm^{-1}cm^2mol^{-1}$. These low values are characteristic of non-electrolytic behaviour, suggesting that the complexes do not dissociate appreciably in solution. The corresponding conductance data are compiled in Table 3.2.

Table 3.2. The molar conductances of the Ce(III) complexes.

Compound	Molar Conductance ($ohm^{-1}cm^2mol^{-1}$)
1	6
2	9
3	7
4	15
5	12
6	10

3.3.3. Mass Spectrometry

The mass spectra of the Ce(III) omplexes were recorded in DMF solution using MALDI time-of-flight BrukerAutoflex max LRF mass spectrometer. The formation and structural composition of the cerium(III) complexes were confirmed through their mass spectral data. Comparison of the observed *m/z* values with the calculated molecular weights of the proposed cerium(III) complexes further supports the assigned molecular formulae.

The mass spectrum of compound **1** exhibits molecular ion peak at *m/z* 617.73 which corresponds to $[M+5H_2O+1Na+H]^+$. For compound **2**, the molecular ion peak is observed at *m/z* 617.86 assigned to $[M+5H_2O+Na]^+$. Compound **3** displays a peak at *m/z* 717.3, attributed to $[M+7H_2O+2H]^+$. For compound **4**, a molecular ion peak at *m/z* 617.917 is observed, corresponding to $[M+Na]^+$, while compound **5** shows a peaks *m/z* is observed at 742.173, which can be to $[M+H_2O+4CH_3OH]^+$. Additionally, the mass spectrum of compound **6** reveals a peak at *m/z* 927.4, corresponding to $[M+7H_2O+3CH_3OH+Na]^+$.(Figs. 3.1 to 3.6).

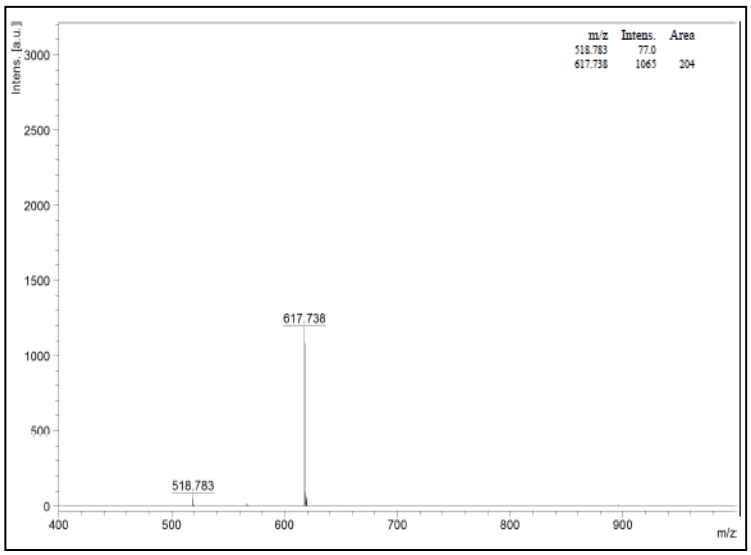

Fig. 3.1. Mass spectrum of **1**

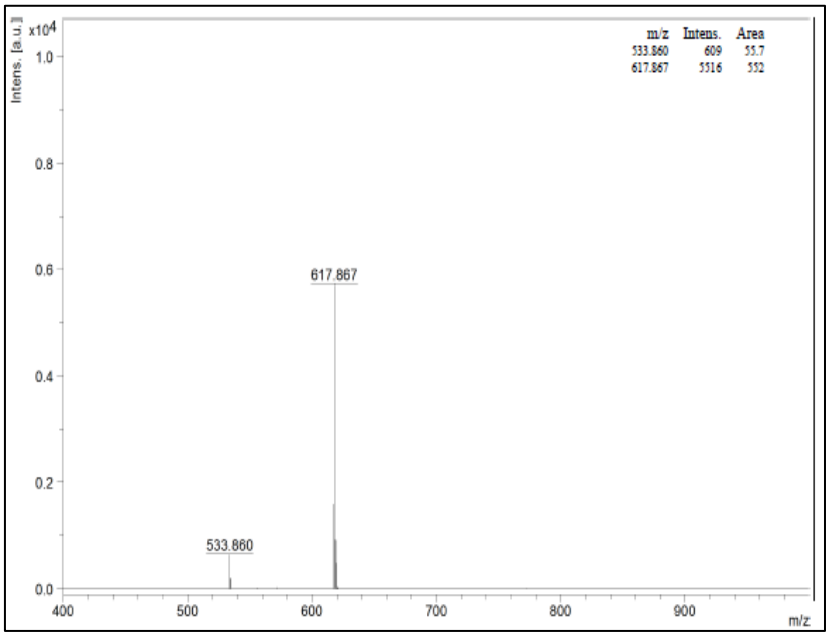

Fig. 3.2. Mass spectrum of **2**

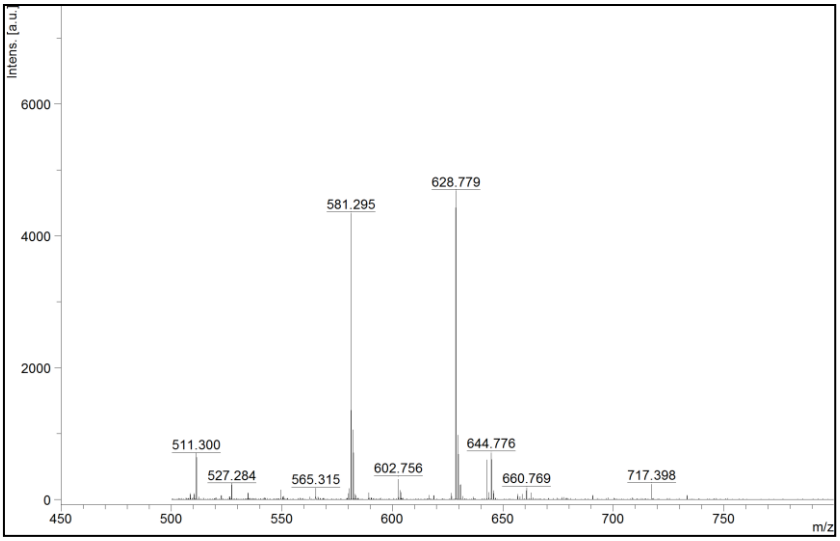

Fig. 3.3. Mass spectrum of **3**

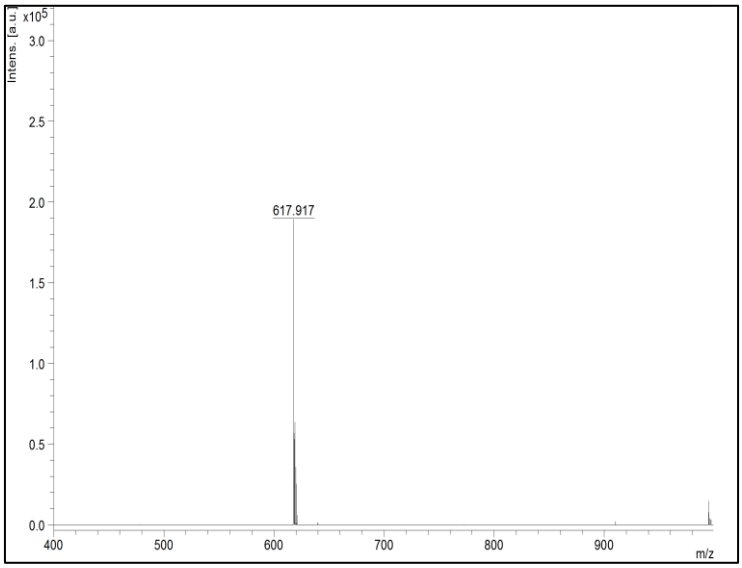

Fig. 3.4. Mass spectrum of **4**

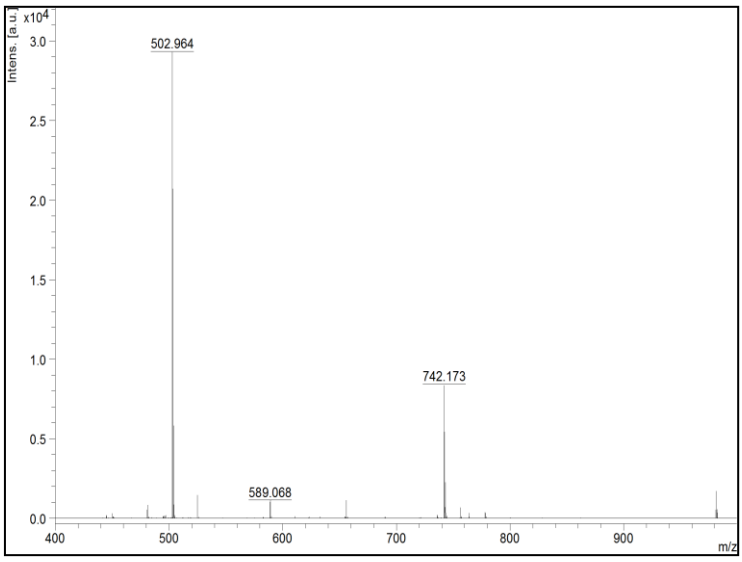

Fig. 3.5. Mass spectrum of **5**

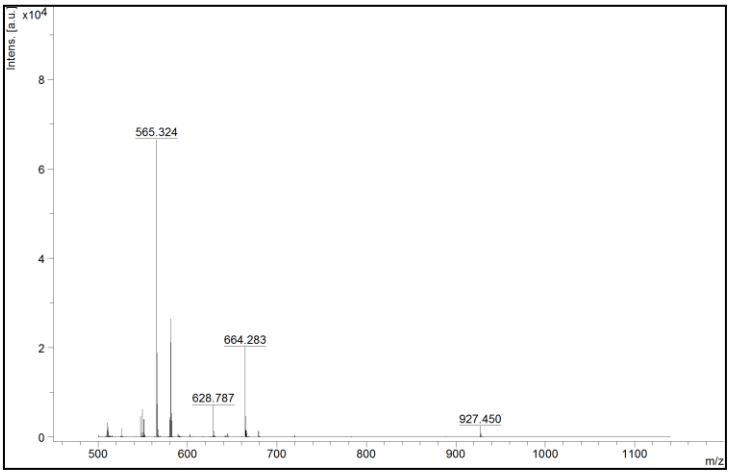

Fig. 3.6. Mass spectrum of **6**

3.3.4. FT-IR Spectroscopy

The FT-IR spectra of the cerium(III) complexes were recorded in the range of 4000-400 cm^{-1}. By comparing the IR spectral bands of the aroylhydrazones and the cerium(III) complexes, the coordination mode of the aroylhydrazones with the metal ions can be well studied.

The absorption band observed at 1677 cm^{-1} in the IR spectrum of H_2salbh is assigned to the stretching vibration of the (N–C=O) functional group [2,10]. For complex **1**, the ν(N–C=O) was shifted to 1608 cm^{-1}, which supports the coordination of the cerium(III) ion with the oxygen atom of the N–C=O group. The IR spectrum of H_2salbh exhibits a strong absorption band at 1622 cm^{-1}, which corresponds to the azomethine group in the hydrazone. But in the case of complex **1**, the corresponding band is lowered to 1547 cm^{-1}, which indicates the coordination of the azomethine nitrogen atom to the cerium(III) ion

[11,12]. The vibrational band at 3270 cm^{-1} is assigned to the ν(N–H) for the metal-free ligand. This ν(N–H) band is also observed in the spectrum of complex **1** [2,13]. This suggests that the ligand remains in keto form in the complex. Further, the new bands at 471 and 455 cm^{-1}, for the complex, would be assigned to ν(M–O) and ν(M–N), respectively [2].

A similar pattern of spectral bands is observed in the case of complex **4**. In complex **4**, the new bands at 510 and 424 cm^{-1} can be attributed to ν(M–O) and ν(M–N) bands, respectively. This clearly implies the successful coordination of the cerium(III) ion with the corresponding hydrazone. Additionally, two new bands were observed at 1485 and 1275 cm^{-1} for complex **1** and at 1473 and 1252 cm^{-1} for complex **4**, which are attributed to the monodentate nature of the nitrate groups in coordination [2,-14-16].

The IR spectrum of Hindbh displays absorption bands at 3231 cm^{-1}, 1635 cm^{-1}, and 1596 cm^{-1}, corresponding to N–H, C=O, and C=N stretching vibrations, respectively. For **3** and **6**, these bands are observed at lower frequencies: at 3212, 1612, and 1553 cm^{-1} for **3**, and 3209, 1611, and 1574 cm^{-1} for **6**, respectively. The downward shift of the ν(C=O) and ν(C=N) bands upon complexation indicates the ligand coordinates to the metal ion through the carbonyl oxygen and azomethine nitrogen atoms. Furthermore, the appearance of new bands at 503 and 448 cm^{-1} in complex **3**, and at 537 and 421 cm^{-1} in complex **6**, is ascribed to ν(M–O) and ν(M–N) vibrations, respectively [15,16]. These observations provide strong evidence for the successful

coordination of both the oxygen and nitrogen donor atoms with the metal centre. The characteristic vibrational bands associated with coordinated nitrate groups are observed at 1434 and 1292 cm^{-1} for complex **3**, and at 1441 and 1244 cm^{-1} for complex **6**. These frequencies are consistent with monodentate coordination of the nitrate ligands [2].

The IR spectrum of H_2salnh exhibits ν(N–C=O) and ν(C=N) bands at 1700 cm^{-1} and 1585 cm^{-1} respectively [2,17]. In complex **2**, the corresponding IR spectral bands are observed at 1656 and 1503 cm^{-1}. This indicates the involvement of carbonyl oxygen and azomethine nitrogen in coordination [2,18]. The appearance of new bands at 483 and 438 cm^{-1}, which is assigned to ν(M–O) and ν(M–N), also supports this assumption. Similarly, in complex **5**, ν(N–C=O) and ν(C=N) bands are observed at lower frequencies when compared to the spectrum of H_2salnh. This suggests that the coordination of the metal complex is through the keto form. Also, in complex **5**, new bands, corresponding to ν(M–O) and ν(M–N), are observed at 493 and 439 cm^{-1}, respectively. The characteristic vibrational peaks of coordinated nitrate groups are observed at 1481 and 1287 cm^{-1} for complex **2** and 1469 and 1252 cm^{-1} for complex **5**. These bands suggest that the nitrate groups are coordinated as monodentate ones [2,14-16]. Table 3.3 presents the FT-IR spectral data of the cerium(III) complexes, and their spectra are presented in Figs. 3.7 to 3.12.

Table 3.3. Infrared spectral data of the Ce(III) complexes

Compound	ν(N–H) cm^{-1}	ν(C=O) cm^{-1}	ν(C=N) cm^{-1}	ν(M–O) cm^{-1}	ν(M–N) cm^{-1}
1	3270	1608	1547	471	455
2	3082	1656	1503	483	438
3	3212	1612	1553	503	448
4	3009	1629	1566	510	424
5	3037	1601	1545	493	439
6	3209	1611	1574	537	421

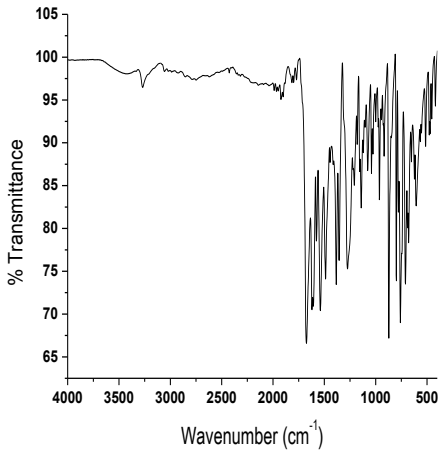

Fig. 3.7. IR spectrum of **1**

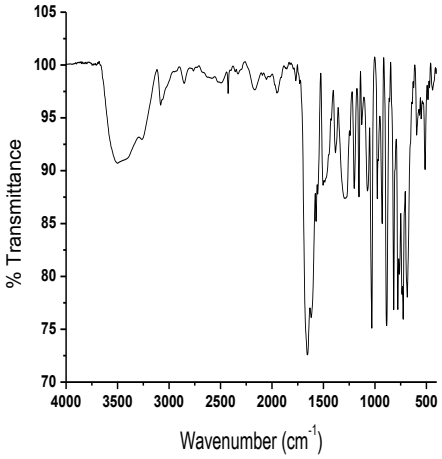

Fig. 3.8. IR spectrum of **2**

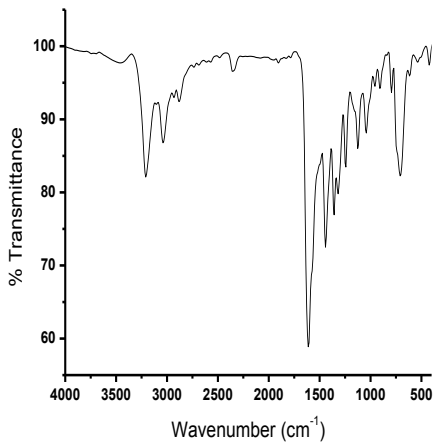

Fig. 3.9. IR spectrum of **3**

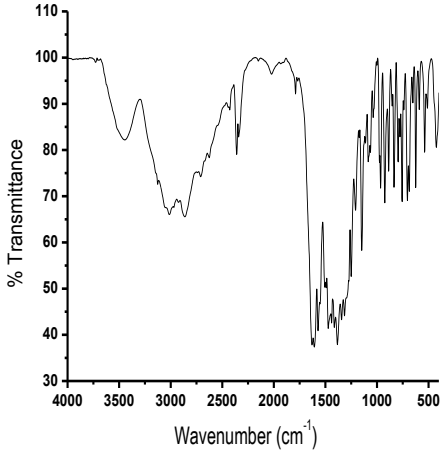

Fig. 3.10. IR spectrum of **4**

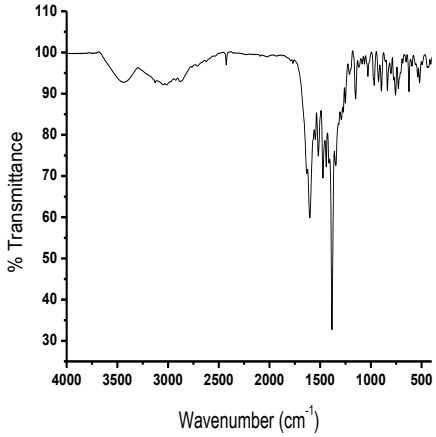

Fig. 3.11. IR spectrum of **5**

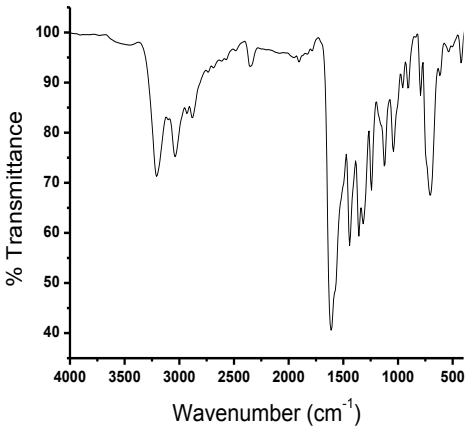

Fig. 3.12. IR spectrum of **6**

3.3.5. Electronic Spectroscopy

The UV–vis absorption spectra of the cerium(III) complexes were recorded in DMF solution (Figs. 3.13 to 3.16). The UV–vis spectrum of H_2salbh resembled the spectrum of H_2salnh displaying three absorption bands in the region 290 to 330 nm. These bands can be ascribed to $\pi \rightarrow \pi^*$ transitions of the aromatic ring and $n \rightarrow \pi^*$ transitions of the azomethine and keto groups [2,11,19]. A new

absorption band was appeared at 381 nm for compound **1** and at 384 nm for the compound **2**, which are assignable to *4f–5d* transitions [2,6,20]. As in the case of complex **1**, the complex **4** also exhibited an additional broad peak at 400 nm. When compared to complex **1**, the absorption bands of complex **4** were shifted to longer wavelength (red shift). The UV–vis absorption spectrum of the complex **5** also followed the same trend that of the complex **4**, showing an additional peak at 388 nm with a slight shift in wavelength. Similarly, compounds **3** and **6** exhibit similar electronic transitions as observed from their UV-vis spectra. Both compounds show absorption bands in the range 300-400 nm, indicating the presence of $\pi \rightarrow \pi^*$, $n \rightarrow \pi^*$, and ligand-to-metal charge transfer (LMCT) transitions. The remarkable red shift observed in these complexes is due to the extended conjugation attained on complexing with cerium(III) and with coligand L-histidine [2,21]. These significant changes observed in the absorption spectra of all complexes confirm the coordination of Ce(III) ions with respective hydrazones. Table 3.4 presents the spectral assignments of the cerium(III) complexes.

Table 3.4. UV-visible spectral data of Ce(III) complexes in DMF (10^{-5} M)

Compound	Electronic spectral bands (nm)	Assignment
1	299, 310, 334, 381	$\pi \rightarrow \pi^*$, $n \rightarrow \pi^*$, 4*f*–5*d* transitions
2	300, 309, 340, 384	$\pi \rightarrow \pi^*$, $n \rightarrow \pi^*$, 4*f*–5*d* transitions
3	302, 316, 330, 400	$\pi \rightarrow \pi^*$, $n \rightarrow \pi^*$, LMCT transitions
4	307, 315, 337, 400	$\pi \rightarrow \pi^*$, $n \rightarrow \pi^*$, 4*f*–5*d* transitions
5	300, 310, 329, 388	$\pi \rightarrow \pi^*$, $n \rightarrow \pi^*$, 4*f*–5*d* transitions
6	303, 315, 330, 400	$\pi \rightarrow \pi^*$, $n \rightarrow \pi^*$, LMCT transitions

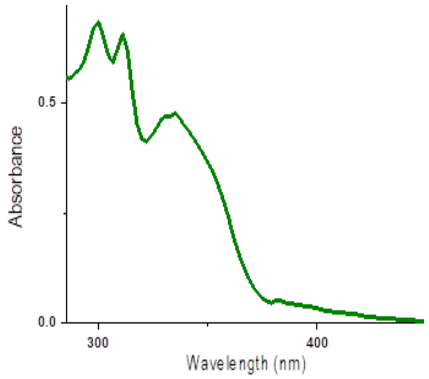

Fig. 3.13. UV-vis spectrum of **1**

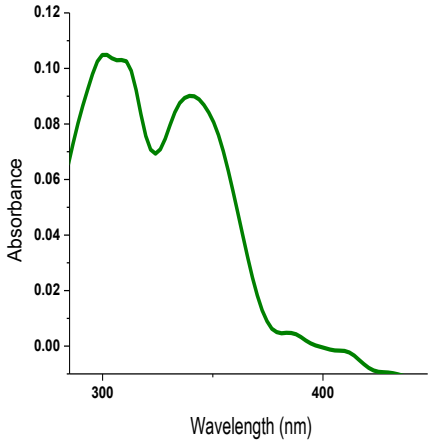

Fig. 3.14. UV-vis spectrum of **2**

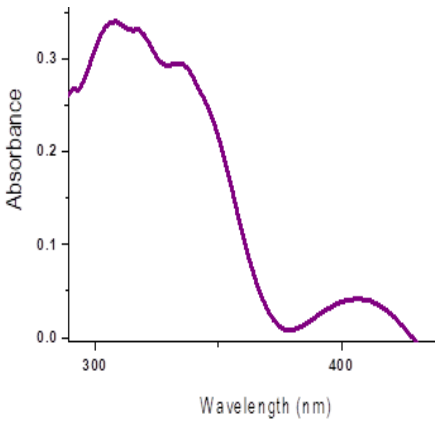

Fig. 3.15. UV-vis spectrum of **4**

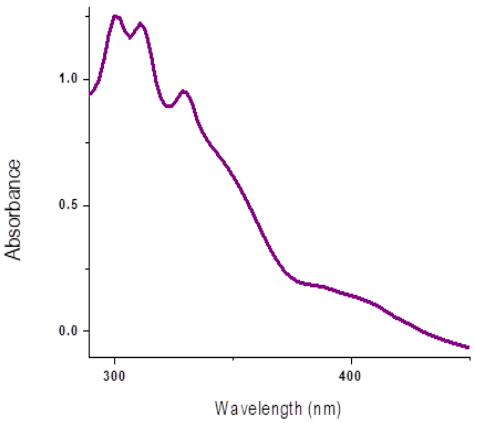

Fig. 3.16. UV-vis spectrum of **5**

3.4. Conclusion

Six novel cerium(III) complexes were synthesized employing three aroylhydrazone ligands, salicylaldehyde benzoylhydrazone (H_2salbh), salicylaldehyde nicotinoylhydrazone (H_2salnh), and indole-

3-carbaldehyde benzoylhydrazone (Hindbh), both in the presence and absence of L-histidine as a coligand. The coordination behaviour and structural features of the resulting complexes were thoroughly investigated through a combination of elemental analysis, molar conductance measurements, FT-IR, UV–visible spectroscopy, and mass spectrometry.

Elemental analyses confirmed the 1:1 metal-to-ligand stoichiometry, with experimental values closely aligning with theoretical predictions. Molar conductance values ranging between 6–15 $ohm^{-1}cm^2mol^{-1}$ in DMF indicate the non-electrolytic behavior of all the complexes in solution.

FT-IR spectra confirmed the successful coordination of metal ion with the aroylhydrazone. The carbonyl (C=O) and azomethine (C=N) bands of the ligands were significantly shifted to lower frequencies. The presence of characteristic metal–oxygen and metal–nitrogen vibrations in the lower frequency region provided additional evidence of successful chelation. Notably, the nitrate groups in the complexes were found to coordinate in a monodentate fashion, as indicated by characteristic IR bands.

Mass spectrometric analysis provided molecular ion peaks consistent with the proposed molecular formulae of the complexes, further validating their compositions. The UV–visible spectral studies exhibited distinct $\pi \rightarrow \pi^*$, $n \rightarrow \pi^*$, and ligand-to-metal charge transfer (LMCT) transitions. Additionally, characteristic $4f \rightarrow 5d$ transitions of Ce^{3+} were observed in the visible region, with red shifts upon

coordination with L-histidine, confirming the influence of the coligand on the electronic environment of the metal centre.

Structurally, the aroylhydrazones H_2salbh and H_2salnh acted as tridentate ONO donors, while Hindbh displayed bidentate coordination. The inclusion of L-histidine as a coligand enhanced the coordination sphere through additional donor sites. All complexes were air-stable, colored and were soluble in polar aprotic solvents such as DMF and DMSO.

In summary, the synthesized Ce(III) complexes exhibit defined coordination geometries, stable bonding, and promising photoluminescence characteristics. These findings not only contribute to the fundamental understanding of Ce(III)-aroylhydrazone chemistry but also pave the way for further exploration of such complexes in fields like photoluminescence, sensor development, and bioinorganic applications.

References

1. Fang, P., Wang, L., Zhan, G., Yan, W., Huo, P., Ying, A., Zhang, Y., Zhao, Z., Yu, G., Huang, Y. and Gong, S., 2021. Lanthanide cerium(III) tris(pyrazolyl)borate complexes: efficient blue emitters for doublet organic light-emitting diodes. *ACS Applied Materials & Interfaces*, 13(38), pp. 45686–45695.

2. Anjana, T.M., Manoj, E., Naseera, C.M., Liyakhath, F.M., Thayyullathil, A., Naduparambath, S., Sheeja, S.R. and Kurup, M.P., 2025. Photophysical properties, DFT calculations and DNA binding studies of a series of deep blue emitting cerium(III) complexes. *Journal of Molecular Structure*, *1327*, p. 141186.

3. Chandran, P.S., Mol, U.S., Drisya, R., Sudarsanakumar, M.R. and Kurup, M.R.P., 2017. Structural studies of poly[(μ_2-acetato)(μ_3-5-aminoisophthalato)diaquacerium(III) monohydrate]: A new three-dimensional fluorescent metal-organic framework constructed from dimers of CeO_9 polyhedra with hydrophilic 'S'-shaped channels. *Journal of Molecular Structure*, 1137, pp. 396–402.

4. Chundawat, N.S., Jadoun, S., Zarrintaj, P. and Chauhan, N.P.S., 2021. Lanthanide complexes as anticancer agents: A review. *Polyhedron*, 207, p. 115387.

5. Jakupec, M.A., Unfried, P. and Keppler, B.K., 2005. Pharmacological properties of cerium compounds. *Reviews of Physiology, Biochemistry and Pharmacology*, pp. 101–111.

6. Sheta, S.M., Akl, M.A. and Saad, H.E., El-Gharkawy, E.S.R., 2020. A novel cerium(III)–isatin Schiff base complex: Spectrofluorometric and DFT studies and application as a kidney biomarker for ultrasensitive detection of human creatinine. *RSC Advances*, 10, pp. 5853–5863.

7. Azenha, M.E., Burrows, H.D., Fonseca, S.M., Ramos, M.L., Rovisco, J., de Melo, J.S. and Kogej, K., 2008. Luminescence from cerium(III) acetate complexes in aqueous solution: considerations on the nature of carboxylate binding to trivalent lanthanides. *New Journal of Chemistry*, 32, pp. 1531–1535.

8. Kumaravel, G., Utthra, P.P. and Raman, N., 2018. Exploiting the biological efficacy of benzimidazole based Schiff base complexes with L-Histidine as a co-ligand: Combined molecular docking, DNA

interaction, antimicrobial and cytotoxic studies. *Bioorganic Chemistry*, 77, pp. 269–279.

9. Yousuf, I. and Arjmand, J., 2016. *In vitro* DNA binding profile of enantiomeric dinuclear Cu(II)/Ni(II) complexes derived from L–/D–histidine–terephthalaldehyde reduced Schiff base as potential chemotherapeutic agents. *Journal of Photochemistry and Photobiology B: Biology*, 164, pp. 83–95.

10. Nishana, L.K., Sakthivel, A., Kurup, M.R.P., Damodaran, K.K., Kulandaisamy, A. and Sithambaresan, M., 2023. Synthesis, spectral characterization and catalytic efficiency of Cu(II) complexes of tridentate aroylhydrazones containing NNO donors. *New Journal of Chemistry*, 47, pp. 20626–20641.

11. Aravindakshan, A.A., Mohan, N., Kurup, M.R.P., Erkan, S., Kaya, S. and Manoj, E., 2024. Mononuclear and binuclear dioxidomolybdenum(VI) chelates derived from a tridentate ONO donor aroylhydrazone: Spectral, structural, DFT and *in silico* biological investigations. *Polyhedron*, 256, p. 116998.

12. Pouralimardan, O., Chamayou, A.C., Janiak, C. and Hosseini-Monfared, H., 2007. Hydrazone Schiff base-manganese(II) complexes: Synthesis, crystal structure and catalytic reactivity. *Inorganica Chimica Acta*, 360, pp. 1599–1608.

13. Mathews, N.A., Jose, A. and Kurup, M.R.P., 2019. Synthesis and characterization of a new aroylhydrazone ligand and its cobalt(III) complexes: X-ray crystallography and *in vitro* evaluation of antibacterial and antifungal activities. *Journal of Molecular Structure*, 1178, pp. 544–553.

14. Shebl, M., 2009. Synthesis, spectral and magnetic studies of mono- and bi-nuclear metal complexes of a new bis(tridentate NO_2) Schiff base ligand derived from 4,6-diacetylresorcinol and ethanolamine. *Spectrochimica Acta Part A: Molecular and Biomolecular Spectroscopy*, 73, pp. 313–323.

15. Shelke, V.A., Jadhav, S.M., Patharkar, V.R., Shankarwar, S.G., Munde, A.S. and Chondhekar, T.K., 2012. Synthesis, spectroscopic characterization and thermal studies of some rare earth metal complexes of unsymmetrical tetradentate Schiff base ligand. *Arabian Journal of Chemistry*, 5, pp. 501–507.

16. Benković, T., Kenđel, A., Parlov-Vuković, J., Kontrec, D., Chiş, V., Miljanić, S. and Galić, N., 2018. Aromatic hydrazones derived from nicotinic acid hydrazide as fluorimetric p^H sensing molecules: Structural analysis by computational and spectroscopic methods in solid phase and in solution. *Spectrochimica Acta Part A: Molecular and Biomolecular Spectroscopy*, 190, pp. 259–267.

17. Kuriakose, M., Kurup, M.R.P. and Suresh, E., 2007. Spectral characterization and crystal structure of 2-benzoylpyridine nicotinoylhydrazone. *Spectrochimica Acta Part A: Molecular and Biomolecular Spectroscopy*, 66, pp. 353–358.

18. Sheeja, S.R., Mangalam, N.A., Kurup, M.R.P., Mary, Y.S., Raju, K., Varghese, H.T. and Panicker, C.Y., 2010. Vibrational spectroscopic studies and computational study of quinoline-2-carbaldehyde benzoyl hydrazone. *Journal of Molecular Structure*, 973, pp. 36–46.

19. Nishana, L.K., Sakthivel, A. and Kurup, M.R.P., 2023. Syntheses, structural characterizations, and catalytic activities of manganese(II)-aroylhydrazone complexes. *Journal of Molecular Structure*, 1281, p. 135128.

20. Sreejith, S.S., Mohan, N. and Kurup, M.R.P., 2018. Experimental and theoretical analysis of a rare nitrato bridged 3*d*–4*f* complex containing $LaZn_2$ core synthesized from a Zn(II) metalloligand. *Journal of Molecular Structure*, 1153, pp. 85–95.

21. Shan, W., Liu, F., Liu, J., Chen, Y., Yang, Z. and Guo, D., 2015. Synthesis and luminescence properties of salicylaldehyde isonicotinoylhydrazone derivatives and their europium complexes. *Journal of Inorganic Biochemistry*, 150, pp. 100–107.

CHAPTER 4

SYNTHESIS AND CHARACTERIZATION OF A SERIES OF DYSPROSIUM(III) COMPLEXES DERIVED FROM SALICYLALDEHYDE BENZOYLHYDRAZONE, SALICYLALDEHYDE NICOTINOYLHYDRAZONE AND INDOLE-3-CARBALDEHYDE BENZOYLHYDRAZONE

4.1. Introduction

The increasing focus on rare earth elements (REE) in recent research highlights their exceptional properties, such as fluorescence, magnetism, and catalytic activity, which present promising opportunities for various technological advancements [1,2]. Among these, complexes of the Dy(III) ion have emerged as an intriguing avenue in various fields of optics because of their exceptional photoluminescence characteristics [3,4].

Aroylhydrazone-based coordination compounds are well-known for their diverse applications in various branches of chemistry. The unique structural features, stability, and outstanding biological activities of aroylhydrazones stem from the presence of the azomethine group [5-8]. Researchers have shown a growing interest in hydrazones because they can be synthesized more easily and cost-effectively. Furthermore, when a second organic ligand, such as an amino acid, is integrated into the coordination sphere, both the biological activities and emission intensities of the complexes are significantly enhanced [9,10]. This synergistic effect provided by the ligands also contributes to the stabilization of the metal complexes [11]. This chapter focuses on the preparation and characterization of dysprosium(III) complexes formed with aroylhydrazones derived from salicylaldehyde benzoylhydrazone, salicylaldehyde nicotinoylhydrazone, indole-3-carbaldehyde benzoylhydrazone and the co-ligand L-Histidine.

4.2. Experimental

4.2.1. Materials

$Dy(OAc)_3 \cdot 4H_2O$ and L-Histidine were of analytical grade and were used as purchased from Sigma Aldrich without further

purification. Solvents such as N,N-dimethylformamide (DMF), methanol, acetic acid, and ether were purchased from commercial suppliers and were used as received.

4.2.2. Synthesis of ligands

Chapter 2 explains the methods of preparation and characterization of the aroylhydrazones, H_2salbh, H_2salnh and Hindbh.

4.2.3. Synthesis of Dy(III) complexes

Dysprosium(III) complexes were synthesized using the aroylhydrazones, H_2salbh, H_2salnh and Hindbh as the primary ligands and L-histidine as the coligand (Scheme 4.1).

4.2.3.1. Synthesis of [Dy(Hsalbh)(OAc)$_2$CH$_3$OH(H$_2$O)$_2$] (7)

A solution of 1 mmol of $Dy(OAc)_3 \cdot 4H_2O$ (0.411 g) in 10 mL of methanol was added to the methanolic solution of H_2salbh (0.240 g, 1 mmol). The solution was refluxed in a water bath for 4 hours. After cooling, the pale yellow-colored precipitate of **7** was filtered off, washed with methanol followed by ether, and then dried. Yield: (0.5897 g) 61.2%. λ_m(DMF): 9 $ohm^{-1}cm^2mol^{-1}$. μ: 10.1 B.M. Elemental Anal. Found (Calcd) %: C: 39.09 (38.82); H: 3.71 (4.29); N: 5.18 (4.76) for [Dy(Hsalbh)$(OAc)_2$ CH_3OH $(H_2O)_2$]. MALDI-TOF-MS *m/z* 642.280 $[M+3H_2O]^+$(Calcd 641.95).

4.2.3.2. Synthesis of [Dy(Hsalnh)(OAc)$_2$(H$_2$O)$_3$] (8)

The complex **8** was synthesized by adding 1 mmol of $Dy(OAc)_3 \cdot 4H_2O$ (0.411 g) dissolved in methanol (10 mL) in 1 mmol of

H_2salnh (0.241 g) dissolved in 10 mL of methanol. The mixture was then refluxed for 4 hours. Then, the pale yellow-colored precipitate obtained was washed with methanol, followed by ether, and air-dried. Yield: (0.5748 g) 58.5%. λ_m(DMF): 11 $ohm^{-1}cm^2mol^{-1}$. μ: 10.4 B.M. Elemental Anal. Found (Calcd) %: 35.13 (35.52); H: 3.35 (3.86); N: 7.64 (7.31) for [Dy(Hsalnh)$(OAc)_2(H_2O)_3$]. MALDI-TOF-MS *m/z* 644.169 $[M+4H_2O-3H]^+$ (Calcd 643.93).

4.2.3.3. Synthesis of [Dy(Hindbh(OAc)$_3$(H_2O)$_3$] (9)

A solution of Hindbh (0.263 g, 1 mmol) in 10 mL of methanol was mixed with a methanolic solution (10 mL) of $Dy(OAc)_3 \cdot 4H_2O$ (0.411 g, 1 mmol). The resulting mixture was refluxed in a water bath for 4 hours. Upon cooling to room temperature, a pale yellow precipitate of complex **9** formed. The solid was isolated by filtration, washed with methanol and diethyl ether, and air-dried. Yield: (0.6569 g) 64.5%. λ_m(DMF): 11 $ohm^{-1}cm^2mol^{-1}$. μ: 10.1 B.M. Elemental Anal. Found (Calcd) %: C: 40.62 (40.22); H: 3.91 (4.30); N: 6.11 (6.40) for [Dy(Hindbh$(OAc)_3(H_2O)_3$]. (MALDI-TOF-MS *m/z* 858.188 $[M +4H_2O+4(CH_3OH)+H]^+$ (Calcd 858.2).

4.2.3.4. Synthesis of [Dy(Hsalbh)(his)$_2$(H_2O)] (10)

To the 10 mL methanolic solution of H_2salbh (0.241 mg, 1 mmol), a methanolic solution of $Dy(OAc)_3 \cdot 4H_2O$ (0.411 g, 1 mmol), and a methanolic solution of L-histidine (0.155 g, 1 mmol) were added. The reaction mixture was refluxed in water bath for 4 hours. The resulting dark yellow precipitate was washed with methanol, followed by ether and air-dried. Yield: (0.7280 g) 55.3%. λ_m(DMF):

14 $ohm^{-1}cm^2mol^{-1}$. μ: 10.5 B.M. Elemental Anal. Found (Calcd) %: C: 42.71 (42.89); H: 3.85 (4.02); N: 15.31 (15.39) for [Dy(Hsalbh)$(his)_2(H_2O)$]. MALDI-TOF-MS *m/z* 801.321 $[M+4H_2O+H]^+$ (Calcd 801.118).

4.2.3.5. Synthesis of [Dy(Hsalnh)his(OAc)$(H_2O)_2$] (11)

Complex **11** was synthesized in a similar method to that of complex **10**, using H_2salnh (0.241 g, 1 mmol) instead of H_2salbh. The dark yellow-colored precipitate was washed with methanol, followed by ether, and air-dried. Yield: (0.6519 g) 44.4%. λ_m(DMF): 12 $ohm^{-1}cm^2mol^{-1}$. μ: 10.4 B.M. Elemental Anal. Found (Calcd) %: C: 38.31 (38.69); H: 3.85 (3.87); N: 12.31 (12.89) for [Dy(Hsalnh)his(OAc)$(H_2O)_2$]. MALDI-TOF-MS *m/z* 671.967 $[M+H_2O+2H]^+$ (Calcd 671.973).

4.2.3.6. Synthesis of [Dy(Hindbh)$(his)_2$(OAc)H_2O] (12)

A solution of Hindbh (0.263 g, 1 mmol) in 10 mL of methanol was added to a methanolic solution (10 mL) containing $Dy(OAc)_3{\cdot}4H_2O$ (0.411 g, 1 mmol) and L-histidine (0.155 g, 1 mmol). The reaction mixture was refluxed in a water bath for 4 hours. Upon cooling to room temperature, a dark yellow precipitate of complex **12** was formed. The product was collected by filtration, washed successively with methanol and diethyl ether, and dried in air. Yield: (0.8111 g) 65.6%. λ_m(DMF): 14 $ohm^{-1}cm^2mol^{-1}$. μ: 10.3 B.M. Elemental Anal. Found (Calcd) %: C: 44.89 (44.42); H: 4.15 (4.22); N: 15.39 (15.54) for [Dy(Hindbh)$(his)_2$(OAc)H_2O]. (MALDI-TOF-MS *m/z* 951.48 $[M+6H_2O+(CH_3OH)+H]^+$ (Calcd 951.28).

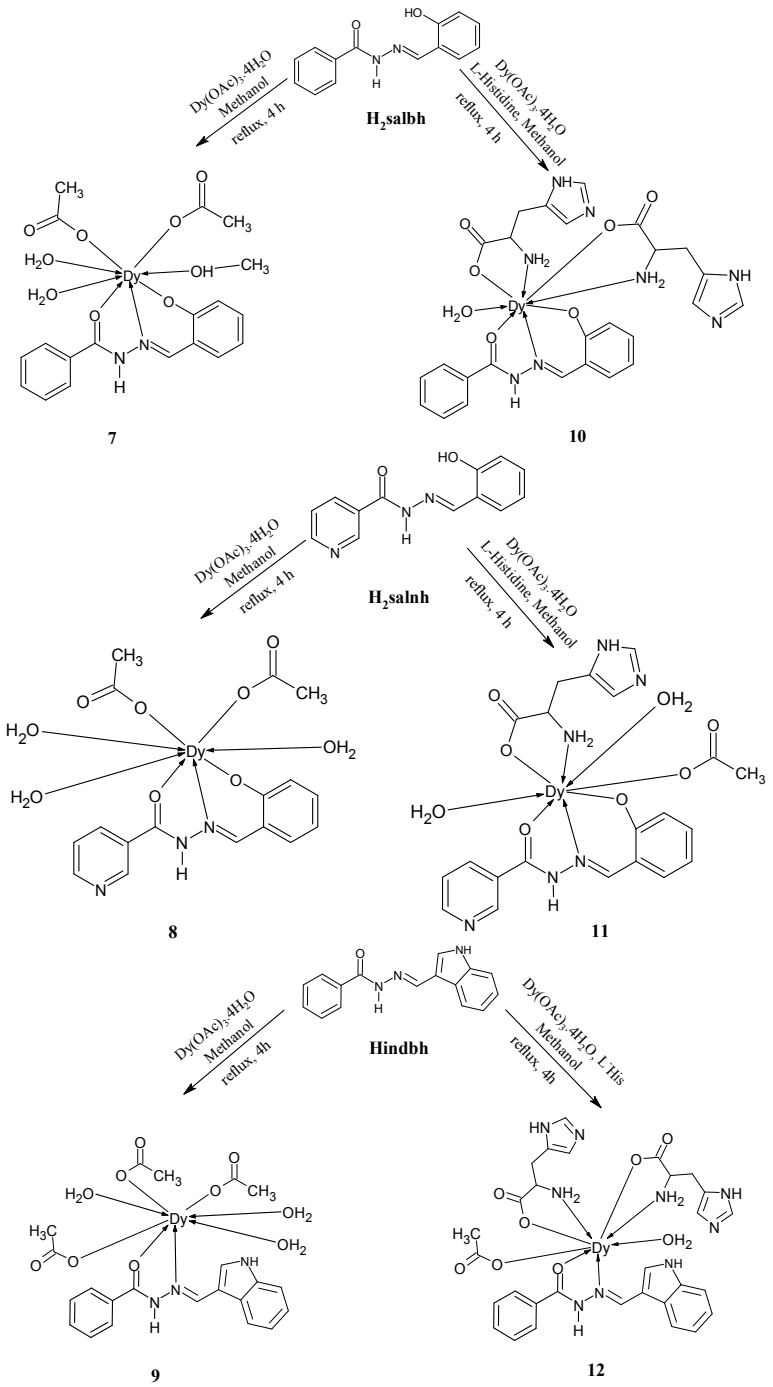

Scheme 4.1. Synthesis of dysprosium(III) complexes

4.3. Results and Discussion

The Dy(III) complexes **7**, **8** and **9** were synthesized by the reaction of a Dy(III) salt with the corresponding aroylhydrazones (H_2salbh, H_2salnh and Hindbh) in 1:1 ratio in methanol. And the Dy(III) complexes **10**, **11** and **12** were synthesized by using the corresponding aroylhydrazones as primary ligand and L-histidine as the coligand in a 1:1:1 ratio, in methanol. All the Dy(III) complexes formed were yellow colored. Also, they are very stable at room temperature and are soluble in dipolar aprotic solvents like DMF and DMSO. The synthesised Dy(III) complexes were characterized by partial elemental analysis, molar conductance, FT-IR, electronic and mass spectroscopy and the structures of the compounds were established. It can be observed that in the Dy(III) complexes, the aroylhydrazones H_2salbh and H_2salnh act as tridentate ONO donors, whereas Hindbh functions as a bidentate ligand.

4.3.1. Partial Elemental analysis

The elemental analysis of all the Dy(III) complexes of aroylhydrazones is presented in Table 4.1. It can be observed that they closely match the expected chemical formula.

Table 4.1. The compositional details of the synthesized Dy(III) complexes

Compound	Empirical formula	Formula Weight (g/mol)	Colour (Yield %)	Found (Calcd %)		
				C	H	N
7	$C_{19}H_{25}DyN_2O_9$	587.90	Pale yellow 61.2	39.09 (38.82)	3.71 (4.29)	5.18 (4.76)
8	$C_{17}H_{22}DyN_3O_9$	574.87	Pale yellow 58.5	35.13 (35.52)	3.35 (3.86)	7.64 (7.31)
9	$C_{22}H_{28}DyN_3O_{10}$	656.97	Pale yellow 64.5	40.62 (40.22)	3.91 (4.30)	6. 11 (6.40)
10	$C_{26}H_{29}DyN_8O_7$	728.05	Dark yellow 55.3	42.71 (42.89)	3.85 (4.01)	15.31 (15.39)
11	$C_{21}H_{25}DyN_6O_8$	651.95	Dark yellow 44.4	38.32 (38.69)	3.85 (3.87)	12.31 (12.89)
12	$C_{30}H_{34}DyN_9O_8$	811.14	Dark yellow 65.6	44.89 (44.42)	4.15 (4.22)	15.39 (15.54)

4.3.2. Conductivity measurements

The molar conductance of Dy(III) complexes (Table 4.2) was evaluated in N,N-dimethylformamide (DMF) at ambient temperature with values in the 9 to 14 $ohm^{-1}cm^2mol^{-1}$ range. These values strongly confirms that the Dy(III) complexes behave as non-electrolytes in solution.

Table 4.2. The molar conductance of the Dy(III) complexes.

Compound	Molar Conductance ($ohm^{-1}cm^2mol^{-1}$)
7	9
8	11
9	11
10	14
11	12
12	14

4.3.3. Mass Spectrometry

Mass spectra of the Dy(III) complexes was recorded in DMF solution using a MALDI time-of-flight Bruker Autoflex max LRF mass spectrometer. The analysis of the mass spectral data confirms the formation of Dy(III) complexes. For compound **7**, molecular ion peak was observed at *m/z* 642.280, corresponding to $[M+3H_2O]^+$. For compound **8**, the molecular ion peak appeared at *m/z* 644.169, which corresponds to $[M+4H_2O-3H]^+$. The mass spectrum of **9** displayed a peak at *m/z* 858.188, assigned to $[M+4H_2O+4CH_3OH+H]^+$, while **10** exhibited a molecular ion peak at *m/z* 801.321, attributed to $[M+4H_2O+H]^+$. Complex **11** showed a peak at *m/z* 671.967, attributing to the molecular ion $[M+H_2O+2H]^+$. Lastly, **12** presented a peak at *m/z* 951.48, assigned to $[M+6H_2O+CH_3OH+H]^+$. These

spectral patterns are consistent with the expected molecular formulations of the synthesized complexes (Figs. 4.1-4.3).

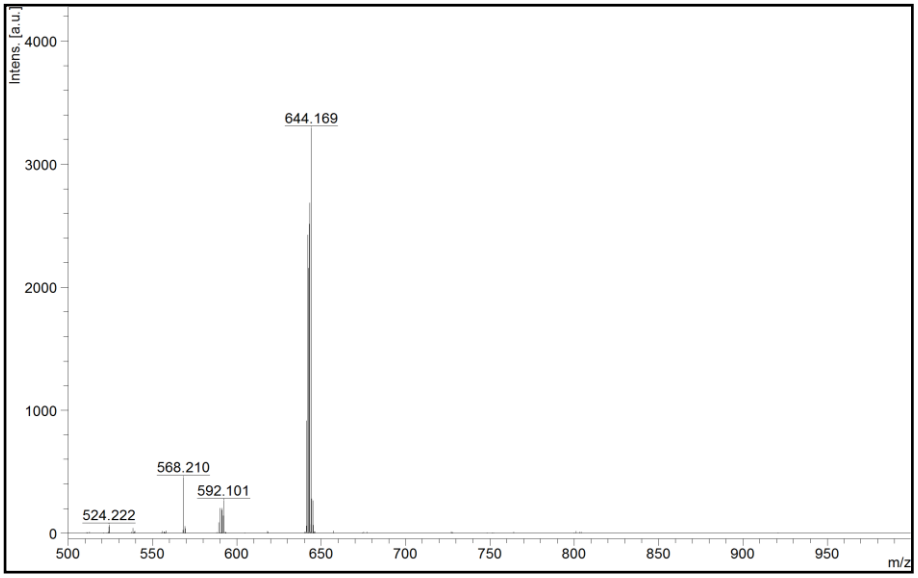

Fig. 4.1. Mass spectrum of **8**

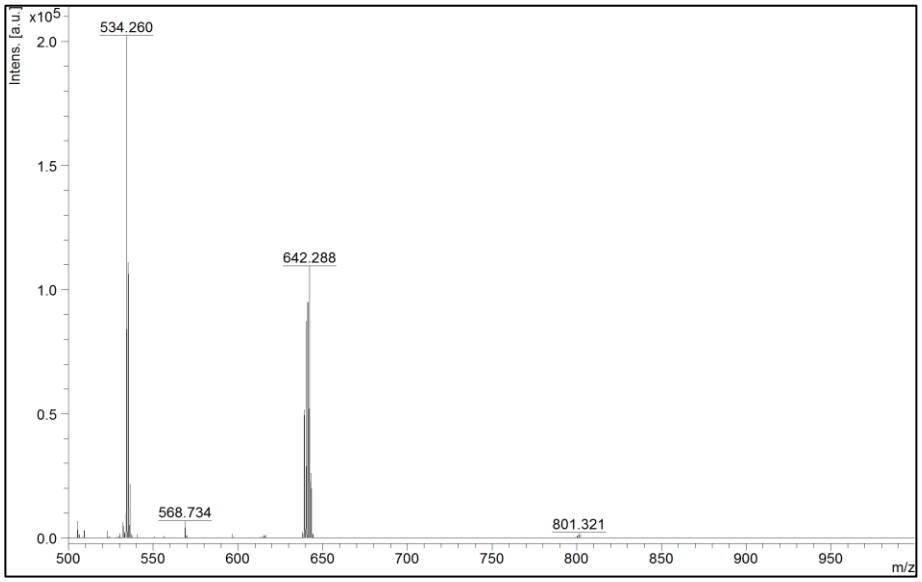

Fig. 4.2. Mass spectrum of **10**

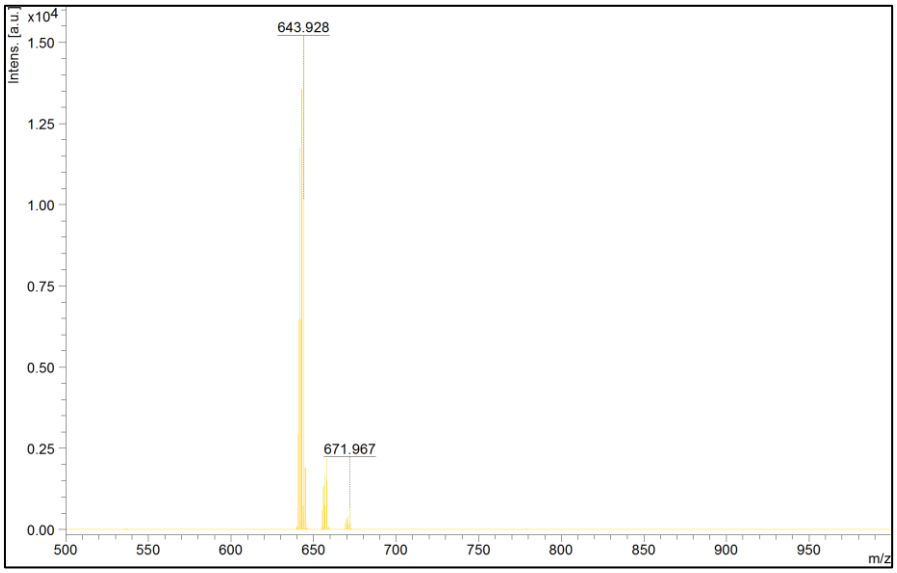

Fig. 4.3. Mass spectrum of **11**

4.3.4. FT-IR Spectroscopy

The FT-IR spectra of the Dy(III) complexes were recorded in the range of 4000-400 cm^{-1} and were compared with those of aroylhydrazones. The spectrum of H_2salbh shows characteristic absorption bands at 1677 and 1622 cm^{-1}, which are attributed to the stretching vibration of the ν(N-C=O) and (C═N) groups [12-14]. These absorption bands were notably shifted to lower frequencies in complexes **7** and **10**, confirming the coordination of Dy(III) with H_2salbh. In complex **7**, these bands appear at 1615 and 1564 cm^{-1}, respectively. A similar shift is observed in complex **10**, with bands appearing at 1615 and 1553 cm^{-1}, respectively. Furthermore, appearance of new bands in complexes **7** and **9**, clearly indicates the successful coordination of hydrazones with Dy(III) ion. The peaks at 547 and 473 cm^{-1} in **7**, and at 524 and 418 cm^{-1} in **10** can be ascribed to ν(M–O) and ν(M–N) respectively [15].

In the IR spectrum of H_2salnh, ν(N-C=O) and ν(C=N) bands were observed at 1700 cm^{-1}, and 1585 cm^{-1}, respectively [14,16]. Upon complexation with Dy(III) ion, these bands were shifted to lower frequencies, indicating the coordination of Dy(III) ion with carbonyl oxygen and azomethine nitrogen. In complex **8**, these bands were observed 1624 cm^{-1} and 1560 cm^{-1}, while in complex **11**, at 1625 cm^{-1} and 1551 cm^{-1}, respectively. Additionally, new bands were observed at 519 and 463 cm^{-1} in **8**, and at 515 and 460 cm^{-1} in **11**. These bands can be assigned to ν(M–O) and ν(M–N) vibrations [17].

The infrared spectrum of the aroylhydrazone Hindbh is characterized by distinct absorption bands at 3231, 1635, and 1596 cm^{-1}, corresponding to the stretching vibrations of N–H, C=O, and C=N functional groups, respectively [13]. Upon coordination with the Dy(III) ion, significant shifts in these bands are observed in complexes **9** and **12**, reflecting changes in the aroylhydrazone's bonding environment. In complex **9**, these bands shift to 3206, 1611, and 1559 cm^{-1}, whereas in complex **12**, they appear at 3444, 1611, and 1577 cm^{-1}. The lowering of the C=O and C=N stretching frequencies indicates that the ligand binds to the metal centre through both the carbonyl oxygen and the azomethine nitrogen atoms. Additionally, new absorption bands emerging at 543 and 415 cm^{-1} for complex **9**, and at 537 and 421 cm^{-1} for complex **12**, which are assigned to the M–O and M–N stretching vibrations [15].

The presence of acetate ions in complexes **7**, **8**, **9**, **11**, and **12** was confirmed by infrared (IR) spectroscopy. The characteristic asymmetric stretching vibration, $\nu_{as}(COO^-)$, and symmetric stretching vibration, $\nu_s(COO^-)$, of the coordinated acetate ions were observed to

overlap with the bands of aroylhydrazones. Specifically, complex **7** exhibited $\nu_{as}(COO^-)$ and $\nu_s(COO^-)$ bands at 1613 and 1400 cm^{-1}, respectively, resulting in a separation (Δ) of 213 cm^{-1}. In complex **8**, these bands appeared at 1625 and 1393 cm^{-1}, with a Δ value of 232 cm^{-1}. Complex **9** showed $\nu_{as}(COO^-)$ and $\nu_s(COO^-)$ at 1611 cm^{-1} and 1448 cm^{-1}, respectively, with a Δ of 163 cm^{-1}. In the case complex **11**, the bands were recorded at 1625 and 1394 cm^{-1}, corresponding to a Δ of 231 cm^{-1}, while complex **12** exhibited bands at 1611 and 1441 cm^{-1} with a Δ value of 170 cm^{-1}. These relatively high Δ values are indicative of monodentate coordination modes of the acetate ions within these complexes [18]. Moreover, the presence of the ν(N-H) band in both the free aroylhydrazones and their corresponding Dy(III) complexes strongly suggests that the aroylhydrazone remains predominantly in the keto form upon complexation.

The FT- IR spectral data of the Dy(III) complexes in the range 4000-400 cm^{-1} are given Table 4.3 and the corresponding spectra are presented in Figs. 4.4 to 4.9.

Table 4.3. Infrared spectral data of the Dy(III) complexes

Compound	ν(N–H) cm^{-1}	ν(C=O) cm^{-1}	ν(C=N) cm^{-1}	ν(M–O) cm^{-1}	ν(M–N) cm^{-1}
7	3347	1615	1564	547	473
8	3364	1624	1560	519	463
9	3206	1611	1559	543	415
10	3267	1615	1553	524	418
11	3363	1625	1551	515	460
12	3444	1611	1577	537	421

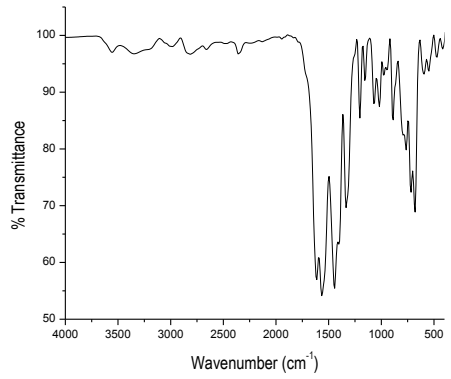

Fig. 4.4. IR spectrum of **7**

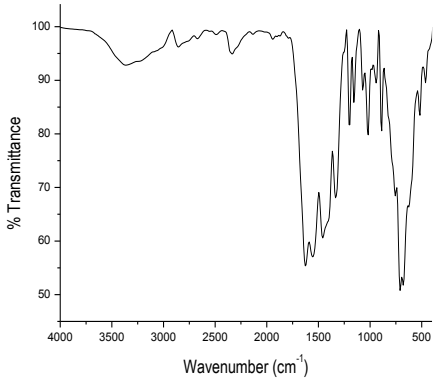

Fig. 4.5. IR spectrum of **8**

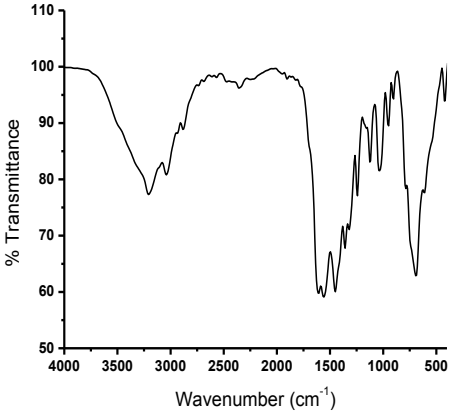

Fig. 4.6. IR spectrum of **9**

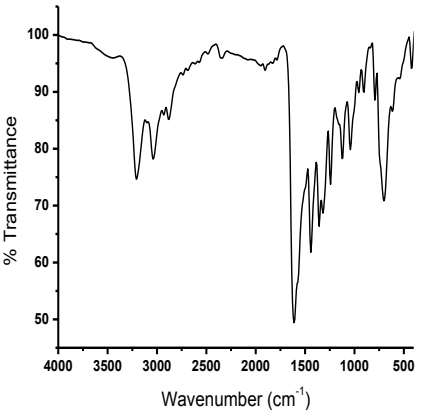

Fig. 4.7. IR spectrum of **10**

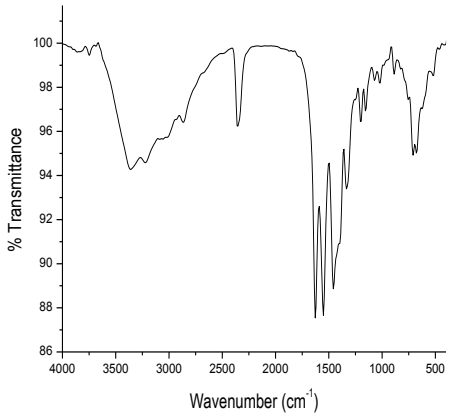

Fig. 4.8. IR spectrum of **11**

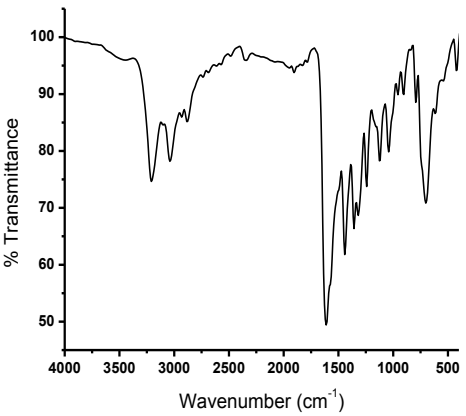

Fig. 4.9. IR spectrum of **12**

4.3.5. Electronic Spectroscopy

The UV-vis spectra of the aroylhydrazones and the Dy(III) complexes were recorded at room temperature in DMF solution (10^{-5} M). The absorption spectrum of H_2salbh exhibits the typical absorption peaks at 299, 311 and 338 nm that can be ascribed to the intra ligand charge transfer (ILCT) transitions of $\pi \rightarrow \pi^*$ and $n \rightarrow \pi^*$ types [19-21]. Upon coordination with Dy(III), a new absorption band was observed at 407 nm for complexes **7** and **10**, respectively which can be ascribed to the ligand-to-metal charge transfer (LMCT) transitions. In addition, compared to the aroylhydrazone, the bands corresponding to $\pi \rightarrow \pi^*$ and $n \rightarrow \pi^*$ transitions are slightly red sifted, clearly indicating the successful coordination of Dy(III) ion to the corresponding aroylhydrazone. Likewise, for H_2salnh, the absorption bands corresponding to ILCT transitions are observed at 299, 310 and 332 nm. And, for the corresponding complexes, **8** and **11**, the LMCT band is observed at 401 and 412 nm. The aroylhydrazone, Hindbh exhibited absorption bands at 302, 315, and 330 nm, can be ascribed to $\pi \rightarrow \pi^*$ and $n \rightarrow \pi^*$ intra-ligand transitions. Upon complexation with Dy(III), complex **9** displayed absorption bands at 302, 316, 330, and 400 nm, while complex **12** showed bands at 302, 316, 333, and 403 nm. The appearance of LMCT bands in addition to red-shifted intra-ligand transitions further confirms successful coordination of the Dy(III) ion with the aroylhydrazone, Hindbh [22,23].

UV-visible spectral data of the Dy(III) complexes in DMF (10^{-5} M) are given in Table 4.4 and the corresponding spectra are presented in Figs. 4.10-4.13.

Table 4.4. UV-visible spectral data of Dy(III) complexes in DMF (10^{-5} M)

Compound	Electronic spectral bands (nm)	Assignment
7	303, 315, 330, 407	$\pi\rightarrow\pi^*$, $n\rightarrow\pi^*$, LMCT transitions
8	302, 315, 330, 401	$\pi\rightarrow\pi^*$, $n\rightarrow\pi^*$, LMCT transitions
9	302, 316, 330, 400	$\pi\rightarrow\pi^*$, $n\rightarrow\pi^*$, LMCT transitions
10	301, 315, 332, 407	$\pi\rightarrow\pi^*$, $n\rightarrow\pi^*$, LMCT transitions
11	319, 331, 342, 412	$\pi\rightarrow\pi^*$, $n\rightarrow\pi^*$, LMCT transitions
12	302, 316, 333, 403	$\pi\rightarrow\pi^*$, $n\rightarrow\pi^*$, LMCT transitions

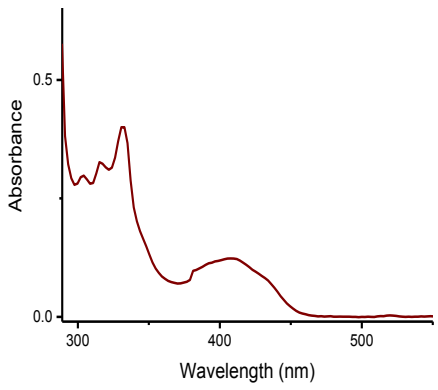

Fig. 4.10. UV-vis spectrum of **7**

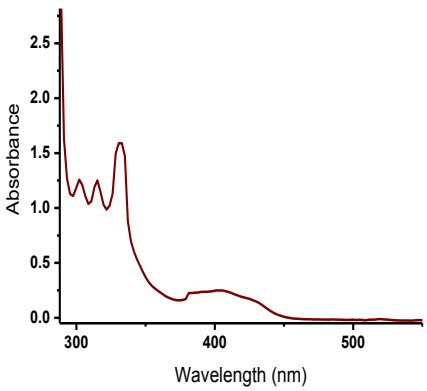

Fig. 4.11. UV-vis spectrum of **8**

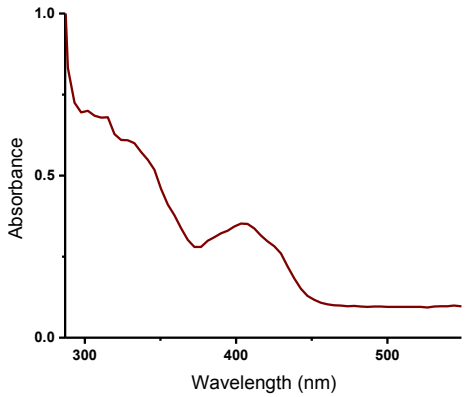

Fig. 4.12. UV-vis spectrum of **9**

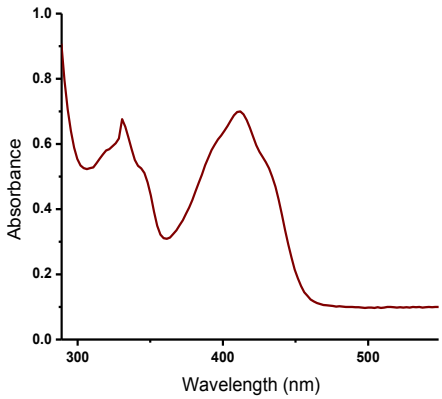

Fig. 4.13. UV-vis spectrum of **10**

4.4. Conclusion

In this chapter, a series of dysprosium(III) complexes were successfully synthesized using aroylhydrazones, H_2salbh, H_2salnh, and Hindbh, as primary ligands, and L-histidine as a co-ligand. The synthetic procedures yielded stable, yellow-colored complexes with good solubility in polar aprotic solvents, confirming their practical utility for further physicochemical and biological investigations.

Comprehensive characterization was carried out using elemental analysis, molar conductance, FT-IR, UV–visible spectroscopy, and mass spectrometry. The elemental analysis results were in close agreement with the theoretical values, verifying the proposed molecular formulae. The molar conductivity data suggested the non-electrolytic nature in all complexes, indicating the absence of free ions in solution.

Spectroscopic studies confirmed the coordination of Dy(III) to the aroylhydrazones. FT-IR analysis demonstrated shifts in key functional group vibrations (C=N, C=O, and N–H), alongside the appearance of new M–O and M–N bands, supporting coordination through oxygen and nitrogen donor atoms. UV-visible spectra exhibited characteristic ligand-to-metal charge transfer (LMCT) bands, further validating successful complex formation. Mass spectrometry corroborated the expected molecular structures, with each complex displaying distinct molecular ion peaks corresponding to their formulations. The coordination behaviour of the ligands varied with their structure: while H_2salbh and H_2salnh acted as tridentate ONO donors, Hindbh functioned as a bidentate ligand.

Overall, this study demonstrates the effective design and synthesis of new Dy(III) complexes with structurally diverse aroylhydrazones, offering valuable insights into their coordination chemistry and laying the groundwork for future studies in photoluminescence, or biomedical applications.

References

1 Balaram, V., 2019. Rare earth elements: A review of applications, occurrence, exploration, analysis, recycling, and environmental impact. *Geoscience Frontiers*, *10*(4), pp. 1285-1303.

2 Paderni, D., Giorgi, L., Fusi, V., Formica, M., Ambrosi, G. and Micheloni, M., 2021. Chemical sensors for rare earth metal ions. *Coordination Chemistry Reviews*, *429*, p. 213639.

3 Punia, M., Bedi, M., Dua, N., Chhillar, P., Taxak, V.B., Khatkar, S.P. and Doon, P.B., 2023. Investigation into photoluminescence possessions of cool white light emanating novel Dy^{3+} complexes with *β*-ketoester antenna for advanced photonic devices. *Journal of Photochemistry and Photobiology A: Chemistry*, *435*, p. 114301.

4 Nair, Y.S., Venkataraman, S.K., Joy, F., Krishna, P.M., Agarwal, A.K., Vinod, T.P., Madathil, P.K. and Kurup, M.P., 2020. Synthesis, spectral and DNA/Protein binding evaluation of novel Cu(II) chelates of an NNO donor tridentate aroylhydrazone: Halogen bonding directed close packing. *Journal of Molecular Structure*, *1217*, p. 128453.

5 Sheeja, S.R., Mangalam, N.A., Sithambaresan, M., Kurup, M.P., Kaya, S. and Serdaroğlu, G., 2021. Spectral studies and quantum chemical *ab initio* calculations for Copper(II) complexes of two heterocyclic aroylhydrazones. *Journal of Molecular Structure*, *1245*, p. 131001.

6 Mangalam, N.A., Kurup, M.P., Suresh, E., Kaya, S. and Serdaroğlu, G., 2021. Diversities in the chelation of aroylhydrazones towards cobalt(II) salts: synthesis, spectral characterization, crystal structure and some theoretical studies. *Journal of Molecular Structure*, *1232*, p. 129978.

7 Kuriakose, D. and Kurup, M.P., 2020. Mononuclear and binuclear dioxidomolybdenum(VI) complexes of ONO appended aroylhydrazone: Crystal structures, interaction energy calculation and cytotoxicity. *Journal of Molecular Structure*, *1204*, p. 127467.

8 Özbek, F.E.Ö., Uğurlu, G., Kalay, E., Necefoğlu, H. and Hökelek, T., 2021. Theoretical and experimental assesment of structural, spectroscopic, electronic and nonlinear optical properties of two

aroylhydrazone derivative. *Journal of Molecular Structure*, *1223*, p. 128982.

9 Devi, R., Bala, M., Khatkar, S.P., Taxak, V.B. and Boora, P., 2016. Investigations of luminescent behavior and intramolecular energy transfer mechanism of europium(III) complexes with fluorinated *β*-ketoester ligand. *Journal of Fluorine Chemistry*, *181*, pp. 36-44.

10 Zhuravlev, K.P., Kudryashova, V.A. and Tsaryuk, V.I., 2016. Luminescence and energy transfer processes in europium and terbium complexes with 2-substituted cycloalkanones and 1,10-phenanthroline derivatives. *Journal of Photochemistry and Photobiology A: Chemistry*, *314*, pp. 14-21.

11 Yang, S., Wang, X., Hu, Z. and Guo, D., 2021. AIE and ESIPT Schiff base ligands and corresponding Eu(III) complexes: Multiple-color and fluorescence properties. *Colloids and Surfaces A: Physicochemical and Engineering Aspects*, *615*, p. 126293.

12 Raja, K., Suseelamma, A. and Reddy, K.H., 2016. Synthesis, X-ray crystal structure, DNA binding and Nuclease activity of lanthanide(III) complexes of 2-benzoylpyridine acetylhydrazone. *Journal of Chemical Sciences*, *128*(8), pp.1265-1275.

13 Pouralimardan, O., Chamayou, A.C., Janiak, C. and Hosseini-Monfared, H., 2007. Hydrazone Schiff base-manganese(II) complexes: Synthesis, crystal structure and catalytic reactivity. *Inorganica chimica acta*, *360*(5), pp. 1599-1608.

14 Anjana, T.M., Manoj, E., Naseera, C.M., Liyakhath, F.M., Thayyullathil, A., Naduparambath, S., Sheeja, S.R. and Kurup, M.P., 2025. Photophysical properties, DFT calculations and DNA binding studies of a series of deep blue emitting cerium(III) complexes. *Journal of Molecular Structure*, *1327*, p. 141186.

15 Chen, H.H., Wu, D.F., Duan, Y.Y., Li, L., Wang, Y.J., Zhang, X.M., Cui, J.Z. and Gao, H.L., 2020. The near-infrared luminescence and magnetism of dinuclear complexes with different local symmetries constructed from a *β*-diketonate co-ligand and bis-Schiff base ligand. *New Journal of Chemistry*, *44*(6), pp. 2561-2570.

16 Benković, T., Kenđel, A., Parlov-Vuković, J., Kontrec, D., Chiş, V., Miljanić, S. and Galić, N., 2018. Aromatic hydrazones derived from

nicotinic acid hydrazide as fluorimetric $_{p}$H sensing molecules: Structural analysis by computational and spectroscopic methods in solid phase and in solution. *Spectrochimica Acta Part A: Molecular and Biomolecular Spectroscopy*, *190*, pp. 259-267.

17 Khan, A., Fuhr, O., Akhtar, M.N., Lan, Y., Thomas, M. and Powell, A.K., 2020. Synthesis, characterization and magnetic studies of dinuclear lanthanide complexes constructed with a Schiff base ligand. *Journal of Coordination Chemistry*, *73*(6), pp. 1045-1054.

18 Sarkar, B., Drew, M.G., Estrader, M., Diaz, C. and Ghosh, A., 2008. Cu^{II} acetate complexes involving N, N, O donor Schiff base ligands: Mono-atomic oxygen bridged dimers and alternating chains of the dimers and $Cu_2(OAc)_4$. *Polyhedron*, *27*(12), pp. 2625-2633.

19 Bagherzadeh, M. and Amini, M., 2009. Synthesis, characterization and catalytic study of a novel iron(III)-tridentate Schiff base complex in sulfide oxidation by UHP. *Inorganic Chemistry Communications*, *12*(1), pp. 21-25.

20 Nishana, L., Sakthivel, A. and Kurup, M.R.P., 2023. Syntheses, structural characterizations, and catalytic activities of manganese(II)-aroylhydrazone complexes. *Journal of Molecular Structure*, *1281*, p. 135128.

21 Krishnamoorthy, P., Sathyadevi, P., Muthiah, P.T. and Dharmaraj, N., 2012. Nickel and cobalt complexes of benzoic acid (2-hydroxy-benzylidene)-hydrazide ligand: synthesis, structure and comparative in vitro evaluations of biological perspectives. *RSC Advances*, *2*(32), pp.12190-12203.

22 Jayendran, M. and Kurup, M.P., 2022. Structural, spectral, cytotoxic and biocatalytic studies of a dinuclear phenoxo bridged Zn(II) complex from NNO donor tridentate Schiff base. *Chemical Data Collections*, *39*, p. 100853.

23 Nishana, L., Sakthivel, A., Kurup, M.P., Damodaran, K.K., Kulandaisamy, A. and Maheswaran, S., 2023. Synthesis, spectral characterization, and catalytic efficiency of aroylhydrazone-based Cu(II) complexes. *New Journal of Chemistry*, *47*(44), pp. 20626-20641.

CHAPTER 5

SYNTHESIS AND CHARACTERIZATION OF A SERIES OF GADOLINIUM(III) COMPLEXES DERIVED FROM SALICYLALDEHYDE BENZOYLHYDRAZONE, SALICYLALDEHYDE NICOTINOYLHYDRAZONE AND INDOLE-3-CARBALDEHYDE BENZOYLHYDRAZONE

5.1. Introduction

Gadolinium(III) complexes have attained significant attention in recent years due to their exciting photophysical and magnetic properties. These complexes have numerous applications across various fields of chemistry, particularly in medicinal inorganic chemistry. They are widely used as a contrast agent in magnetic resonance imaging (MRI) due to their exceptional paramagnetic characteristics [1,2]. Additionally, their unique photoluminescent properties make them suitable candidates for designing optical devices, displays, sensors, and superconductors [3,4].

Among the Schiff base ligands, aroylhydrazones represent an important class of organic compounds capable of forming stable coordination compounds with both transition and inner transition metal ions [5,6]. The tendency of inner transition metal ions, such as Gd(III), to adopt high coordination numbers is suitably supported by the versatile binding environment offered by this class of compounds. The biological activities and other applications exhibited by aroylhydrazones stem from their azomethine functionality [7-9]. Notably, when a second organic ligand, such as L-histidine, is introduced into the coordination sphere, these properties are significantly enhanced [10,11]. This chapter deals with the preparation and characterization of gadolinium(III) complexes of aroylhydrazones derived from salicylaldehyde benzoylhydrazone, salicylaldehyde nicotinoylhydrazone, indole-3-carbaldehyde benzoylhydrazone, and the co-ligand L-Histidine.

5.2. Experimental

5.2.1. Materials

$Gd(OAc)_3 \cdot H_2O$ and L-Histidine were procured from Sigma Aldrich. Solvents, including N,N-dimethylformamide (DMF), methanol, acetic acid, and ether, were obtained from commercial suppliers and were used without additional purification.

5.2.2. Synthesis of ligands

Chapter 2 explains the method of preparation and characterization of the aroylhydrazones, H_2salbh, H_2salnh and Hindbh.

5.2.3. Synthesis of Gd(III) complexes

Gadolinium(III) complexes were synthesized using the aroylhydrazones, H_2salbh, H_2salnh and Hindbh as the primary ligands and L-histidine as the coligand (Scheme 5.1).

5.2.3.1. Synthesis of [Gd(Hsalbh)$_2$(OAc)(H$_2$O)] (13)

$Gd(OAc)_3 \cdot H_2O$ (1 mmol, 0.352 g) was dissolved in methanol (10 mL) and was added to the methanolic solution of H_2salbh (0.240 g, 1 mmol). The resulting solution was refluxed in a water bath for 4 hours. After cooling, the pale-yellow colored precipitate of **13** was filtered off, washed with methanol followed by ether, and then dried. Yield: (0.7128 g) 61.2%. λ_m(DMF): 12 $ohm^{-1}m^2mol^{-1}$. μ: 7.9 B.M. Elemental Anal. Found (Calcd) %: C: 50.88 (50.55); H: 3.64 (3.82); N:

7.98 (7.86) for [Gd(Hsalbh)$_2$(OAc)(H$_2$O)]. MALDI-TOF-MS *m/z* 798.20 [M+3H$_2$O+CH$_3$OH]$^+$, (Calcd 798.89).

5.2.3.2. Synthesis of [Gd(Hsalnh)$_2$(OAc)(H$_2$O)] (14)

The complex **14** was synthesized with the similar method as that of **13**, using H$_2$salnh (0.241 g, 1 mmol) instead of H$_2$salbh. The mixture was then refluxed for 4 hours. Then, the dark yellow colored precipitate was washed with methanol, followed by ether, and air-dried. Yield: (0.7148 g) 58.5%. λ_m(DMF): 10 ohm^{-1}cm^{2}mol^{-1}. μ: 7.9 B.M. Elemental Anal. Found (Calcd) %: C: 47.23 (47.05); H: 3.84 (3.53); N: 11.42 (11.76) for [Gd(Hsalnh)$_2$(OAc)H$_2$O]. MALDI-TOF-MS *m/z* 715.68 [M+H]$^+$, (Calcd 715.78).

5.2.3.3. Synthesis of [Gd(Hindbh(OAc)$_3$(H$_2$O)$_3$] (15)

Hindbh (0.263 g, 1 mmol) was dissolved in 10 mL of methanol and mixed with a 10 mL methanolic solution of Gd(OAc)$_3$·H$_2$O (0.352 g, 1 mmol). The resulting mixture was heated under reflux in a water bath for 4 hours. After allowing the reaction mixture to cool to room temperature, a pale-yellow precipitate of complex **15** was formed. The product was collected by filtration, washed thoroughly with methanol followed by diethyl ether, and dried in air. Yield: (0.6517 g) 65.3%. λ_m(DMF): 14 ohm^{-1}cm^{2}mol^{-1}. μ: 7.8 B.M. Elemental Anal. Found (Calcd) %: C: 40.42 (40.54); H: 4.12 (4.33); N: 6.31 (6.45) for [Gd(Hindbh(OAc)$_3$(H$_2$O)$_3$]. (MALDI-TOF-MS *m/z* 727.85 [M+3H$_2$O+Na-H]$^+$, (Calcd 727.75)

5.2.3.4. Synthesis of [Gd(Hsalbh)$_2$his] (16)

The aroylhydrazone, H_2salbh (0.241 mg, 1 mmol), was dissolved in 10 mL of methanol. To this solution, a methanolic solution of $Gd(OAc)_3 \cdot H_2O$ (0.352 g, 1 mmol) and a methanolic solution of L-histidine (0.155 g, 1 mmol) were added. The reaction mixture was refluxed in a water bath for 4 hours. The resulting pale-yellow precipitate was washed with methanol, followed by ether, and air-dried. Yield: (0.7899 g) 55.3%. λ_m(DMF): 7 $ohm^{-1}cm^2mol^{-1}$. μ: 7.7 B.M. Elemental Anal. Found (Calcd) %: C: 51.54 (51.70); H: 3.42 (3.83); N: 12.11 (12.41) $[Gd(Hsalbh)_2his] \cdot 3H_2O$. MALDI-TOF-MS *m/z* 946.05 $[M+H_2O+AcOH+Na+H]^+$, (Calcd 945.99).

5.2.3.5. Synthesis of [Gd(Hsalnh)$_2$his] (17)

Complex **17** was synthesized by a method similar to that of complex **16**, using H_2salnh (0.241 g, 1 mmol) instead of H_2salbh. Pale yellow colored precipitate was washed with methanol, followed by ether, and air-dried. Yield: (0.7919 g) 44.4%. λ_m(DMF): 9 $ohm^{-1}cm^2mol^{-1}$. μ: 7.9 B.M. Elemental Anal. Found (Calcd) %: C: 48.75 (48.54); H: 3.24 (3.56); N: 15.64 (15.92) for $[Gd(H_2salnh)_2his]$. MALDI-TOF-MS *m/z* 982.53 $[M+6H_2O+AcOH+Na]^+$, (Calcd 983.00).

5.2.3.6. Synthesis of [Gd(Hindbh)(his)$_2$(OAc)H$_2$O] (18)

A solution of Hindbh (0.263 g, 1 mmol) in methanol (10 mL) was added to a methanolic solution (10 mL) containing $Gd(OAc)_3 \cdot H_2O$ (0.352 g, 1 mmol) and L-histidine (0.155 g, 1 mmol). The resulting reaction mixture was refluxed in a water bath for 4 hours. Upon

cooling to room temperature, a pale-yellow precipitate of complex **18** was obtained. The product was collected by filtration, washed successively with methanol and diethyl ether, and dried in air. Yield: (0.8059 g) 55.2%. λ_m(DMF): 15 ohm^{-1}cm^{2}mol^{-1}. μ: 7.8 B.M. Elemental Anal. Found (Calcd) %: C: 44.89 (44.71); H: 4.15 (4.25); N: 15.11 (15.64) for [Gd(Hindbh)(his)$_2$(OAc)H$_2$O]. (MALDI-TOF-MS *m/z* 923.58 [M +3H$_2$O+2(CH$_3$OH)]$^+$, (Calcd 924.02).

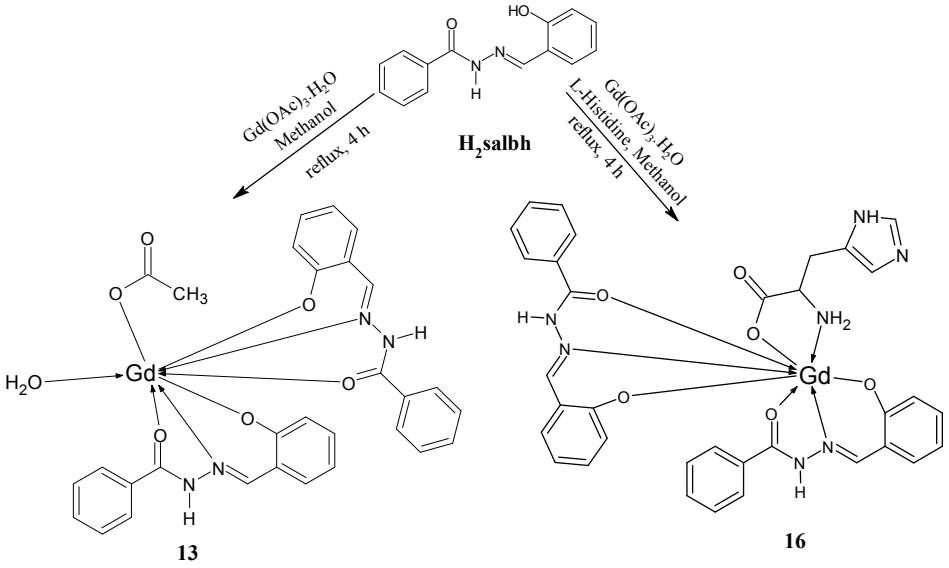

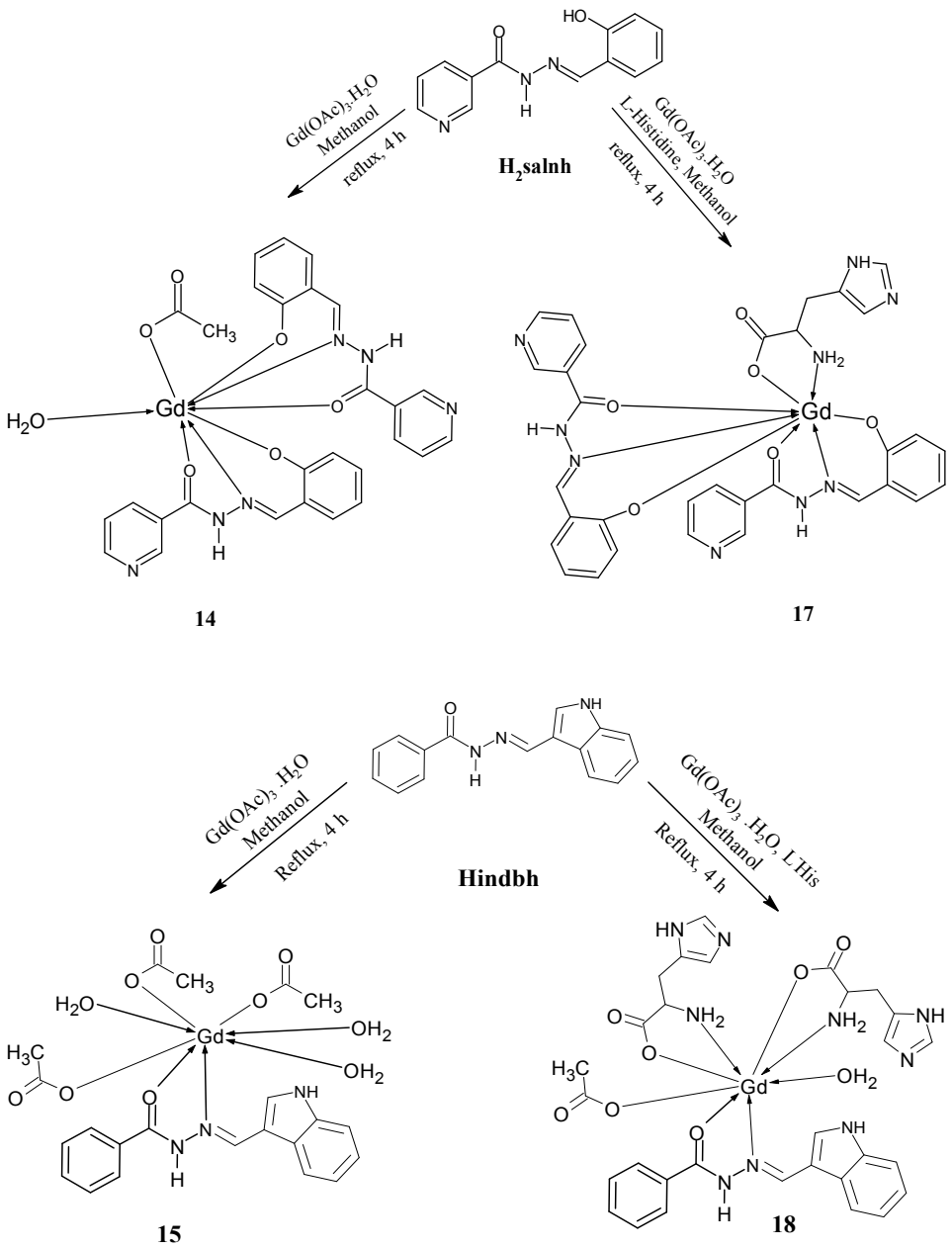

Scheme 5.1. Synthesis of gadolinium(III) complexes

5.3. Results and Discussion

The gadolinium(III) complexes, **13**, **14**, and **15**, were synthesized by the reaction of $Gd(OAc)_3 \cdot H_2O$ with the respective aroylhydrazones, H_2salbh, H_2salnh and Hindbh, in a 1:1 molar ratio in methanol. Complexes **16**, **17**, and **18** were prepared using a similar procedure, with the addition of L-histidine as a co-ligand, maintaining a 1:1:1 metal-to-ligand-to-coligand ratio in methanol. All six Gd(III) complexes were obtained as yellow-colored solids, which were stable at room temperature and showed good solubility in dipolar aprotic solvents, such as DMF and DMSO.

The synthesized Gd(III) complexes were characterized by partial elemental analysis, molar conductance, FT-IR, UV-visible spectroscopy, and mass spectrometry. The combined spectral and analytical data confirmed the successful formation of the complexes. Coordination behaviour studies revealed that H_2salbh and H_2salnh act as tridentate ligands through ONO donor atoms, while Hindbh functions as a bidentate ligand, coordinating through the azomethine nitrogen and carbonyl oxygen atom. In the complexes **16**–**18**, L-histidine coordinates through its amino and carboxylate groups, contributing to a more extended and stable coordination environment around the Gd(III) ion.

5.3.1. Partial Elemental analysis

The CHN data of the Gd(III) complexes of aroylhydrazones are outlined in Tables 5.1. The calculated and the observed data are showing good correlation with one another.

Table 5.1. The compositional details of the synthesized Gd(III) complexes

Compound	Empirical formula	Formula Weight (g/mol)	Color (Yield %)	Found (Calcd %)		
				C	**H**	**N**
13	$C_{30}H_{27}GdN_4O_7$	712.80	Pale yellow 61.2	50.88 (50.55)	3.64 (3.82)	7.98 (7.86)
14	$C_{28}H_{25}GdN_6O_7$	714.78	Dark yellow 58.5	(47.23) 47.05	(3.84) 3.53	(11.42) 11.76
15	$C_{22}H_{28}GdN_3O_{10}$	651.72	Pale yellow 65.3	40.42 (40.54)	4.12 (4.33)	6.31 (6.45)
16	$C_{34}H_{30}GdN_7O_6$	789.89	Pale yellow 55.3	51.54 (51.70)	3.42 (3.83)	12.11 (12.41)
17	$C_{32}H_{28}GdN_9O_6$	791.87	Pale yellow 44.4	48.75 (48.54)	3.24 (3.56)	15.64 (15.92)
18	$C_{30}H_{34}GdN_9O_8$	805.89	Pale yellow 55.2	44.89 (44.71)	4.15 (4.25)	15.11 (15.64)

5.3.2. Conductivity measurements

The molar conductance of all the Gd(III) complexes are measured in DMF and are listed in Table 5.2. The values range from 7-15 $ohm^{-1}cm^2mol^{-1}$and thus the Gd(III) complexes can be regarded as non-electrolytes.

Table 5.2. The molar conductance of the Gd(III) complexes

Compound	Molar Conductance ($ohm^{-1}cm^2mol^{-1}$)
13	12
14	10
15	14
16	7
17	9
18	15

5.3.3. Mass Spectrometry

Mass spectra of the synthesized Gd(III) complexes were recorded in DMF solution using a MALDI time-of-flight (TOF) Bruker Autoflex max LRF mass spectrometer, which serves as an essential technique for the characterization and identification of metal complexes. The mass spectrum of compound **13** exibits a molecular ion peak at *m/z* 798.20, corresponding to $[M+3H_2O+CH_3OH]^+$, while compound **14** showed a peak at *m/z* 715.68, assigned to $[M+H]^+$. For compound **15**, the peak appeared at *m/z* 727.85, which corresponds to $[M+3H_2O+Na–H]^+$. Compound **16** exhibited a peak at *m/z* 946.05,

attributed to [M+H_2O+AcOH+Na+H]. Similarly, compound **17** showed a molecular ion peak at *m/z* 982.54, assigned to [M+6H_2O+AcOH+Na]$^+$. For compound **18**, the molecular ion peak was observed at *m/z* 923.58, assigned to [M+3H_2O+2(CH_3OH)].

5.3.4. FT-IR Spectroscopy

The FT-IR spectra of the aroylhydrazones and their Gd(III) complexes were recorded over the range of 4000-400 cm^{-1}, comparative analysis of the FT-IR spectra of Gd(III) complexes with aroylhydrazones helps to identify the binding modes and coordination sites present in these complexes. The FT-IR spectra of the aroylhydrazones, H_2salbh and H_2salnh, exhibit intense broad bands at 3500 and 3501 cm^{-1}, respectively, which corresponds to the stretching vibrations of the –OH group [12].

In the FT-IR spectrum of H_2salbh, ν(N–C=O) band was observed at 1677 cm^{-1} [13,14]. For complexes **13** and **16**, these absorption bands shifted to lower frequencies, appearing at 1615 and 1614 cm^{-1}, respectively. This shift indicates the coordination of carbonyl oxygen to the Gd(III) ion. Additionally, an important band corresponding to ν(C=N) appeared at 1622 cm^{-1} was also moved to a lower frequency region upon coordination [14,15]. In complex **13**, this band was observed at 1547 cm^{-1}, while in complex **16**, it was at 1563 cm^{-1}. Furthermore, the emergence of new bands corresponding to ν(M–O) and ν(M–N) at 595 and 446 cm^{-1} in complex **13**, as well as at 522 and 419 cm^{-1} in complex **16**, clearly demonstrates the successful coordination of Gd(III) ion with aroylhydrazone [14,16].

In the case of H_2salnh, the ν(N–C=O) and ν(C=N) bands were seen at 1700 and 1585 cm^{-1} respectively [14]. In the spectrum of complex **14**, these bands shifted to 1619 and 1553 cm^{-1} respectively. A similar trend was also seen in the case of complex **17**, where the ν(N-C=O) and ν(C=N) appeared at 1626 and 1552 cm^{-1} [14,17]. This observation indicates the involvement of azomethine nitrogen and carbonyl oxygen in metal coordination. Additionally, the formation of new bands corresponding to ν(M–O) and ν(M–N) at 519 and 450 cm^{-1} for complex **14**, and at 531 and 426 cm^{-1} for complex **17**, further supports this finding [14,18].

The analysis of the IR spectrum provides compelling evidence for the presence of acetate ions within complexes **13**, **14**, **15** and **18**. This is particularly evident in the observation of the asymmetric stretching vibration $\nu(COO^-)_{as}$ and the symmetric stretching vibration $\nu(COO^-)_s$ of the coordinated acetate ions, both of which overlap with the characteristic bands associated with aroylhydrazones [19]. For complex **13**, the $\nu(COO^-)_{as}$ band is clearly detected at a wavelength of 1614 cm^{-1}, while in complex **14**, this band is observed slightly higher at 1619 cm^{-1}. In addition to this, the $\nu(COO^-)_s$ bands corresponding to the symmetric stretching vibrations are recorded at 1393 cm^{-1} for complex **13** and at 1386 cm^{-1} for complex **14**, providing further confirmation of the acetate [19]. The calculated separation between the two stretching frequencies (denoted as Δ) is found to be 221 cm^{-1} for complex **13** and 233 cm^{-1} for complex **14** with the metal centre in the complex. In complex **15**, the $\nu(COO^-)_{as}$ and $\nu(COO^-)_s$ bands were found at 1614 and 1400 cm^{-1}, respectively, with a Δ value of 214 cm^{-1}. For complex **18**, these bands were recorded at 1611 cm^{-1} and 1448

cm^{-1}, respectively, giving a Δ value of 163 cm^{-1}. This high difference in Δ values suggests a stronger indication of monodentate acetate coordination modes for these complexes. Furthermore, the presence of the *ν*(N-H) band in the hydrazones and their corresponding Gd(III) complexes suggests that the ligand retains its keto form upon coordination. These observations further support the presence and mode of coordination of acetate ions in the complexes [20,21]. The FT-IR spectral data of the Gd(III) complexes in the range of 4000-400 cm^{-1} are presented in Table 5.3, with the corresponding spectra illustrated in Figs. 5.1 to 5.4.

Table 5.3. Infrared spectral data of the Gd(III) complexes

Compound	*ν*(N–H) cm^{-1}	*ν*(C=O) cm^{-1}	*ν*(C=N) cm^{-1}	*ν*(M–O) cm^{-1}	*ν*(M–N) cm^{-1}
13	3202	1615	1547	595	446
14	3009	1619	1553	519	450
15	3208	1618	1559	537	415
16	3198	1614	1563	522	419
17	3231	1626	1552	531	426
18	3209	1610	1570	543	421

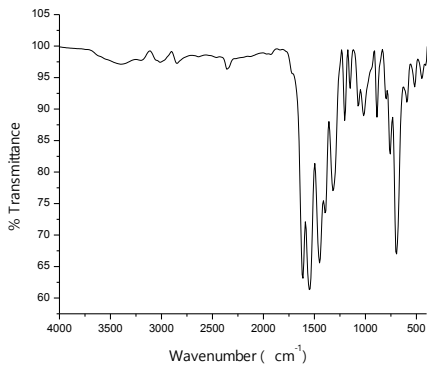

Fig. 5.1. IR spectrum of **13**

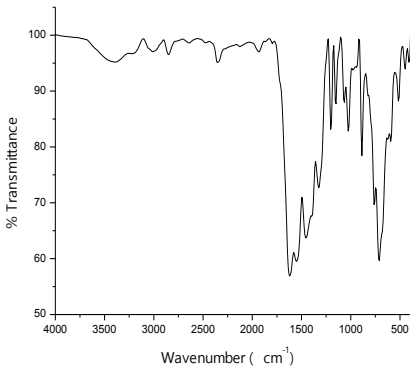

Fig. 5.2. IR spectrum of **14**

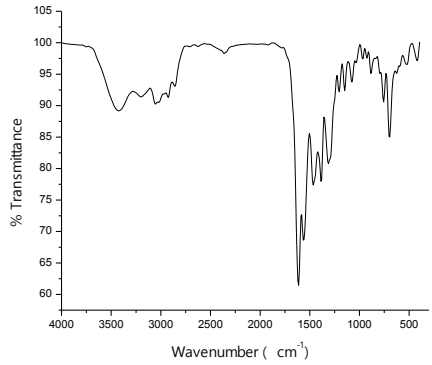

Fig. 5.3. IR spectrum of **16**

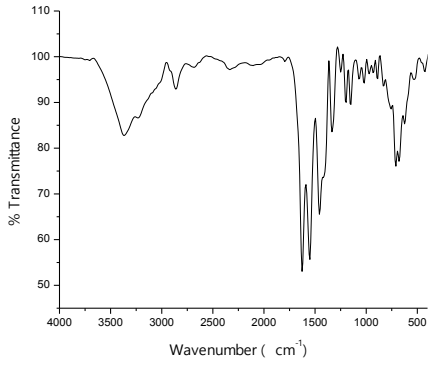

Fig. 5.4. IR spectrum of **17**

5.3.5. Electronic Spectroscopy

The UV-vis absorption spectra of the aroylhydrazones and the Gd(III) complexes were recorded at room temperature in DMF solution (10^{-5} M) and are shown in Figs. 5.5 to 5.8. The spectral data is summarized in Table 5.4. The aroylhydrazones exhibit absorption bands in the range of 299 to 338 nm, corresponding to the $\pi \rightarrow \pi^*$ transitions of the aromatic rings, as well as the $n \rightarrow \pi^*$ transitions of the non-bonding electrons present in the nitrogen atom of the azomethine group and oxygen atom of the C=O group. In the case of Gd(III) complexes, an additional absorption band is observed in the range 388-410 nm, along with the $\pi \rightarrow \pi^*$ and $n \rightarrow \pi^*$ transitions. This new absorption band can be primarly due to the intraligand charge transfer transitions [22].

Table 5.4. UV-visible spectral data of Gd(III) complexes in DMF (10^{-5} M)

Compound	Electronic spectral bands (nm)	Assignment
13	285, 296, 326, 336, 388	$\pi\rightarrow\pi^*$, $n\rightarrow\pi^*$, intraligand charge transfer transitions
14	303, 315, 332, 405	$\pi\rightarrow\pi^*$, $n\rightarrow\pi^*$, intraligand charge transfer transitions
15	304, 316, 334, 400	$\pi\rightarrow\pi^*$, $n\rightarrow\pi^*$, intraligand charge transfer transitions
16	301, 314, 330, 408	$\pi\rightarrow\pi^*$, $n\rightarrow\pi^*$, intraligand charge transfer transitions
17	300, 318, 331, 410	$\pi\rightarrow\pi^*$, $n\rightarrow\pi^*$, intraligand charge transfer transitions
18	300, 314, 330, 401	$\pi\rightarrow\pi^*$, $n\rightarrow\pi^*$, intraligand charge transfer transitions

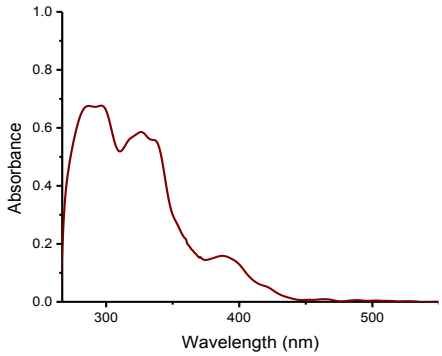

Fig. 5.5. UV-vis spectrum of **13**

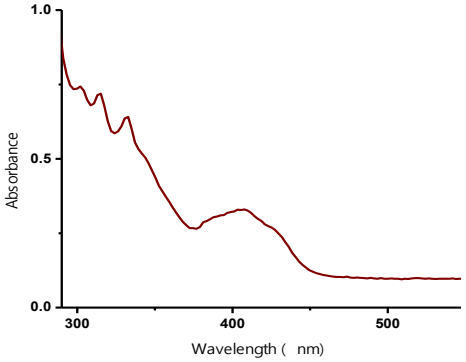

Fig. 5.6. UV-vis spectrum of **14**

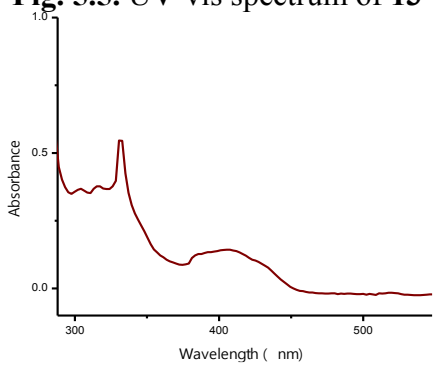

Fig. 5.7. UV-vis spectrum of **16**

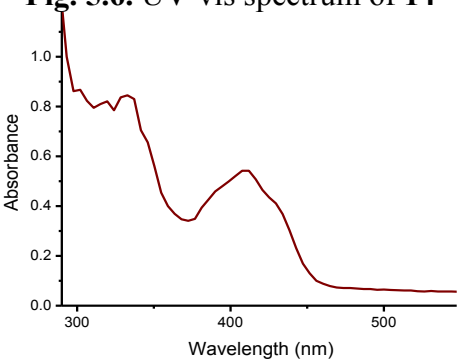

Fig. 5.8. UV-vis spectrum of **17**

5.4. Conclusion

The investigations presented in this chapter focused on the synthesis and characterization of six Gadolinium(III) complexes using aroylhydrazones, H_2salbh, H_2salnh, and Hindbh, as primary ligands and L-histidine as a co-ligand. The successful formation of these complexes was confirmed by a combination of analytical techniques including elemental analysis, molar conductance measurements, FT-IR, UV–vis spectroscopy, and MALDI-TOF mass spectrometer.

Spectroscopic evidence indicates that H_2salbh and H_2salnh function as tridentate ligands, coordinating to the Gd(III) ion through ONO donor atoms, while Hindbh coordinates in a bidentate mode. In ternary complexes, L-histidine was found to coordinate through both amino and carboxylate donor sites, contributing to enhanced coordination geometry and stability of the resulting complexes.

Infrared spectral data supported metal–ligand coordination through azomethine nitrogen and carbonyl oxygen, with characteristic shifts in stretching frequencies. UV–vis spectra showed intraligand charge-transfer transitions indicative of ligand-metal interactions. The mass spectra validated the proposed molecular formulations, while the low molar conductance values clearly demonstrates the non-electrolytic nature of all complexes. Overall, the results demonstrate the versatility of aroylhydrazones in forming stable Gd(III) complexes.

References

1. Pilichos, E., Font-Bardia, M., Escuer, A. and Mayans, J., 2021. Structural and magnetic studies of mononuclear lanthanide complexes derived from N-rich chiral Schiff bases. *Dalton Transactions*, 50(5), pp. 1746–1753.

2. Liao, H., Wang, Z., Chen, S., Wu, H., Ma, X. and Tan, M., 2015. One-pot synthesis of gadolinium(III) doped carbon dots for fluorescence/magnetic resonance bimodal imaging. *RSC Advances*, 5, pp. 66575–66581.

3. Moulick, A., Heger, Z., Milosavljevic, V., Richtera, L., Barroso-Flores, J., Merlos Rodrigo, M.A., Buchtelova, H., Podgajny, R., Hynek, D., Kopel, P. and Adam, V., 2018. Real-time visualization of cell membrane damage using gadolinium–Schiff base complex-doped quantum dots. *ACS Applied Materials & Interfaces*, 10, pp. 35859–35868.

4. da Silveira, C.O., Oliveira, W.X., da Silva Júnior, E.N., Alvarenga, M.E., Martins, F.T., Gatto, C.C., Pinheiro, C.B., Pedroso, E.F., Silva, J.P., Marques, L.F. and Santos, M.V., 2024. Photoluminescence and magnetic properties of isostructural europium(III), gadolinium(III) and terbium(III) oxamate-based coordination polymers. *Dalton Transactions*, 53, pp. 14995–15009.

5. Reshma, P.R., Tom, L., Dhanya, N.P., Hussan, K.S., Raphael, V.P., Bhagyesh, V.B. and Joseph, B., 2025. Two novel Aroyl Hydrazones from 4-methoxybenzhydrazide: comprehensive study including synthesis, X-ray crystallography, DFT analysis, antibacterial activity and molecular docking. *Journal of Molecular Structure*, *1335*, p. 141866.

6. Nishana, L., Sakthivel, A. and Kurup, M.R.P., 2023. Syntheses, structural characterizations, and catalytic activities of manganese(II)-aroylhydrazone complexes. *Journal of Molecular Structure*, *1281*, p. 135128.

7. Tafere, D.A., Gebrezgiabher, M., Elemo, F., Atisme, T.B., Ashebr, T.G. and Ahmed, I.N., 2024. Hydrazones, hydrazone-based coinage metal complexes, and their biological applications. *RSC Advances*, 15, pp. 6191–6207.

8. Kaczmarek, M.T., Zabiszak, M., Nowak, M. and Jastrzab, R., 2018. Lanthanides: Schiff base complexes, applications in cancer diagnosis, therapy, and antibacterial activity. *Coordination Chemistry Reviews*, *370*, pp. 42-54.

9. Banerjee, S., Selim, M., Saha, A. and Mukherjea, K.K., 2019. Radiation induced DNA damage and its protection by a gadolinium(III) complex: spectroscopic, molecular docking and gel electrophoretic studies. International Journal of Biological Macromolecules, 127, pp. 520–528.

10. Tüfekyapan, T., Bastemur, G.Y., Bıçak, B., Akpinar, R., Sanli, N.O., Gündüz, S.K., Ozkorucuklu, S.P. and Karipcin, F., 2025. Syntheses of new ternary complexes with 1-benzoyl-3-(benzimidazoyl) thiourea) and amino acids: Experimental, theoretical, electrochemical, antioxidant, antibacterial, and molecular docking studies. *Inorganic Chemistry Communications*, *173*, p. 113859.

11. Kumaravel, G., Utthra, P.P. and Raman, N., 2018. Exploiting the biological efficacy of benzimidazole based Schiff base complexes with L-histidine as a co-ligand: Combined molecular docking, DNA interaction, antimicrobial and cytotoxic studies. *Bioorganic Chemistry*, 77, pp. 269–279.

12. Silverstein, R.M. and Bassler, G.C., 1962. Spectrometric identification of organic compounds. *Journal of Chemical Education*, 39(11), p. 546.

13. L.K. Nishana, A. Sakthivel, M.R.P. Kurup, K.K. Damodaran, A. Kulandaisamy, M. Sithambaresan, Synthesis, spectral characterization and catalytic efficiency of Cu(II) complexes of tridentate aroylhydrazones containing NNO donors, New J. Chem. 47 (2023) 20626 – 20641.

14. Anjana, T.M., Manoj, E., Naseera, C.M., Liyakhath, F.M., Thayyullathil, A., Naduparambath, S., Sheeja, S.R. and Kurup, M.P., 2025. Photophysical properties, DFT calculations and DNA binding studies of deep blue emitting cerium(III) complexes. *Journal of Molecular Structure*, 1327, p. 141186.

15. A.A. Aravindakshan, N. Mohan, M.R.P. Kurup, S. Erkan, S. Kaya, E. Manoj, Mononuclear and binuclear dioxidomolybdenum(VI) chelates derived from a tridentate ONO donor aroylhydrazone: Spectral, structural, DFT and *in silico* biological investigations, Polyhedron 256 (2024) 116998.

16. Sogukomerogullari, H.G., Başaran, E., Kepekçi, R.A., Türkmenoğlu, B., Sarıoğlu, A.O. and Köse, M., 2025. Novel europium(III), terbium(III), and gadolinium(III) Schiff base complexes: Synthesis, structural, photoluminescence, antimicrobial, antioxidant, and molecular docking studies. *Polyhedron*, *265*, p. 117275.

17. M. Kuriakose, M.R.P. Kurup, E. Suresh, Spectral characterization and crystal structure of 2-benzoylpyridine nicotinoyl hydrazone Spectrochim. Acta A 66 (2007) 353-358.

18. Kumari, N., Singh, S., Baral, M., Kumar, D. and Kanungo, B.K., 2024. Highly selective Gd(III) fluorimetric sensor based on thiosemicarbazone scaffold: A dual function ensemble for fluorescence and naked eye sensing of CN^- and $H_2PO_4^-$ anions. *Journal of Photochemistry and Photobiology A: Chemistry*, 454, p. 115724.

19. Xu, Y., Pan, T., Ren, G., Wang, J., Yang, H., Wang, L., Zhang, D., Sun, Y., Deng, R., Zhou, S. and Tian, L., 2024. Efficient Organic Light-Emitting Diodes Obtained by Introducing Gadolinium (Gd) Complexes Based on Pyrazolone Derivative Ligands as Hole Trappers. *ACS Applied Materials & Interfaces*, *16*(47), pp. 65100-65107.

20. Sarkar, B., Drew, M.G., Estrader, M., Diaz, C. and Ghosh, A., 2008. Cu^{II} acetate complexes involving N, N, O donor Schiff base ligands: Mono-atomic oxygen bridged dimers and alternating chains of the dimers and $Cu_2(OAc)_4$. *Polyhedron*, *27*(12), pp. 2625-2633.

21. Bartyzel, A., 2017. Synthesis, thermal study and some properties of N_2O_4—donor Schiff base and its Mn(III), Co(II), Ni(II), Cu(II) and Zn(II) complexes. *Journal of Thermal Analysis and Calorimetry*, *127*(3), pp.2133-2147.

22. Harraf, E., Bikas, R., Soltani, B. and Lis, T., 2024. Synthesis, spectroscopic properties, crystal structure and Hirshfeld surface analysis of Pr(III), Sm(III), Gd(III), Dy(III), and Ho(III) coordination compounds with Schiff base ligand derived from 4-aminoantipyrine. *Journal of Molecular Structure*, *1316*, p. 139013.

CHAPTER 6

PHOTOLUMINESCENCE STUDIES OF COMPLEXES OF AROYLHYDRAZONES

6.1. Introduction

The study of luminescence began in the early 17th century with the discovery of the "Bolognian stone" by Vincenzo Cascariolo in 1603. This naturally occurring material, later identified as barium sulfate doped with metal ions such as Zn^{2+}, Sn^{2+}, or Cd^{2+}, was the first documented inorganic phosphor. Later, in 1888, the term *luminescence* was first defined by Eilhard Wiedemann to refer specifically to light that occur independently of thermal excitation [1,2].

In recent years, there has been a marked and sustained growth in the investigations of photoluminescent materials, largely driven by the increasing demand for advanced technologies across various domains. Photoluminescence plays a critical role in a wide array of applications, including solid-state lighting, high-resolution electronic displays, laser technologies, anticounterfeiting strategies, biological imaging, and fluorescent labeling. Among the many luminescent materials, lanthanide ions have attracted particular attention due to their exceptional and tunable photophysical properties, such as narrow emission bands, long-lived excited states, large Stokes shifts, and high quantum yields. These properties make them especially suitable for cutting-edge developments in bioassays, chemical and environmental sensor systems, optical data storage, and next-generation photonic and optoelectronic devices [3,4].

6.1.1. Mechanisms of lanthanide luminescence

The unique spectroscopic characteristics of lanthanide ions stem from the fact that their 4*f* orbitals have a smaller radial extension

than the outer filled $5s^2$ and $5p^6$ orbitals, which shield the 4*f* electrons from external influences. This leads to parity-forbidden 4*f*–4*f* absorptions with smaller molar absorption coefficients and prolonged luminescence lifetimes. Lanthanide compounds exhibit three primary types of optical transitions: allowed *f-d* transitions, charge-transfer transitions, and formally forbidden *f-f* transitions [5,6].

6.1.1.1. Interconfigurational $4f^n$ - $4f^n5d^1$ transitions

The 4*f*-5*d* electronic transitions, being parity-allowed, exhibit significantly greater intensity and broader spectral features compared to the parity-forbidden 4*f*–4*f* transitions, and typically occur at high energies, often exceeding 200 nm. These transitions are most prominently observed in lanthanide ions such as Ce^{3+}, Pr^{3+}, and Tb^{3+}. Owing to the extension of the 5*d* orbitals, these transitions are highly sensitive to the surrounding ligand field, which is markedly stronger than that experienced by the more shielded 4*f* orbitals. This results in pronounced ligand-field splitting and corresponding red shifts in emission with increasing field strength. In complexes of ions such as Ce^{3+} and Eu^{2+}, strong ligand-field interactions can sufficiently stabilize the 5*d* levels, leading to observable emissions in the visible region rather than the ultraviolet. The $4f^n$-$4f^{n-1}5d^1$ transitions are electric dipole-allowed, resulting in broad absorption and emission bands and short excited-state lifetimes [5-7].

6.1.1.2. Charge-transfer transitions

Charge transfer (CT) transitions play a dual role in lanthanide luminescence, acting either as efficient sensitizers or as quenchers depending on their energy relative to the lanthanide excited states.

When ligand-to-metal charge transfer (LMCT) states lie at sufficiently high energy, they can effectively transfer energy to the excited 4*f* states, thereby enhancing luminescence. However, if their energy is comparable to that of the emitting level, they often act as nonradiative deactivation pathways, quenching luminescence.

Three primary types of charge transfer transitions are typically considered. The LMCT transitions involve the transfer of an electron from the ligand to the metal ion. They are often observed in the UV region due to their higher transition energies, particularly in easily reducible ions such as Sm^{3+}, Eu^{3+}, Tm^{3+}, and Yb^{3+}. Metal-to-ligand charge transfer (MLCT) transitions, while common in *d*-block metal complexes, are rarely seen in lanthanide systems, Ce^{3+} being a notable exception due to its tendency to oxidize to Ce^{4+}. In addition, ligand-centred charge transfer such as intraligand CT or ICT transitions can also efficiently sensitize lanthanide luminescence [5,8].

6.1.1.3. Intraconfigurational *f-f* transitions

The 4*f*–4*f* electronic transitions in trivalent lanthanide ions (Ln^{3+}) are characterized by their sharp spectral features and long excited-state lifetimes, owing to the effective shielding of 4*f* electrons by the filled 5*s* and 5*p* orbitals. These transitions are intra-configurational and primarily parity-forbidden electric dipole (ED) transitions according to Laporte's selection rule, resulting in weak absorption bands [9]. However, partial relaxation of the selection rules can occur through mechanisms such as spin-orbit coupling, vibronic coupling, *J*-mixing, and ligand-field-induced parity mixing, resulting in induced electric dipole transitions, some of which are hypersensitive to the Ln(III) environment. Magnetic dipole (MD) transitions, while

allowed, remain weak in intensity but are often comparable to induced ED transitions, whereas electric quadrupole (EQ) transitions are parity-allowed but rarely significant. Consequently, despite their low absorption coefficients, 4*f*–4*f* transitions are extensively exploited in optical materials, including lasers, phosphors, and biosensors, due to their narrow emission lines, stability across various host environments, and potential for long-lived excited states [5,10].

The inherently weak absorption of lanthanide ions can be overcome by the phenomenon of *luminescence sensitization*, also known as the *antenna effect*, which was first reported by S.I. Weissman in 1942, who demonstrated that lanthanide luminescence could be induced by exciting the ligand absorption bands in metal–organic complexes. This indirect excitation mechanism, which involves three key steps light absorption by organic ligands (chromophores), energy transfer to the excited states of the lanthanide ion (Ln^{3+}), and subsequent light emission has since become a cornerstone in the design of lanthanide-based luminescent materials. The inherently low molar absorption coefficients of lanthanide ions render direct *f*–*f* excitation inefficient; however, by introducing organic ligands, this limitation is overcome *via* efficient energy transfer pathways. These pathways commonly involve singlet–triplet intersystem crossing ($S_1 \rightarrow T_1$) within the ligand, followed by triplet-to-lanthanide energy transfer ($T_1 \rightarrow Ln^{3+}$), provided that the triplet energy matches the lanthanide excited state. The efficiency of this process is further enhanced by the use of chelating ligands or antenna chromophores that bring the donor and acceptor orbitals into close proximity, lower the orbital distance, and induce partial covalency

through *f–d* orbital mixing by breaking the local symmetry of the lanthanide ion [11,12].

6.1.2. Application of Photoluminescence: Lanthanide complexes as fluorescent probes

Due to the extensive use of rare earth elements (REEs) in various fields, the scarcity of certain REE such as Eu, Dy and Er is also expected in the coming future. Therefore, the detection of REE is a major challenge. The most common techniques of detection include inductively-coupled plasma mass spectrometry (ICP-MS), optical emission spectroscopy (ICP-OES), instrumental neutron activation analysis (INAA), glow discharge mass spectrometry (GD-MS) and laser induced breakdown spectroscopy (LIBS). However, these methods are often expensive and sophisticated. In this context, the development of fluorescent Schiff base sensors for REEs is receiving immense attention due to the greater selectivity, sensitivity, faster response, cost effectiveness and simplicity [13].

Fluorescent probes are meticulously designed to undergo distinct photophysical changes such as fluorescence enhancement (turn-on) or shifts in emission maxima upon interaction with specific analytes. These emission responses are governed by several well-established mechanisms, including chelation-enhanced fluorescence (CHEF), intramolecular charge transfer (ICT), photoinduced electron transfer (PET), excimer/exciplex formation, excited-state intramolecular proton transfer (ESIPT), and fluorescence resonance energy transfer (FRET). Among these, CHEF plays a particularly prominent role in metal ion sensing due to the strong chelating affinity of metal ions toward organic donor ligands. When a metal ion

coordinates with a Schiff base ligand, there can be a considerable enhancement or quenching of fluorescence intensity. This leads to phenomena known as chelation-enhanced fluorescence (CHEF) or chelation-enhanced quenching (CHEQ). These significant changes observed are primarily attributed to the photo-induced electron transfer (PET) mechanism [14].

Photoinduced Electron Transfer (PET) is a widely employed mechanism in the development of fluorescent sensors, where electron transfer occurs from a donor to an acceptor in the excited state. PET-based systems typically consist of a fluorophore, spacer, and receptor, with the receptor playing a critical role in modulating fluorescence upon interaction with specific analytes. Upon light excitation, an electron transitions from the highest occupied molecular orbital (HOMO) to the lowest unoccupied molecular orbital (LUMO). If the receptor is unbound, PET from the receptor to the fluorophore can quench fluorescence. However, when the receptor binds to a target analyte such as a metal ion in Schiff base complexes this interaction can alter the HOMO–LUMO alignment and either suppress or activate PET, resulting in an "off–on" or "on–off" fluorescence signal. This modulation of fluorescence intensity, quantum yield, or lifetime based on analyte recognition makes PET a powerful and sensitive strategy for designing selective molecular sensors, and they hold significant potential for applications in live cell imaging [15].

6.1.3. Fluorescence quantum yield

The fluorescence quantum yield is defined as the ratio of the number of photons emitted through fluorescence to the number of photons absorbed, representing the efficiency of the fluorescence

process. It quantifies the fraction of excited fluorophores that return to the ground state *via* radiative emission rather than non-radiative pathways. A high quantum yield, approaching unity, indicates that radiative decay dominates over non-radiative pathways [16].

6.1.4. Fluorescence lifetime (τ)

The fluorescence lifetime (τ) is a photophysical parameter that describes the average time a molecule remains in its excited electronic state before returning to the ground state. It is defined as the reciprocal of the total decay rate constant, that is, the rate constants for radiative and non-radiative processes, respectively. The lifetime corresponds to the time required for an excited molecular population to decay to $1/e$ (~36.8%) of its original number, assuming first-order kinetics. In simple systems, this decay is single-exponential, but in more complex environments such as mixtures of fluorophores or molecules with multiple conformational states the decay is often multiexponential and represented as a weighted average of multiple lifetimes. Fluorescence lifetime is not entirely intrinsic, as it is influenced by factors such as quenching, solvent effects, and molecular interactions. It spans a broad temporal range depending on the decay pathway involved, from femtoseconds for internal conversion to nanoseconds for fluorescence and up to microseconds or seconds for phosphorescence [17,18].

6.2. Fluorescence studies

6.2.1. Experimental

The reaction scheme for the synthesis of aroylhydrazones and their complexes are discussed in Chapters 2, 3, 4, & 5.

6.2.2. Results and discussion

In this section, the photoluminescence properties of the aroylhydrazones and their complexes of Ce(III), Dy(III), and Gd(III) ions is discussed. Photoluminescence spectroscopy, lifetime measurements, and quantum yield studies were employed to investigate the impact of metal coordination on the luminescent behaviour of the ligands. The Ce(III) complexes of H_2salbh and H_2salnh, in particular, exhibit characteristic emissions that confirm efficient ligand-to-metal energy transfer, facilitated by the antenna effect of the hydrazone moieties.

The observed enhancement in fluorescence in all the Ce(III), Dy(III) and Gd(III) complexes of Hindbh is primarily attributed to the suppression of photo-induced electron transfer (PET) and the activation of the chelation-enhanced fluorescence (CHEF) mechanism. A comparative evaluation of the hydrazones and their metal complexes demonstrates a marked improvement in emission efficiency upon coordination. These findings provide valuable insights into the structure–property relationships governing lanthanide photoluminescence and contribute to the rational design of luminescent materials for potential applications in sensing, bioimaging, and optoelectronic devices.

6.2.2.1. Photoluminescence studies of aroylhydrazones

6.2.2.1.1. Fluorescence studies

Fluorescence emission spectra of aroylhydrazones have been performed in methanolic solution with a concentration of 10^{-5} M, for excitation at 330 nm. The emission spectra of H_2salbh and H_2salnh

exhibited similar band patterns, indicating the similarity in their structures (Fig. 6.1). The most prominent fluorescence emission peaks of H_2salbh were observed at 430 and 494 nm, while for H_2salnh, the peaks were at 432 and 502 nm. In the case of Hindbh, the emission peaks are located at 406, 419 and 457 nm which isalso attributed to $\pi^* \rightarrow \pi$ transitions [19].

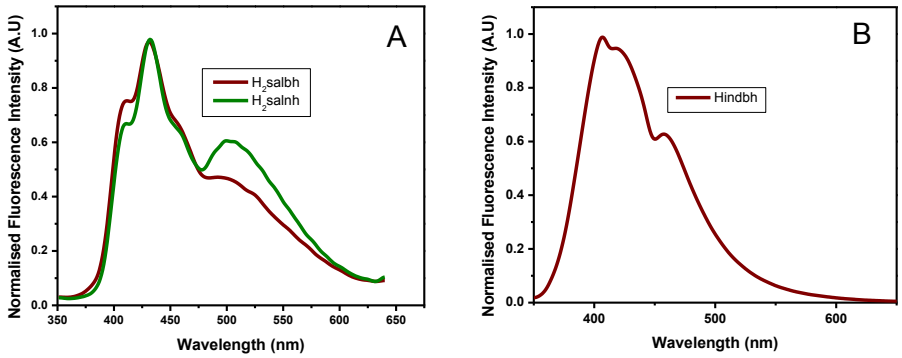

Fig. 6.1. (A) Emission spectra of H_2salbh and H_2salnh in DMF solution (10^{-5} M) at room temperature with excitation at 330 nm. (B) Emission spectra of Hindbh in DMF solution (10^{-5} M) at room temperature with excitation at 330 nm.

6.2.2.1.2. Fluorescence lifetime decay studies and quantum yields

To gain deeper insight into the photoluminescence properties of the aroylhydrazones-H_2salbh, H_2salnh, and Hindbh- both fluorescence decay and quantum yield measurements were carried out. The fluorescence decay profiles of H_2salbh, H_2salnh were best fitted to a triexponential decay function, indicating the presence of multiple emissive states or decay pathways. For H_2salbh, the fitted lifetime components were τ_1 = 2.82 ns (20.61%), τ_2 = 13.8 ns (2.78%), and τ_3 = 0.930 ns (76.68%), with a chi-squared (χ^2) value of 1.267, indicating a good fit to the experimental data. Similarly, H_2salnh exhibited lifetime

components of τ_1 = 2.78 ns (23.27%), τ_2 = 14.10 ns (3.17%), and τ_3 = 0.897 ns (73.26%), with a χ^2 value of 1.296. The predominance of the shortest lifetime component (τ_3) in both ligands suggests that non-radiative deactivation pathways dominate the photolminescence behaviour of the uncoordinated hydrazones [19].

The average lifetimes were calculated as 1.67 ns for H_2salbh and 1.74 ns for H_2salnh, reflecting the overall excited-state behaviour of the ligands in solution. Corresponding photoluminescence quantum yields (ϕ) were determined to be 11.19% and 11.92%, respectively (Table 6.1). The relatively lower quantum yields are indicative of efficient non-radiative decay mechanisms in the free ligands, likely arising from active photo-induced electron transfer (PET) processes or conformational flexibility [12].

In the case of Hindbh, the fluorescence decay profile was best fitted to a biexponential function, indicating a relatively simpler excited-state relaxation process compared to the other hydrazones. The dominant lifetime component was observed at τ_1 = 1.65 μs (99.92%), with a minor longer-lived component at τ_2 = 14.04 μs (0.08%). The average fluorescence lifetime was calculated to be 1.67 μs, with a chi-squared (χ^2) value of 0.97, confirming an excellent fit to the experimental data. The photoluminescence quantum yield (Φ) for Hindbh was determined to be 16.39%, notably higher than those of H_2salbh and H_2salnh.

Table 6.1. Photoluminescene parameters of hydrazones in DMF solutions

Compound	τ_1, (b_1)	τ_2, (b_2)	τ_3, (b_3)	τ_{av}	χ^2	ϕ (%)
H_2salbh	2.82 ns, (20.61%)	13.8 ns, (2.78%)	0.930 ns, (76.68%)	1.67 ns	1.26	11.19
H_2salnh	2.78 ns, (23.27%)	14.10 ns, (3.17%)	0.897 ns, (73.26%)	1.74 ns	1.29	11.92
Hindbh	1.65 μs, (99.92%)	14.04 μs, (0.08)	------	1.67 μs	0.97	16.39

6.2.2.2. Photoluminescence studies of Ce(III) complexes

6.2.2.2.1. Fluorescence studies

The emission spectra of the cerium(III) complexes were recorded in DMF at room temperature. Upon excitation at 330 nm, the complexes of H_2salbh and H_2salnh, **1** and **2**, exhibited strong emission peaks at 434 and 457 nm, which can be attributed to $\pi \rightarrow \pi^*$ transition. The fluorescent intensities of the complexes **1** and **2** are marginally increased, and the emission spectra of the complexes are broadened in comparison with the metal-free ligands. This significant increase in the emission intensity of the complexes confirms the coordination of ligands to cerium(III) ion [19]. The enhancement in luminescence intensity observed in the complexes suggests that the hydrazone effectively functions as a sensitizer, facilitating energy transfer to the metal centre through the antenna effect. When metal ions coordinate with chelating antennas, the absorbed energy is efficiently transferred by the aroylhydrazones (donor) to the excited states of Ce^{3+}(acceptor) [5,11,20]. Further, the broadening of the emission spectra of the complexes **1** and **2** (Fig. 6.2) strengthens the possibility of overlapping the characteristic bands of cerium(III) and π to π^* transitions. Thus,

the emission peaks located at 434 and 457 nm may correspond to emission from the lowest excited state $^2D_{3/2}$ to ground states $^2F_{7/2,5/2}$ of cerium(III) ion. Moreover, the energy difference between the two peaks is around 2000 cm^{-1}, which eventually validates this assumption [21,22]. In addition, the observed blue shift in these emission bands, in comparison to that of the hydrazone, is because of the decrease in conjugation length and enhanced molecular rigidity, which restricts intramolecular rotation [19,23,24].

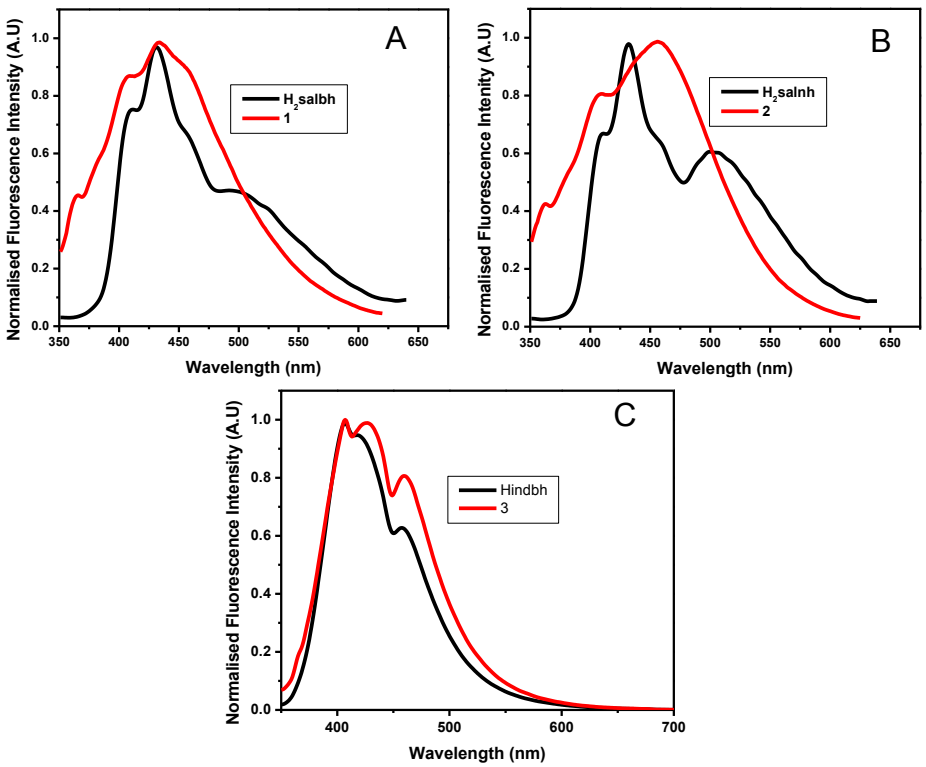

Fig. 6.2. (A). Emission spectra of H_2salbh and **1** in DMF solution (10^{-5} M) at room temperature with excitation at 330 nm. (B) Emission spectra of H_2salnh and **2** in DMF solution (10^{-5} M) at room temperature with excitation at 330 nm, (C) Emission spectra of Hindbh and **3** in DMF solution (10^{-5} M) at room temperature with excitation at 330 nm.

As expected, the emission spectra for the complexes of H_2salbh and H_2salnh, **4** and **5**, also exhibited an increase in emission intensity compared to the hydrazones. With the introduction of L-histidine into the coordination complex, the emission maxima are red-shifted in both complexes. This may be due to the enlargement of the conjugation offered by L-histidine. The conformational rigidity attained on complexation may also lead to a stronger emission [19,23,25]. But the fluorescence intensity of complexes **4** and **5** is less when compared to the complexes **1** and **2** (Fig. 6.3). This reflects the fact that the intermolecular energy transfer between L-histidine and Ce(III) ion is comparatively weaker. This may be due to the lower energy gap between the triplet energy level of L-histidine and the excited state energy level of Ce(III) ion. In addition, as most of the energy was absorbed by L-histidine, the absorption of energy by the hydrazones was eventually reduced [19,22,25]. The fluorescence emission spectra of all the cerium(III) complexes prove that they are suitable for photochemical applications.

In the study of metal complexes derived from the aroylhydrazone, Hindbh, both compound **3** and compound **6** exhibit emission spectra that closely resemble that of Hindbh, while notable red shifts in their emission maxima. Compound **3** displays emission peaks at 406, 426, and 459 nm, each shifted to longer wavelengths compared to the ligand, alongside a notable increase in emission intensity. Compound **6** demonstrates a further red shift in emission peaks to 416, 432, and 462 nm, accompanied by a significant enhancement in fluorescence intensity.

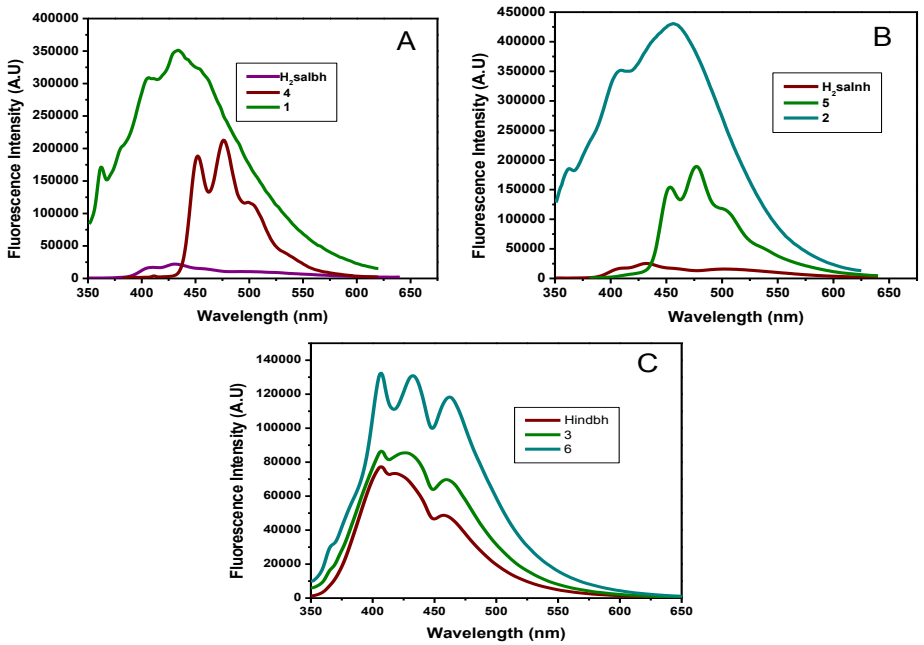

Fig. 6.3. (A) Emission spectra of H_2salbh, **1** and **4** in DMF solution (10^{-5} M) at room temperature with excitation at 330 nm. (B) Emission spectra of H_2salnh, **2** and **5** in DMF solution (10^{-5} M) at room temperature with excitation at 330 nm. (C) Emission spectra of Hindbh, **3** and **6** in DMF solution (10^{-5} M) at room temperature with excitation at 330 nm.

These red shifts indicate an enhanced planarity and increased π-electron delocalization within the metal complexes [21]. The substantial increase in emission intensity observed in compound **3** and **6** is consistent with the Chelation-Enhanced Fluorescence (CHEF) effect. L-histidine, acting as a co-ligand in compound **6**, participates in bidentate coordination and contributes additional π-conjugation. This coordination increases the rigidity and planarity of the metal-ligand framework, effectively suppressing non-radiative decay pathways and facilitating radiative transitions, thus leading to enhanced fluorescence. Moreover, the extended conjugation due to L-histidine stabilizes the

excited state, further accounting for the observed red shifts in emission [14].

6.2.2.2.2. Fluorescence lifetime decay studies and quantum yields

The luminescent decay profiles of complexes **1** and **2** are best fitted to a fourth exponential with average lifetimes 4.80 and 5.22 ns, whereas complexes **4** and **5** are best fitted to a third exponential with average fluorescence lifetimes 3.02 and 2.01 ns [19]. Fig. 6.4 illustrates the comparative fluorescence decay profiles of the hydrazone and their cerium(III) complexes, highlighting differences in their excited-state lifetimes. It is interesting to note that the lifetime of the complexes was increased on complexing with Ce(III), which suggests that the excited states of all the complexes are stable in comparison with the hydrazones [26]. Also, the complex **2** is found to exhibit the highest value of lifetime [19].

In contrast, complexes **3** and **6** exhibit significantly longer excited-state lifetimes in the microsecond range compared to the nanosecond lifetimes observed for complexes **1**, **2**, **4**, and **5**, reflecting distinctly different photoluinescence behaviour. Both complexes follow biexponential decay, with complex **3** showing decay components of 1.83 μs (99.88%) and 16.50 μs (0.12%), and complex **6** exhibiting components of 2.09 μs (99.68%) and 16.45 μs (0.32%), resulting in an average lifetime of 1.84 μs and 2.14 μs respectively. The reliability of the decay fitting is confirmed by high χ^2 probability values of 0.97 for complex **3** and 0.98 for complex **6**.

Furthermore, the photoluminescence quantum yield of all the Ce(III) complexes was determined in DMF solution at room temperature. It is interesting to note that the incorporation of L-

histidine in the coordination sphere substantially leads to an increase in the photoluminescence quantum yield from 24.37% to 27.47% for **1** and **4**, and 20.14% to 30.05% for **2** and **5**. These results suggest that the photoluminescence quantum yield of the Ce(III) complexes is influenced by their structural rigidity, which limits geometric relaxation processes following excitation [19].

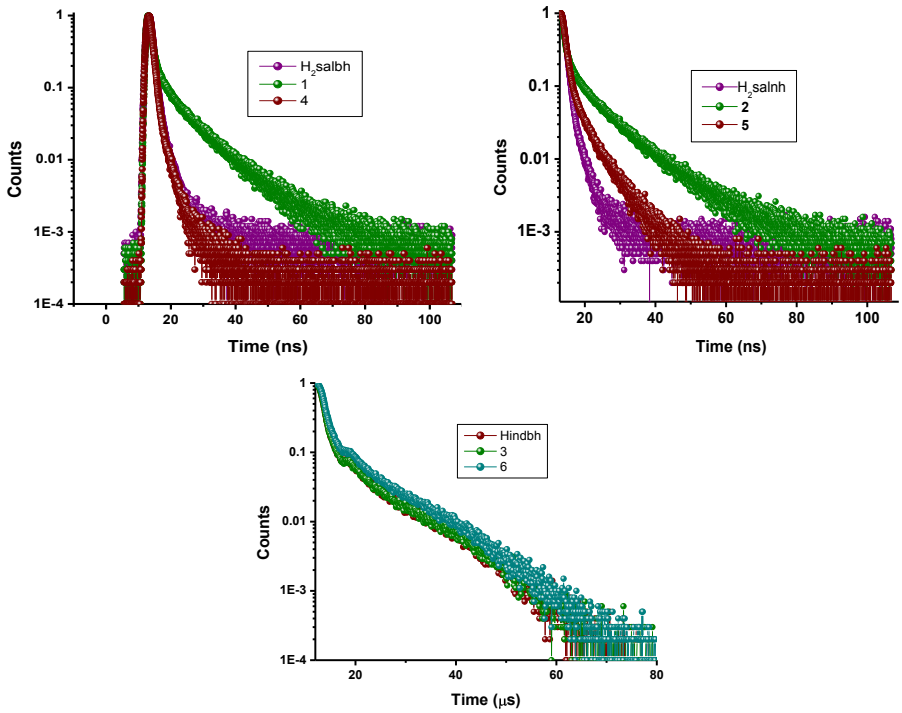

Fig. 6.4. The comparative fluorescence decay measurements of the hydrazones and their cerium(III) complexes.

In the case of complexes **3** and **6**, also, there is a notable increase in photoluminescence quantum yield, with values of 18.62% and 19.47%, respectively, compared to 16.39% for aroylhydrazone, Hindbh. This enhancement indicates that coordination with Ce(III) improves excited-state stability and reduces non-radiative decay, likely

due to increased structural rigidity and stronger metal–ligand interactions. The combination of prolonged microsecond lifetimes and moderate quantum yields highlights the potential of these complexes for applications requiring long-lived and efficient luminescence. The photoluminescence properties of hydrazones and Ce(III) complexes in DMF solutions are presented in Table 6.2.

Table 6.2. Photoluminescence parameters Ce(III) complexes in DMF solutions

Compound	τ_1, (b_1)	τ_2, (b_2)	τ_3, (b_3)	τ_4, (b_4)	τ_{av}	χ^2	ϕ (%)
1	1.31 ns, (22.58%)	7.28 ns, (28.71%)	15.60 ns, (15.22%)	0.13 ns, (33.49%)	4.80 ns	1.14	24.37
2	1.35 ns, (18.94%)	7.07 ns, (28.41%)	15.09 ns, (19.41%)	0.14 ns, (33.23%)	5.22 ns	1.07	20.14
3	1.8 μs, (99.88)	16.50 μs, (0.12)	-----	------	1.84 μs	0.97	18.62
4	2.24 ns, (69.88%)	7.701 ns, (18.02%)	0.590 ns, (12.10%)	-------	3.02 ns	0.82	27.47
5	0.87 ns, (71.30%)	3.03 ns, (13.89%)	6.605 ns, (14.81%)	-------	2.01 ns	0.93	30.05
6	2.09 μs, (99.68%)	16.45 μs, (0.32%)	------	-------	2.14 μs	0.98	19.47

6.2.2.3. Photoluminescence studies of Dy(III) complexes

6.2.2.3.1. Fluorescence studies

The emission spectra of Dy(III) complexes were recorded in DMF solution (10^{-5} M) at room temperature with an excitation wavelength of 330 nm. For the H_2salbh based complexes, complex **7** exhibits strong emission bands in the 406–461 nm regions, with significantly enhanced intensity compared to the aroylhydrazone. Complex **10** shows a broad emission band centred around 447 nm and

displays higher fluorescence intensity than H_2salbh. Although its intensity is lower than that of complex **7**, the increase relative to H_2salbh, indicates successful coordination and enhancement of photoluminescence properties. The red-shifted, broad nature of the band is attributed to $\pi^* \rightarrow \pi$ transitions. Also the broad and similar emission profiles of the complexes, in comparison to the aroylhydrazones, indicate that the luminescence originates from ligand centred transitions.

In the H_2salnh complexes, complex **8** demonstrates the highest fluorescence intensity among all studied complexes, with an emission profile closely resembling that of the free ligand but with substantial enhancement. This suggests highly efficient ligand-to-metal energy transfer upon complexation. Complex **11**, while showing a broad emission band at 435 nm, also exhibits higher fluorescence intensity than the free ligand, although less than that of complex **8**. This further supports successful coordination and an improvement in emission behaviour.

For the complexes of Hindbh, complexes **9** and **12** show emission bands in the 406–461 nm range, similar in shape to the Hindbh, but with a clear and significant increase in fluorescence intensity. This enhancement strongly supports the conclusion that the emission is still ligand-centred and that coordination to Dy(III) improves the efficiency of the emissive process. The observed red shifts further confirm changes in the electronic environment due to complex formation (Fig. 6.5).

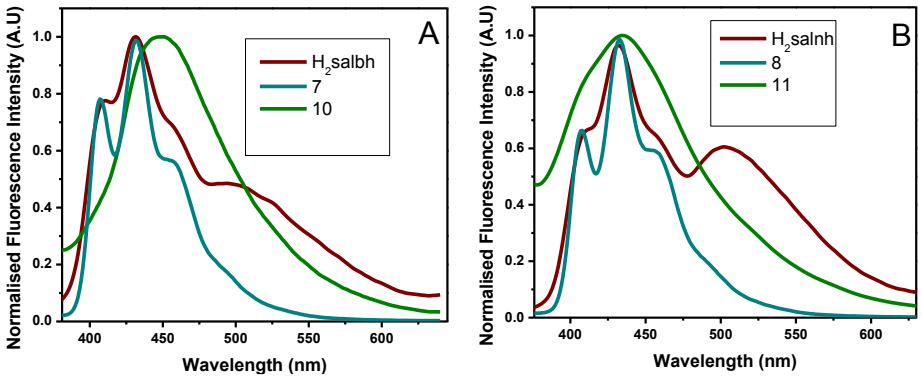

Fig. 6.5. (A). Normalised fluorescence emission spectra of H_2salbh, **7** and **10** in DMF solution (10^{-5} M) at room temperature with excitation at 330 nm. (B) Normalised fluorescence emission spectra of H_2salnh, **8** and **11** in DMF solution (10^{-5} M) at room temperature with excitation at 330 nm.

Compared with the hydrazones, the fluorescence intensities of all the Dy(III) complexes are greatly enhanced (Fig. 6.6). When hydrazones coordinate with Dy(III) ions, it leads to increased conjugation and structural rigidity in the complexes. This eventually enhances the luminescence intensity and proves that non-radiative transitions are lowered upon complexation [21,25]

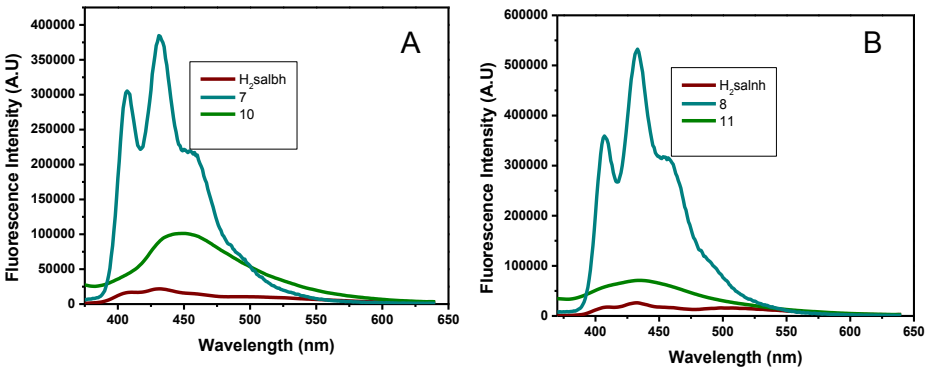

Fig. 6.6. (A) Fluorescence Emission spectra of H_2salbh, **7** and **10** in DMF solution (10^{-5} M) at room temperature with excitation at 330 nm. (B) Fluorescence Emission spectra of H_2salnh, **8** and **11** in DMF solution (10^{-5} M) at room temperature with excitation at 330 nm.

The enhancement of fluorescence intensity in the Dy(III) complexes can be mainly explained by CHEF and PET mechanisms. The weak fluorescence of the hydrazones can be attributed to the PET mechanism. On irradiating with light, an electron from the HOMO of the fluorophore is transferred to the LUMO. Subsequently, an electron from the imine nitrogen or hydroxyl group of the hydrazone is transferred to the ground state of the fluorophore. Thus, the excited electron cannot come back to the ground state, and it eventually leads to the deactivation of the fluorophore. But, upon complexation, the fluorescence intensity is greatly enhanced. This *turn-on* fluorescence is attributed to the CHEF mechanism through the inhibition of PET. On chelation, the electron transfer is hindered as the imine nitrogen and hydroxyl oxygen are coordinated to the Dy(III) ion [12,27-29].

6.2.2.3.2. Fluorescence lifetime decay studies and quantum yields

The fluorescence lifetime was measured in DMF at room temperature. The decay curves of all the Dy(III) complexes are best fitted to a triexponential function, except for complexes **9** and **12**, which exhibit a biexponential decay profile. The triexponential nature of lifetime observed in most of the complexes leads to an assumption of having the presence of three luminescence emission centers in the hydrazones and also in the corresponding Dy(III) complexes. In contrast, complexes **9** and **12** show dominant long-lived components of 1.705 μs (99.92%) and 1.964 μs (99.68%), respectively, along with negligible contributions from minor components. The increase in the average lifetime of the Dy(III) complexes **7** and **8** with respect to the hydrazones suggests that the excited states of the complexes are stable in comparison with the hydrazones [30,31]. A comparative

fluorescence decay measurements of the hydrazones and their Dy(III) complexes are shown in Fig. 6.7.

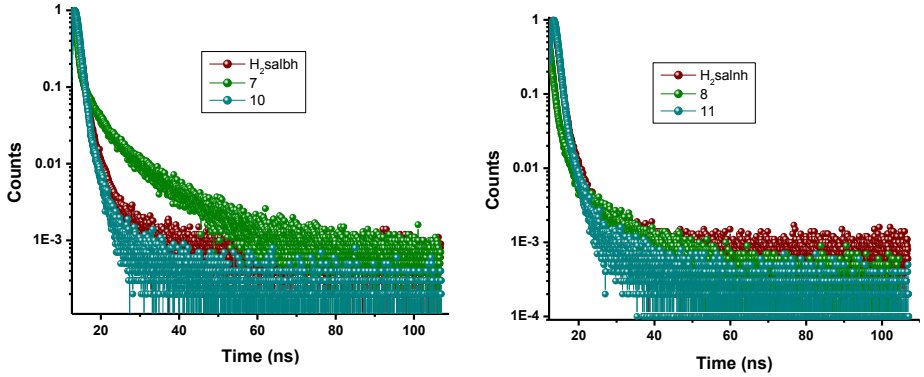

Fig. 6.7. The comparative fluorescence decay measurements of the hydrazones and their Dy(III) complexes.

The life time decay curve of **7** yields lifetimes of τ_1 = 3.13 ns (20.99%), τ_2 = 11.79 ns (17.37%) and τ_3 = 0.303 ns (61.65%) with χ^2 1.172, and **8** yields lifetimes of τ_1 = 2.946 ns (26.90%), τ_2 = 12.28 ns (24.3%) and τ_3 = 0.362 ns (48.81) with χ^2 1.160. The average lifetime calculated for **7** and **8** is 2.87 and 3.95 ns, respectively. The luminescence lifetime obtained for **10** is τ_1 = 0.759 (88.55%), τ_2 = 2.218 (10.77%) and τ_3 = 13.9 ns (0.69%), yielding the average fluorescence lifetime 1.003 ns. In the case of **11**, τ_1 = 0.746 (86.48%), τ_2 = 2.13 (12.40%) and τ_3 = 10.24 ns (1.12%), leading to an average lifetime of 1.09 ns.

Complexes **9** and **12** exhibit biexponential decay with long-lived components in the microsecond range, τ_1 = 1.705 μs (99.92%) and τ_2 = 15.170 μs (0.08%) for complex **9**, and τ_1 = 1.964 μs (99.68%) and τ_2 = 13.69 μs (0.32%) for complex **12**, resulting in average

lifetimes of 1.72 μs and 1.99 μs, respectively. The microsecond lifetimes observed in complexes **9** and **12** are attributed to delayed fluorescence arising from their unique emissive properties.

On account of the exciting photoluminescence properties of the Dy(III) complexes, the photoluminescence quantum yield was also calculated. For all the complexes, it is surprising to note that there is a drastic increase in the quantum yield values. The photoluminescence parameters of the Dy(III) complexes in DMF solutions are presented in Table 6.3.

For complexes of H_2salbh, the quantum yield obtained is 53.44% for **7** and 43.82% for **10** respectively. For the complex **8**, the quantum yield is obtained 67.76% and for the complex **11**, 52.05%. For complexes of Hindbh, the quantum yield obtained is 16.96% for **9** and 17.69 for compound **12**. Complexes exhibiting a photoluminescence quantum yield >50% are well known for their promising applications in the field of OLED fabrication. Thus, the compounds **7**, **8** and **11** can be best utilized for further photoluminescent applications in the future. This significant increase in quantum yields of Dy(III) complexes can be attributed to the CHEF mechanism. In addition, the lower value of quantum yield observed in the aroylhydrazones can presumably be due to the free rotation.

Table 6.3. Photoluminescence parameters of the Dy(III) complexes in DMF solutions

Compound	$\tau_1$ns (b_1)	τ_2, (b_2)	τ_3,(b_3)	τ_{av}	χ^2	ϕ (%)
7	3.13 ns, (20.99%)	11.79 ns, (17.37%)	0.303 ns, (61.65%)	2.87 ns	1.172	53.44
8	2.946 ns, (26.90%)	12.28 ns, (24.3%)	0.362 ns, (48.81)	3.95 ns	1.60	67.76
9	1.705 μs, (99.92%)	15.170 μs, (0.08%)	--------	1.72 μs	0.979	16.96
10	0.759 ns, (88.55%)	2.218 ns, (10.77%)	13.9 ns, (0.69%)	1.00 ns	1.043	43.82
11	0.746 ns, (86.48%)	2.13 ns, (12.40%)	10.24 ns, (1.12%)	1.09 ns	1.096	52.05
12	1.964 μs, (99.68%)	13.69 μs, (0.32%)	-------	1.99 μs	0.979	17.69

6.2.2.4. Photoluminescence studies of Gd(III) complexes

6.2.2.4.1. Fluorescence studies

The emission spectra of Gd(III) complexes were measured in DMF solution (10^{-5} M) at room temperature, using an excitation wavelength of 330 nm. The fluorescence emission peaks of compounds **13** and **14** are akin to those of the aroylhydrazones (Fig.6.8). In contrast, compound **16** shows a broad emission peak at 462 nm whereas compound **17** shows a similar peak at 482 nm.

Notably, the emission intensities of all the Gd(III) complexes were significantly enhanced. Complexes **15** and **18**, derived from Hindbh, display fluorescence within the 406–462 nm region, maintaining spectral features similar to the aroylhydrazone.

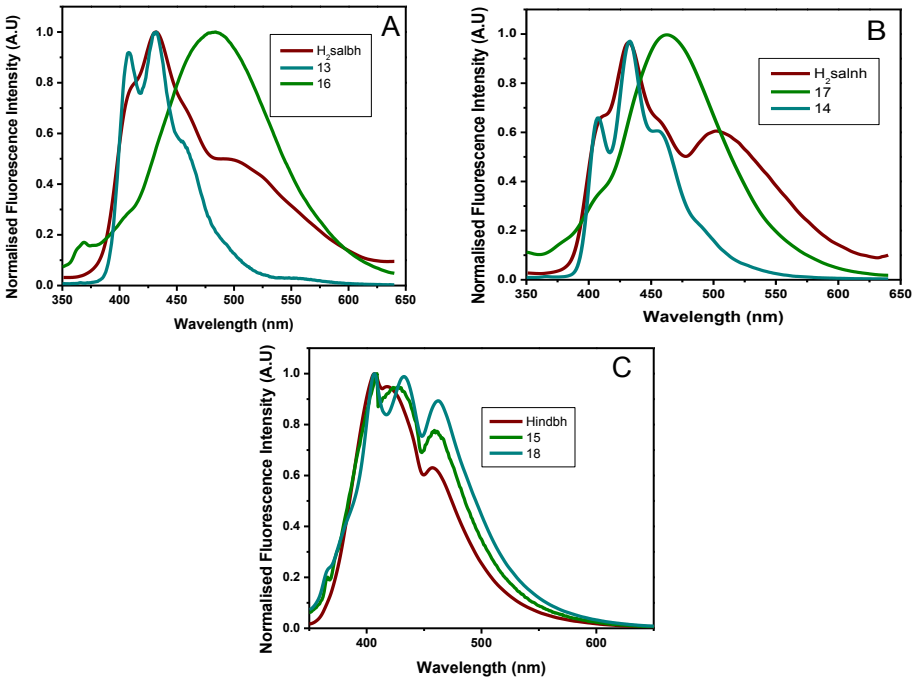

Fig. 6.8. (A). Normalised fluorescence emission spectra of H_2salbh, **13** and **16** in DMF solution (10^{-5} M) at room temperature with excitation at 330 nm. (B) Normalised fluorescence emission spectra of H_2salnh, **14** and **17** in DMF solution (10^{-5} M) at room temperature with excitation at 330 nm. (C) Normalised fluorescence emission spectra of Hindbh, **15** and **18** in DMF solution (10^{-5} M) at room temperature with excitation at 330 nm.

However, the coordination to Gd(III) ion leads to a marked enhancement in emission intensity with a remarkable red shift. This suggests that while the emission remains primarily ligand-centred, the metal ion plays a key role in enhancing the photoluminescence efficiency. However, the characteristic emission peaks of the Gd(III) ion were not observed in any of the complexes, suggesting weaker energy transfer from the aroylhydrazones to the Gd(III) ion.

The rapid increase in emission intensities of the Gd(III) complexes can mainly be attributed to the processes of photo-induced electron transfer (PET) and the chelation-enhanced fluorescence (CHEF) mechanism. The hydrazone, which initially exhibited weak emission intensity, shows a significant increase in emission intensity upon complexation with the Gd(III) ion (Fig. 6.9) [32]. This emission band corresponds to a ligand-based $\pi^* \rightarrow \pi$ transition. Notably, the anticipated sensitization of the metal ion through the antenna effect is not observed. This may be attributed to the significant energy gap between the electronic levels of the Gd(III) ion and the ligand-centered electronic levels of aroylhydrazones. The Gd(III) ion's main emitting level is at $^6P_{7/2}$, which is higher than that of most organic ligands. But, the coordination has increased structural rigidity, and as a result, the emission intensity and quantum yield have been significantly improved. This enhancement can also be linked to the increased stability of the half-filled *4f* subshell of the Gd(III) ion [33].

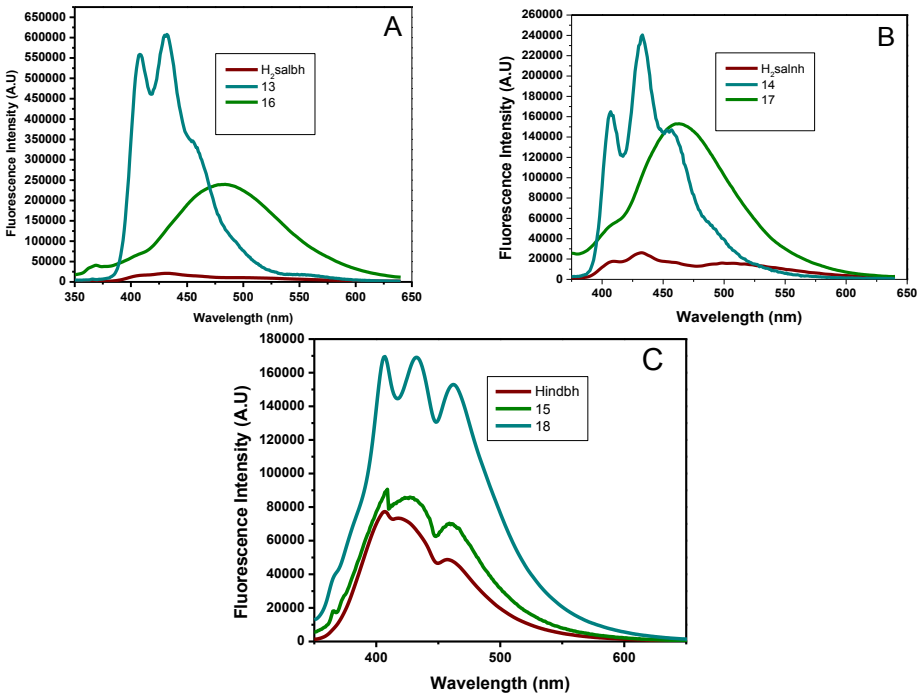

Fig. 6.9. (A) Fluorescence Emission spectra of H_2salbh, **13** and **16** in DMF solution (10^{-5} M) at room temperature with excitation at 330 nm. (B) Fluorescence Emission spectra of H_2salnh, **14** and **17** in DMF solution (10^{-5} M) at room temperature with excitation at 330 nm. (C) Fluorescence Emission spectra of H_2salnh, **15** and **18** in DMF solution (10^{-5} M) at room temperature with excitation at 330 nm.

6.2.2.4.2. Fluorescence lifetime decay studies and quantum yields

The fluorescence decay profiles of the Gd(III) complexes derived from H_2salbh and H_2salnh displayed triexponential decay and for those related to Hindbh displayed biexponential decay. Notable differences were found in both the individual lifetime components and the average fluorescence lifetimes. Compounds **13** and **16** exhibited average lifetimes of 3.07 and 0.84 ns, respectively, while compounds **14** and **17** showed slightly shorter average lifetimes of 1.55 and 1.09 ns. In contrast, compounds **15** and **18** displayed biexponential decay

with significantly longer lifetimes in the microsecond range indicative of long-lived excited states. A comparative fluorescence decay measurements of the hydrazones and their Gd(III) complexes are shown in Fig.6.10.

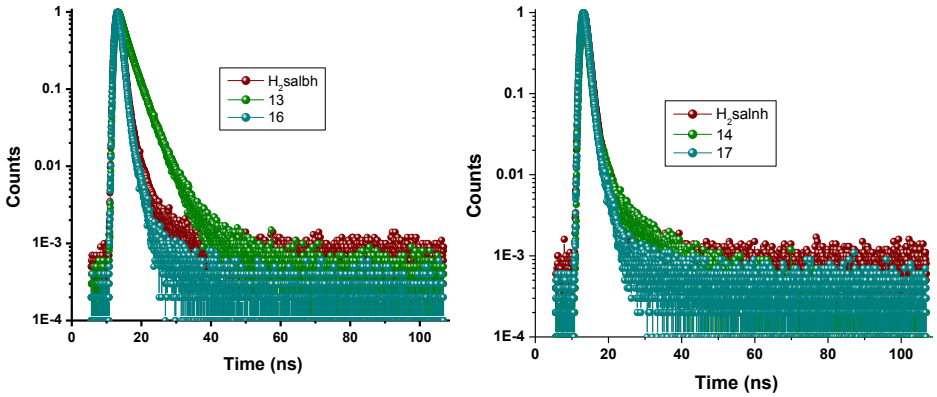

Fig. 6.10. The comparative fluorescence decay measurements of the hydrazones and their Gd(III) complexes.

For complex **13**, the fluorescence decay curve yielded three components: τ_1= 0.733 ns (11.73%), τ_2= 3.02 ns (81.04%), and τ_3 = 7.44 ns (7.23%), with a goodness-of-fit value (χ^2) of 1.172. Complex **14** showed decay components of τ_1= 2.974 (10.55%), τ_2 = 11.569 (8.73%), and τ_3 = 0.286 ns (80.72%), with χ^2 = 1.129. The calculated average lifetimes for **13** and **14** were 3.07 and 1.55 ns, respectively. For complex **16**, the fluorescence lifetimes were τ_1 = 0.0581 ns (17.62%), τ_2 = 0.857 ns (75.97%), and τ_3 = 2.863 ns (6.41%), resulting in an average lifetime of 0.84 ns. Similarly, complex **17** exhibited τ_1 = 0.759 (89.28%), τ_2 = 2.256 (10.22%), and τ_3 = 14.92 ns (0.50%), with an average lifetime of 1.09 ns. Photoluminescence parameters of the Gd(III) complexes in DMF solutions are listed in Table 6.4.

In contrast, complexes **15** and **18** demonstrate biexponential decay behaviour characterized by microsecond-range lifetimes. For complex **15**, the decay components are τ_1 = 1.77 μs (99.89%) and τ_2 = 14.869 μs (0.11%), while complex **18** exhibits τ_1 = 1.757 μs (99.88%) and τ_2 = 14.342 μs (0.12%). These decay profiles yield average lifetimes of 1.78 μs for complex **15** and 1.77 μs for complex **18**. The observed microsecond-scale lifetimes are indicative of delayed fluorescence.

Despite the slight decrease in lifetime values, a significant enhancement in quantum yield was observed for all Gd(III) complexes, particularly for complexes **13** and **14**. The observed enhancement in quantum yield is likely attributed to the increased structural rigidity of the ligand framework induced by chelate ring formation upon coordination with the Gd(III) ion. This structural reinforcement may reduce non-radiative decay pathways, thereby improving the overall emission efficiency.

Table 6.4. Photoluminescence parameters of the Gd(III) complexes in DMF solutions

Compound	τ_1, (b_1)	τ_2, (b_2)	τ_3, (b_3)	τ_{av}	χ^2	ϕ (%)
13	0.733 ns, (11.73%)	3.02 ns, (81.04%),	7.44 ns, (7.23%)	3.07 ns	1.071	29.53
14	2.974 ns, (10.55%)	11.569 ns, (8.73%)	0.286 ns, (80.72)	1.55 ns	1.129	24.50
15	1.77 μs, (99.89%)	14.869 μs, (0.11%)	-------	1.78 μs	0.979	17.25
16	0.0581 ns, (17.62%)	0.857 ns, (75.97%)	2.863 ns, (6.41%)	0.84 ns	0.992	19.05
17	0.759 ns, (89.28%)	2.256 ns, (10.22%)	14.92 ns, (0.50%)	1.09 ns	1.252	20.49
18	1.757 μs, (99.88%)	14.342 μs, (0.12%)	-------	1.77 μs	0.979	20.9

6.2.2.5. Bioimaging

Owing to its superior photoluminiscent properties and the highest quantum yield, compound **8** was further investigated for its potential application in fluorescence bioimaging (FBI). FBI represents a versatile and sensitive technique extensively utilized in contemporary medicine and biological research for the visualization of cellular morphology and physiological processes in living systems [34].

The HeLa cells were cultured in Dulbecco's Modified Eagles Medium (DMEM-Himedia), supplemented with 10% heat-inactivated Fetal Bovine Serum (FBS) and 1% antibiotic cocktail containing Penicillin (100 U/mL), Streptomycin (0.1 mg/mL), and Amphotericin B (0.25 μg/mL). The cells containing TC flasks (25 cm^2) were incubated at 37 °C in a 5% CO_2 environment with humidity in a cell culture incubator [35]. After 24 hours of incubation, a green fluorescence was emitted by the compound **8**, while observed under the blue filter of the inverted phase contrast fluorescence microscope [36]. Fig. 6.11 shows the bright field and fluorescence images of the HeLa cells (control) alone and Fig. 6.12 shows the fluorescence images of the HeLa cells treated with 25, 50 and 100 μg/mL of compound **8**. It can be noted that fluorescence emission was observed when highest exposure and gain was provided [36]. So this observation suggests that at higher concentrations, the compound **8** can be considered as a potential candidate for bioimaging.

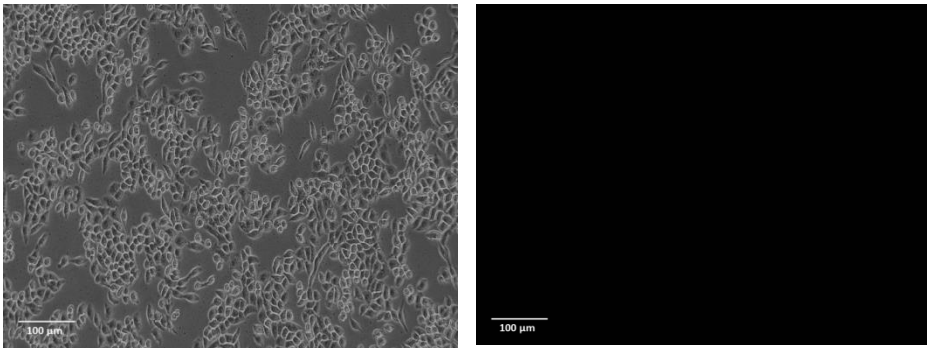

Fig. 6.11. Cell imaging in HeLa cells. A and B: Bright and fluorescence images of HeLa cells (control) alone.

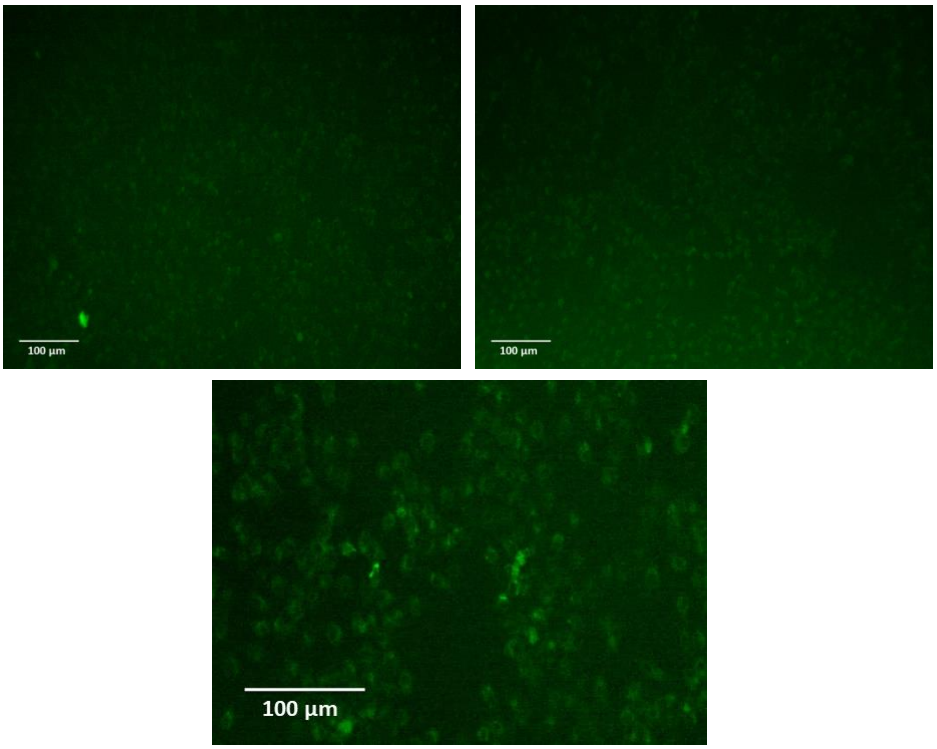

Fig. 6.12. C, D and E: Fluorescence images of the HeLa cells treated with 25, 50 and 100 μg/mL of compound **8**.

6.3. Conclusion

The photoluminescent properties of hydrazones and their lanthanide complexes with Ce(III), Dy(III), and Gd(III) ions have been systematically explored, revealing significant improvements in optical behaviour upon metal coordination. For Ce(III) complexes of H_2salbh and H_2salnh, the characteristic *d–f* transitions confirm efficient energy transfer from the aroylhydrazones, which act as effective chelating antennae. Photoluminescence lifetime (τ) measurements, extending into the microsecond range, indicate enhanced excited-state stability in the complexes relative to the aroylhydrazones. Additionally, the incorporation of L-histidine into the coordination environment further increases the quantum yield, highlighting the impact of ligand architecture on emission efficiency. These promising optical features position Ce(III) complexes as potential candidates for high-performance blue organic light-emitting diodes (OLEDs).

For Dy(III) complexes, a notable increase in fluorescence intensity upon chelation is observed, primarily attributed to the suppression of photo-induced electron transfer (PET) and the activation of the chelation-enhanced fluorescence (CHEF) mechanism. This turn-on fluorescence behaviour is highly advantageous for the design of responsive fluorescent sensors. Moreover, the Dy(III) complex with the highest quantum yield was successfully utilized in bioimaging applications, demonstrating its dual functionality in optical sensing and biomedical imaging.

In the case of Gd(III) complexes, the pronounced enhancement in emission intensity is predominantly governed by the inhibition of PET and the CHEF mechanism. The hydrazone ligands, which exhibit weak fluorescence due to non-radiative PET pathways, undergo significant photophysical changes upon coordination with Gd(III) ions. Metal coordination suppresses PET while inducing structural rigidity and extended conjugation through chelation, thereby promoting radiative decay pathways. These combined effects result in a substantial fluorescence enhancement, underscoring the pivotal role of metal–ligand interactions in modulating luminescent behaviour.

Overall, the study demonstrates that careful ligand design and strategic coordination with lanthanide ions can significantly enhance photoluminescent properties. These findings provide a foundation for developing advanced materials for applications in optoelectronics, sensing, and biomedical imaging.

References

1. Zwinkels, J., 2023. Luminescence. In: *Encyclopedia of Color Science and Technology*, pp. 1116–1120. Cham: Springer International Publishing.
2. Jain, M. and Singh, P., 2024. Luminescence: types and mechanism. In: *Mechanoluminescence in Organic and Inorganic Compounds*, pp. 1–18. Elsevier.
3. Tessitore, G., Mandl, G.A., Maurizio, S.L., Kaur, M. and Capobianco, J.A., 2023. The role of lanthanide luminescence in advancing technology. *RSC Advances*, 13(26), pp. 17787–17811.
4. Bünzli, J.C.G. and Eliseeva, S.V., 2013. Intriguing aspects of lanthanide luminescence. *Chemical Science*, 4(5), pp. 1939–1949.
5. Bünzli, J.C.G., 2016. Lanthanide luminescence: from a mystery to rationalization, understanding and applications. In: *Handbook on the Physics and Chemistry of Rare Earths*, Vol. 50, pp. 141–176. Elsevier.
6. Eliseeva, S.V. and Bünzli, J.C.G., 2010. Lanthanide luminescence for functional materials and bio-sciences. *Chemical Society Reviews*, 39(1), pp. 189–227.
7. Bünzli, J.C.G. and Piguet, C., 2005. Taking advantage of luminescent lanthanide ions. *Chemical Society Reviews*, 34(12), pp. 1048–1077.
8. Hasegawa, M., Ohmagari, H., Tanaka, H. and Machida, K., 2022. Luminescence of lanthanide complexes: from fundamental to prospective approaches related to water- and molecular-stimuli. *Journal of Photochemistry and Photobiology C: Photochemistry Reviews*, 50, p. 100484.
9. Costantini, J.M., Guillaumet, M., Lelong, G., Ishikawa, N., Seo, P. and Yasuda, K., 2025. Near-infrared study of radiation damage in ion-irradiated cerium dioxide and cerium-gadolinium dioxide. *Nuclear Instruments and Methods in Physics Research Section B: Beam Interactions with Materials and Atoms*, *558*, p.165567.
10. Görller-Walrand, C. and Binnemans, K., 1998. Spectral intensities of *f–f* transitions. *Handbook on the Physics and Chemistry of Rare Earths*, 25, pp. 101–264.
11. Bünzli, J.C.G., 2015. On the design of highly luminescent lanthanide complexes. *Coordination Chemistry Reviews*, 293, pp. 19–47.

12. Indelli, M.T., Ghirotti, M., Prodi, A., Chiorboli, C., Scandola, F., McClenaghan, N.D., Puntoriero, F. and Campagna, S., 2003. Solvent switching of intramolecular energy transfer in bichromophoric systems: Photophysics of (2,2-Bipyridine) tetracyanoruthenate (II)/pyrenyl complexes. *Inorganic chemistry*, *42*(18), pp.5489-5497.

13. Afrin, A., Jayaraj, A. and Gayathri, M.S., 2023. An overview of Schiff base-based fluorescent turn-on probes: a potential candidate for tracking live cell imaging of biologically active metal ions. *Sensors & Diagnostics*, 2(5), pp. 988–1076.

14. Sharma, S. and Ghosh, K.S., 2021. Recent advances (2017–20) in the detection of copper ion by fluorescence sensors working through PET, ESIPT and FRET. *Spectrochimica Acta Part A: Molecular and Biomolecular Spectroscopy*, 254, p. 119610.

15. Niu, H., Liu, J., O'Connor, H.M., Gunnlaugsson, T., James, T.D. and Zhang, H., 2023. Photoinduced electron transfer (PeT) based fluorescent probes for cellular imaging and disease therapy. *Chemical Society Reviews*, 52(7), pp. 2322–2357.

16. Lakowicz, J.R. (ed.), 2006. *Principles of Fluorescence Spectroscopy*. Boston, MA: Springer US.

17. Berezin, M.Y. and Achilefu, S., 2010. Fluorescence lifetime measurements and biological imaging. *Chemical Reviews*, 110(5), pp. 2641–2684.

18. Murali, K., Sparkes, H.A., Pandiyan, B.V. and Prasad, K.J.R., 2017. Synthesis, photophysical properties and DFT analysis of highly substituted pyrido carbazole-based "push pull" chromophores. *New Journal of Chemistry*, *41*(16), pp.8242-8252.

19. Anjana, T.M., Manoj, E., Naseera, C.M., Liyakhath, F.M., Thayyullathil, A., Naduparambath, S., Sheeja, S.R. and Kurup, M.P., 2025. Photophysical properties, DFT calculations and DNA binding studies of deep blue emitting cerium(III) complexes. *Journal of Molecular Structure*, 1327, p. 141186.

20. Azenha, M.E., Burrows, H.D., Fonseca, S.M., Ramos, M.L., Rovisco, J., de Melo, J.S., Sobral, A.J. and Kogej, K., 2008. Luminescence from cerium(III) acetate complexes in aqueous solution: considerations on the nature of carboxylate binding. *New Journal of Chemistry*, 32(9), pp. 1531–1535.

21. Ma, C.G., Brik, M.G., Liu, D.X., Feng, B., Tian, Y. and Suchocki, A., 2016. Energy level schemes of f^N electronic configurations for di-

, tri- and tetravalent lanthanides and actinides in a free state. *Journal of Luminescence*, 170, pp. 369–374.

22. Wang, L., Zhao, Z., Zhan, G., Fang, H., Yang, H., Huang, T., Zhang, Y., Jiang, N., Duan, L., Liu, Z. and Bian, Z., 2020. Deep-blue OLEDs based on a doublet *d–f* transition cerium(III) complex with 100% exciton utilization efficiency. *Light: Science & Applications*, 9(1), p. 157.

23. Zhang, J., Xu, L. and Wong, W.Y., 2018. Energy materials based on metal Schiff base complexes. *Coordination Chemistry Reviews*, 355, pp. 180–198.

24. Fujii, K., Iyi, N., Sasai, R. and Hayashi, S., 2008. Preparation of a luminous heterogeneous system: rhodamine/coumarin/phyllosilicate hybrid and blue-shift in fluorescence emission. *Chemistry of Materials*, 20(9), pp. 2994–3002.

25. Taha, Z.A., Ajlouni, A.M., Al-Hassan, K.A., Hijazi, A.K. and Faiq, A.B., 2011. Syntheses, characterization, biological activity and fluorescence properties of bis(salicylaldehyde)-1,3-propylenediimine Schiff base and its lanthanide complexes. *Spectrochimica Acta Part A: Molecular and Biomolecular Spectroscopy*, 81(1), pp. 317–323.

26. Majumdar, D., Das, D., Sreejith, S.S., Das, S., Biswas, J.K., Mondal, M., Ghosh, D., Bankura, K. and Mishra, D., 2019. Dicyanamide-interlaced assembly of Zn(II)-Schiff-base complexes: synthesis, structures, TD-DFT, fluorescence lifetime and antibacterial studies. *Inorganica Chimica Acta*, 489, pp. 244–254.

27. Ganguly, A., Ghosh, S., Kar, S. and Guchhait, N., 2015. Selective fluorescence sensing of Cu(II) and Zn(II) using a simple Schiff base ligand. *Spectrochimica Acta Part A: Molecular and Biomolecular Spectroscopy*, 143, pp. 72–80.

28. Muthusamy, S., Rajalakshmi, K., Zhu, D., Zhu, W., Wang, S., Lee, K.B., Xu, H. and Zhao, L., 2021. Dual detection of Hg(II) and Pb(II) using a coumarin-based fluorescent probe via ESIPT and PET. *Sensors and Actuators B: Chemical*, 346, p. 130534.

29. Chen, H.H., Wu, D.F., Duan, Y.Y., Li, L., Wang, Y.J., Zhang, X.M., Cui, J.Z. and Gao, H.L., 2020. Near-infrared luminescence and magnetism of dinuclear complexes with *β*-diketonate and bis-Schiff base ligands. *New Journal of Chemistry*, 44(6), pp. 2561–2570.

30. Shavaleev, N.M., Eliseeva, S.V., Scopelliti, R. and Bünzli, J.C.G., 2015. Influence of symmetry on luminescence and radiative lifetime

of nine-coordinate europium complexes. *Inorganic Chemistry*, 54(18), pp. 9166–9173.

31. Chai, W.J., Li, W.X., Sun, X.J., Ren, T. and Shi, X.Y., 2011. Fluorescence enhancement of lanthanide(III) perchlorate by 1,10-phenanthroline in bis(benzoylmethyl)sulfoxide complexes. *Journal of Luminescence*, 131(2), pp. 225–230.

32. Woźnicka, E., Zapała, L., Miłoś, A., Ciszkowicz, E., Lecka-Szlachta, K., Woźnicki, P., Przygórzewska, A., Kosińska-Pezda, M. and Byczyński, Ł., 2024. Synthesis, spectroscopic characterization and biological activities of light-lanthanide complexes with 3-hydroxyflavone. *Spectrochimica Acta Part A: Molecular and Biomolecular Spectroscopy*, 322, p. 124870.

33. da Silveira, C.O., Oliveira, W.X., da Silva Júnior, E.N., Alvarenga, M.E., Martins, F.T., Gatto, C.C., Pinheiro, C.B., Pedroso, E.F., Silva, J.P., Marques, L.F. and Santos, M.V., 2024. Photoluminescence and magnetic properties of isostructural europium(III), gadolinium(III) and terbium(III) oxamate polymers. *Dalton Transactions*, 53(36), pp. 14995–15009.

34. Berrones-Reyes, J.C., Vidyasagar, C.C., Flores, B.M.M. and Jiménez-Pérez, V.M., 2018. Luminescent molecules of main group elements: advances in synthesis, properties and applications in fluorescent bioimaging. *Journal of Luminescence*, 195, pp. 290–313.

35. Mayeen, A., Santhosh, A., Joseph, N., Jose, J., Manoj, A., Joseph, S., Bhat, S. and John, H., 2024. Flexible, electrospun boron nitride nanosheets (BNNS)/hydroxyapatite–PVDF nanofibers with superior piezoelectric/ferroelectric, biocompatible features for effective bone tissue regeneration. *Journal of Alloys and Compounds*, *1002*, p.175111.

36. Roy, A. and Narayanan, D.P., 2025. Carbon Dots Derived from Edible Fern (Stenochlaena palustris (Burm. fil.) Bedd.) for Heavy Metal Sensing and Biomedical Applications. *Results in Surfaces and Interfaces*, p.100660.

CHAPTER 7

DNA BINDING STUDIES OF COMPLEXES OF AROYLHYDRAZONES

7.1. Introduction

DNA is a primary intracellular target of various drugs, particularly in the case of anticancer medications [1,2]. When anticancer drugs interact with DNA in cancer cells, they can cause damage that halts cell division, ultimately leading to cell death. It's noteworthy to emphasize that platinum-based anticancer drugs, such as cisplatin, the first metallodrug, play a pivotal role in the landscape of chemotherapy, being an integral component of all treatments. Despite their excellent anticancer activity, these drugs are associated with serious side effects, high toxicity, and a narrow spectrum of activity. This is primarily due to cisplatin's binding with non-DNA targets, such as nucleophilic sites in intracellular components like thiol-containing peptides, proteins, replication enzymes, and RNA [3-5].

In this context, the development of metal complexes for anticancer drugs has gained significant attention. The design of planar hydrophilic complexes has proven to be highly effective as potential agents in the creation of anticancer drugs [6]. Additionally, the nature of the metal and the structure of the coordinated ligands have a significant impact on drug action. Among these, the metal complexes of aroylhydrazones are particularly notable for their promising role in drug development [7]. These complexes demonstrate remarkable potential in inhibiting cell growth and forming effective bonds with DNA molecules. This unique interaction is essential not only for targeting diseases but also for inhibiting key enzymes, such as acyltransferases and ribonucleotide reductases. Additionally, they significantly impact DNA replication, highlighting the exciting therapeutic possibilities that aroylhydrazones present in medicine [8].

Recent investigations by Samala Deepa and co-workers have focused on the synthesis of transition metal complexes of aroylhydrazones. *In vitro* cytotoxicity studies, conducted using the CTG assay, against the SKOV3 and MDA-MB231 cell lines, revealed effective anticancer activity [9].

These complexes are known to exhibit a diverse range of activities, including anticancer, antiplatelet, anti-tubercular, antifungal, antioxidant, analgesic, antibacterial, anti-inflammatory, antitumoral, and antimalarial effects. The antimalarial and anti-tuberculosis activities of metal complexes derived from isonicotinic acid hydrazide are well documented [10]. For instance, Rusul Oday Khalid and her team synthesized hydrazone-based transition metal complexes, finding that the palladium(II) complexes displayed antibacterial activity comparable to ciprofloxacin [11]. Similarly, copper(II) complexes of benzoylhydrazone show high antitumor potency and effectively inhibit DNA synthesis and cell growth in both human and rodent cell lines. Moreover, molybdenum complexes of salicylaldehyde benzoylhydrazones act as groove binders [12].

The versatile coordination behaviour, chemical stability, and ease of synthesis of aroylhydrazones are largely attributed to the azomethine group present in these compounds. The carbon atom in the C=N imine bond of Schiff bases acts as a potent electrophile, while the nitrogen functions as a versatile nucleophile, offering remarkable binding opportunities. The presence of aromatic groups in these hydrazones contributes to the planar structure of the resulting metal complexes, facilitating intercalative binding through π–π stacking interactions [13]. Recently, Jennifer Meyer Moreira and her team

synthesized zinc(II) and cadmium(II) complexes of hydrazones, conducting CT-DNA binding studies that identified the intercalative mode of interaction [14]. Additionally, Hala A. Kiwan and team synthesized cobalt(II), nickel(II), and copper(II) complexes of hydrazones, finding that these complexes interact with CT-DNA with relatively high binding constants [15].

Currently, studies investigating the DNA-binding properties of lanthanide metal complexes are emerging as a significant research focus. The excellent ability of trivalent lanthanide ions and their complexes to coordinate with biomolecules has garnered considerable attention among researchers designing new lanthanide-based drugs. The strong Lewis acidity, high coordination number, greater charge density, and rapid ligand exchange capabilities of these complexes make them effective catalysts for the phosphate ester hydrolysis of the DNA backbone [16]. Moreover, lanthanide ions can replace calcium-dependent reactions in biological systems due to their similar ionic radii to Ca^{2+} [16-18]. This feature has led to the development of cerium(III) based antithrombotic drugs over the past decades. Recently, Sheta and colleagues synthesized a cerium-Schiff base complex, which serves as a kidney biomarker for the selective detection of human creatinine [16,19].

7.2. DNA binding studies

7.2.1. Modes of binding

There are two primary types of binding interactions between metal complexes and DNA: irreversible and reversible. In the irreversible binding mode, a stable covalent bond is formed between the central metal ion and specific components of the DNA strand, such

as the nitrogenous bases (adenine, thymine, cytosine, and guanine) or the phosphate backbone. Conversely, reversible binding relies on noncovalent interactions. This involves the binding of positively charged metal complexes to the exterior of the DNA helix, which includes electrostatic attraction to the negatively charged sugar-phosphate backbone, hydrogen bonding, and van der Waals forces, as well as $\pi\cdots\pi$ stacking and CH$\cdots$ interactions [20].

7.2.1.1. Covalent binding

Covalent binding involves the formation of a strong and irreversible bond between complexes of metal ions and DNA bases, particularly the nitrogen atoms in guanine or adenine. A prominent example is cisplatin, a well-established anti-cancer agent. Although it is neutral, cisplatin aquates within cells to form a reactive cationic species, *cis*-$[PtCl(NH_3)_2(H_2O)]^+$. The monoaqua cisplatin compound formed is very reactive and easily attaches to DNA by disrupting the DNA replication, and ultimately leads to cell death [2].

7.2.1.2. Non covalent binding

Non covalent binding modes mainly include; intercalation, groove binding and electrostatic interactions.

7.2.1.2.1. Intercalation

Intercalation involves the insertion of molecules, such as metal complexes, between adjacent base pairs of double-stranded DNA, facilitating the stacking of these molecules within the DNA structure. The efficacy of intercalation is intricately shaped by a variety of factors, including the planarity of the ligands, nature of metal ion and the coordination geometry [21].

7.2.1.2.2. Groove binding

Groove binding refers to a reversible interaction between the major or minor grooves of DNA and metal complexes that are located outside the DNA double helix. The negative electrostatic potential present in the grooves of the DNA enhances the binding of small, flexible molecules, especially in the minor groove. Consequently, groove binding is highly specific and results in only minor structural changes to the DNA double helix. This binding is primarily driven by intermolecular interactions, including electrostatic forces, hydrogen bonding, and van der Waals attractions [22].

7.2.1.2.3. Electrostatic binding

Electrostatic binding is a weaker external mode of interaction in which cationic metal complexes bind to the negatively charged sugar-phosphate backbone of DNA.

7.2.2. Experimental

The study of interaction of drugs with DNA molecule is a significant criterion for the development of potential anticancer drugs. Absorption spectroscopy is an important tool to evaluate the interactions of metal complexes with DNA [23]. The efficiency of binding and interaction of DNA with metal complexes is related to the changes in absorbance and wavelength observed in the electronic absorption spectra. The binding of DNA with metal complexes can be attained either through the covalent interaction or through the non-covalent interactions like intercalative, electrostatic, minor or major groove binding [18,24,25].

7.2.2.1. Absorption spectroscopic study

The DNA binding properties of the hydrazones and metal complexes were studied using electronic absorption spectroscopy. A

fixed concentration of CT genomic DNA in nuclease-free water was incubated individually with different concentrations (25, 50, 100 μg/mL) of the synthesized aroylhydrazones and complexes in phosphate buffer at $_p$H 7.4 and incubated at 37 °C for 2 hours [16,26].

The intrinsic CT-DNA binding constant of the ligands and complexes were determined from the UV-vis spectral data using the Benesi Hildebrand equation [16].

$$\frac{1}{\Delta A} = \frac{1}{K_b \Delta\varepsilon[H]} + \frac{1}{\Delta\varepsilon[G]}$$

where [H] is the concentration of the host (DNA), [G] is the concentration of the guest (complex), ΔA is the change in absorbance of the DNA on the addition of complex and $\Delta\varepsilon$ is the difference in molar extinction coefficient between the free DNA and DNA-cerium complex. The plot of $\frac{1}{\Delta A}$ versus$\frac{1}{[complex]}$gives a straight line. The K_b value can be obtained from the ratio of Y intercept to the slope of straight line [16].

7.3. Results and discussion

DNA binds with metal complexes through various modes like covalent, noncovalent and electrostatic interaction. Intercalation and groove binding are the noncovalent modes of interaction [16]. Intercalation arises from the strong π–π stacking interaction between the aromatic chromophore ligand of a metal complex and the DNA bases. Planarity, conjugation, number of donor atoms in the ligand and the geometry of the complex determine the ability of intercalation. And the groove binding arises from the highly negative electrostatic potential in the DNA grooves. The distortion of the DNA backbone

caused by groove binding is smaller in comparison with intercalation [16,22].

7.3.1. DNA Binding study of aroylhydrazones

The mode of interaction between the aroylhydrazones with DNA base pairs can be identified from the changes in the absorbance and shift in wavelength obtained in the UV-vis spectra. The electronic absorption spectra of CT-DNA with different concentrations (25, 50, 100 μg/mL) of hydrazones are shown in Fig. 7.1 [16]. As the concentration of aroylhydrazones increased, a notable increase in absorbance accompanied by a significant red shift in the wavelength was observed. This hyperchromism suggests that the hydrazones may interact with DNA through either external groove binding or partial intercalation, where the hydrazone molecules insert themselves between the base pairs of the DNA [27].

To quantitatively evaluate the binding strength of the synthesized aroylhydrazones with CT-DNA, the intrinsic binding constants (K_b) were determined from UV–vis absorption data and are presented in Table 7.1. Among the three compounds, H_2salbh exhibited the lowest binding constant (K_b=0.497×10^3 M^{-1}), indicating a relatively weak interaction with DNA. A moderate increase in binding affinity was observed for H_2salnh (K_b=0.970×10^3 M^{-1}), which can be attributed to the presence of a pyridine ring in its structure [28,29,30]. The nitrogen atom within the heteroaromatic ring may enhance the electronic interaction with nucleobases of DNA.

In contrast, Hindbh showed a significantly higher binding constant (K_b=4.000×10^5 M^{-1}), indicating a much stronger interaction

with CT-DNA. This enhanced binding affinity is likely due to the presence of an indole moiety, which introduces a larger, more conjugated π-system capable of stronger interactions with the DNA base pairs. The increased molecular planarity and electron delocalization in Hindbh further support its enhanced binding capability. These structural features collectively contribute to the significantly higher DNA-binding affinity observed for Hindbh in comparison to H_2salbh and H_2salnh.

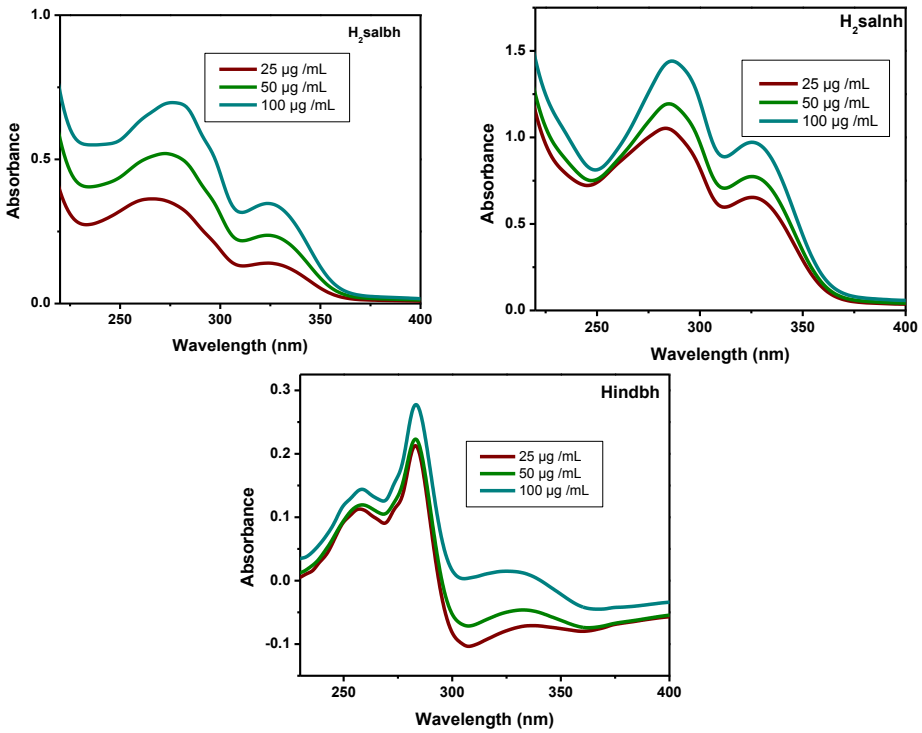

Fig. 7.1. Electronic absorption spectra of CT-DNA with different concentrations (25, 50, 100 μg/mL) of the aroylhydrazones.

Table 7.1. The DNA binding constants of aroylhydrazones

Compound	Binding constant (K_b) M^{-1}
H_2salbh	$0.497x10^3$
H_2salnh	$0.970x10^3$
Hindbh	$4.000x10^5$

7.3.2. DNA Binding study of Ce(III) complexes

The electronic absorption spectra of CT-DNA with different concentrations (25, 50, 100 μg/mL) cerium(III) complexes are shown in Fig. 7.2. The incremental addition of cerium(III) complexes to CT-DNA caused an increase in absorbance with a red shift, which is a clear indication of partial intercalation or surface binding [16,27].

The synthesized Ce(III) complexes exhibit distinct DNA-binding behaviours influenced by their ligand structures and metal coordination. The cerium(III) complexes of the Hindbh, **3** and **6**, demonstrate an exceptionally strong binding constant, indicative of a strong groove binding. This behaviour is attributed to their favorable coordination geometries, which facilitate the effective interaction along the grooves of the DNA helix.

In contrast, compounds **1** and **4**, derived from H_2salbh, exhibit comparatively modest DNA-binding constants, indicative of weak groove-binding interactions. The slightly enhanced affinity of compound **1** compared to **4** may result from its increased structural rigidity and phenyl-ring planarity, which can promote stronger interactions with the DNA helix.

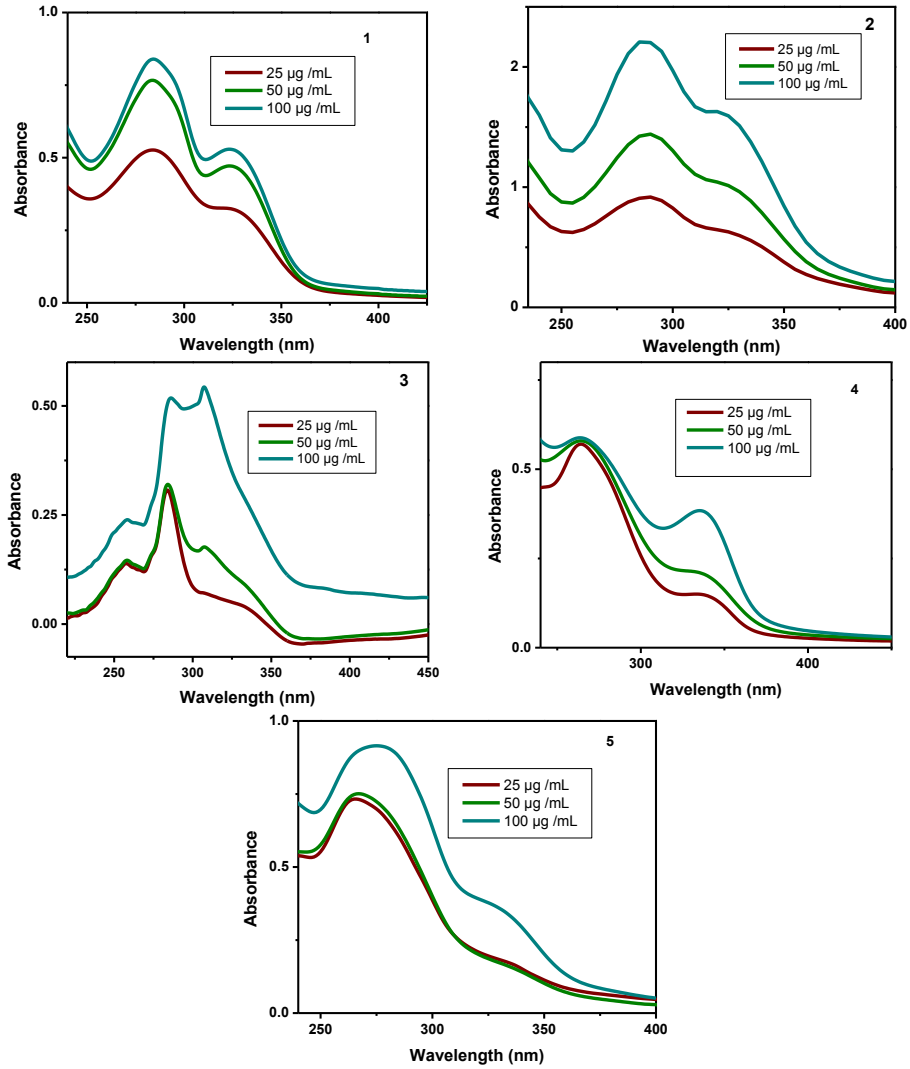

Fig. 7.2. Electronic absorption spectra of CT-DNA with different concentrations (25, 50, 100 μg/mL) of the Ce(III) complexes.

Similarly, the H_2salnh-derived complexes, compound **2** and compound **5**, also show comparatively weak DNA affinity, consistent with groove-binding behaviour [16,29-31]. These observations highlight the influence of ligand structure and metal coordination on DNA-binding modes. The cerium(III)-Hindbh complexes (particularly

3 and **6**) engage in strong groove binding, while the H_2salbh- (**1** and **4**) and H_2salnh-derived complexes (**2** and **5**) predominantly engage *via* weak groove-binding interactions.

Table 7.2. The DNA binding constants of Ce(III) complexes

Compound	Binding constant (K_b) M^{-1}
1	0.614×10^3
2	0.618×10^3
3	7.114×10^5
4	0.408×10^3
5	0.654×10^3
6	1.530×10^5

7.3.3. DNA Binding study of Dy(III) complexes

The electronic absorption spectra of CT-DNA with different concentrations (25, 50, 100 μg/mL) Dy(III) complexes are shown in Fig. 7.3. The Dy(III) complexes exhibited significant hyperchromism in their UV-vis spectra upon interaction with DNA, suggesting a non-intercalative binding mode. This observation indicates that the complexes likely bind through groove binding and electrostatic interactions, rather than intercalating between DNA base pairs.

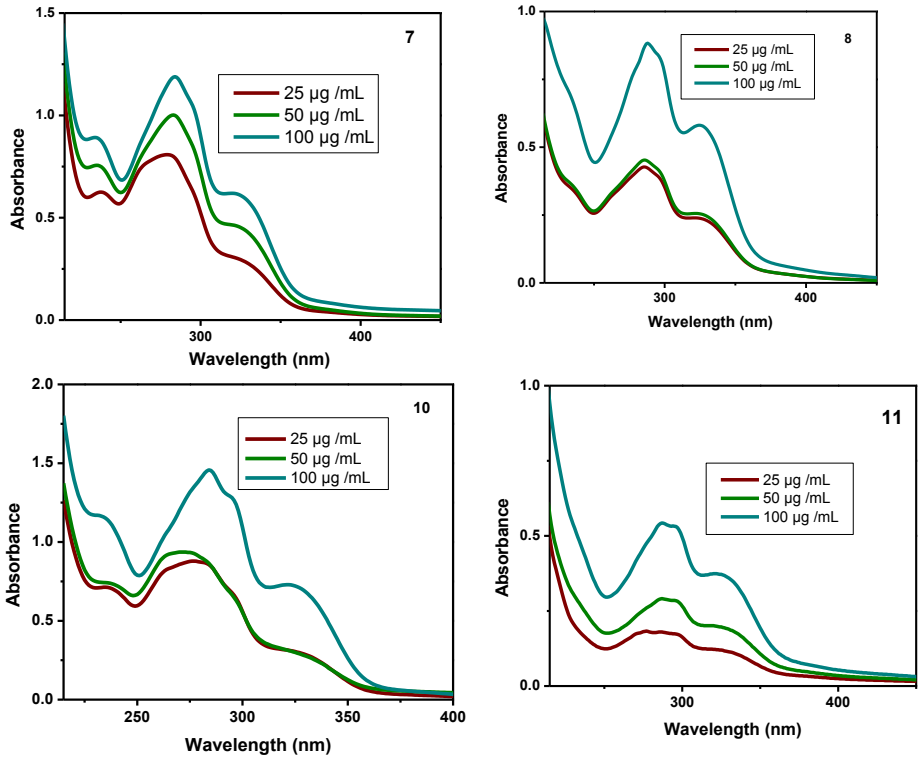

Fig. 7.3. Electronic absorption spectra of CT-DNA with different concentrations (25, 50, 100 μg/mL) Dy(III) complexes.

To further validate this binding mode, the intrinsic binding constants of the Dy(III) complexes were determined. A general enhancement in DNA-binding affinity was observed upon complexation with Dy(III), except for complex **12** (Table 7.3.). The increase in K_b value of the Dy(III) complexes can be attributed to its greater planar area and extended conjugation, leading to stronger interactions of the coordinated hydrazones with the DNA base pairs.

A more significant enhancement was observed in the case of complexes of Hindbh. The binding affinity of the Dy(III) complex derived from Hindbh was substantially higher than that of the

aroylhydrazone, marking it as the most effective DNA binder among the studied complexes. This strong interaction can be attributed to the presence of the indole ring in the aroylhydrazone and extended conjugated structure and its favorable coordination with the metal center, promoting stronger interactions and groove binding with DNA. Similarly, the presence of N-donor aromatic ligand, pyridine, in complexes of H_2salnh also contributes to a stronger interaction with DNA bases [26,32].

However, an exception to this trend was observed in complex **12**, where the K_b value decreased to 1.90×10^5 M^{-1}, which is lower than that of the corresponding aroylhydrazone, Hindbh. This decrease suggests that the coordination environment and steric hindrance in complex **12** may limit its ability to interact effectively with DNA.

The Dy(III) complexes derived from Hindbh (notably complexes **9** and **12**) exhibit strong groove-binding interactions with DNA, whereas the complexes derived from H_2salbh (**7** and **10**) and H_2salnh (**8** and **11**) display comparatively weaker groove-binding affinity [33,34].

Table 7.3. The DNA binding constants of Dy(III) complexes

Compound	Binding constant (K_b) M^{-1}
7	$0.8x10^3$
8	$2.5x10^3$
9	$5.3x10^5$
10	$1.0x10^3$
11	$3.9x10^3$
12	$1.9x10^5$

7.3.4. DNA Binding study of Gd(III) complexes

The DNA binding affinity of the Gd(III) complexes was also determined using UV-vis absorption spectroscopy. Similar to the Ce(III) and Dy(III) complexes, the Gd(III) complexes exhibited pronounced hyperchromism in their UV–vis spectra, indicating a comparable mode of interaction with DNA. The electronic absorption spectra of CT-DNA with different concentrations (25, 50, 100 μg/mL) the Gd(III) complexes are shown in Fig.7.4.

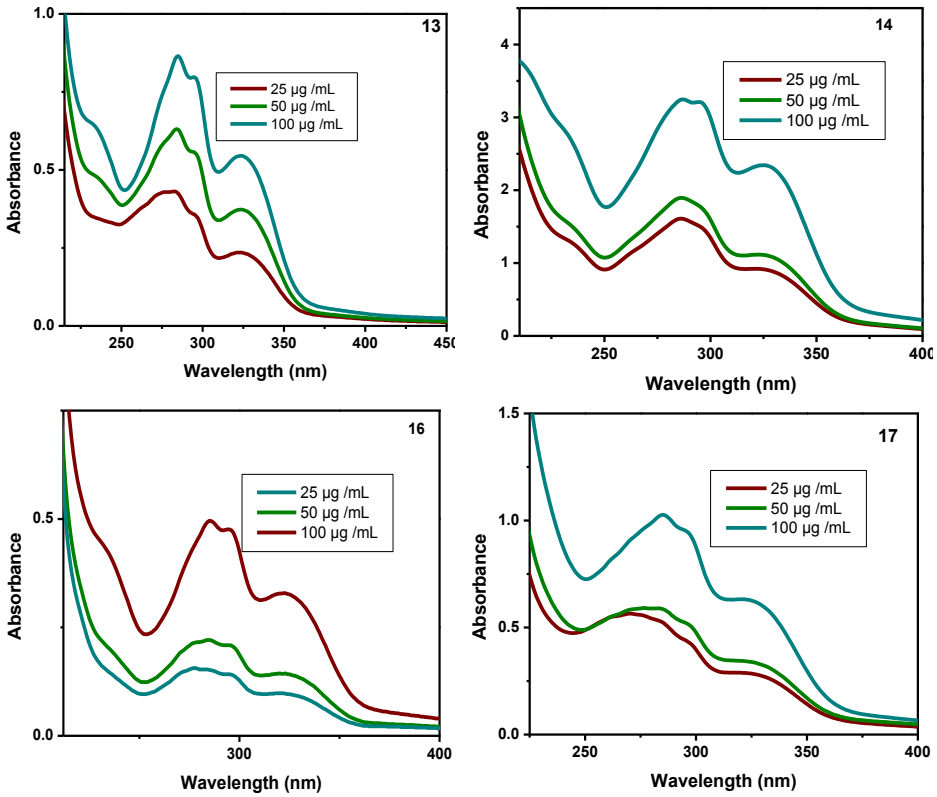

Fig. 7.4. Electronic absorption spectra of CT-DNA with different concentrations (25, 50, 100 μg/mL) Gd(III) complexes.

The intrinsic binding constants (K_b) of compounds **13** to **18** further support the trends observed in earlier complexes. Complexes **13** and **16**, derived from H_2salbh, exhibited moderate DNA-binding affinities, while complexes **14** and **17**, based on H_2salnh, showed slightly higher values, reflecting the influence of the pyridine N-donor ligand on enhancing DNA interactions. Notably, complexes **15** and **18**, originating from the Hindbh ligand, which contains an indole moiety, demonstrated significantly higher binding constants. This pronounced increase highlights the critical role of the indole ring's extended conjugation in facilitating strong π–π stacking and groove binding with DNA. The data reinforce that ligand structure, particularly the presence of aromatic systems such as indole, combined with favorable metal coordination, is pivotal in modulating the DNA-binding affinity of these Gd(III) complexes [31].

Table 7.4. The DNA binding constants of Gd(III) complexes

Compound	Binding constant (K_b) M^{-1}
13	0.614×10^3
14	2.354×10^3
15	1.160×10^5
16	4.639×10^3
17	0.729×10^3
18	6.977×10^5

7.4. Conclusion

This chapter explores the DNA binding activity of aroylhydrazones and their metal complexes with Ce(III), Dy(III), and

Gd(III) ion. The binding affinities of the aroylhydrazones and their corresponding metal complexes were assessed both quantitatively and qualitatively using UV-vis spectroscopy. All compounds exhibited a consistent trend of hyperchromism upon incremental addition of the aroylhydrazones and their Ce(III), Dy(III), and Gd(III) complexes, indicating an external binding mode.

The DNA binding studies of the synthesized aroylhydrazones and their Ce(III), Dy(III), and Gd(III) complexes reveal a consistent trend: metal complexation enhances the DNA-binding affinity of the ligands, with the extent of enhancement strongly influenced by the nature of the aroylhydrazones and the central metal ion. Among the aroylhydrazones, Hindbh, which contains an indole moiety, showed the highest binding constants, both in its free form and in its complexes. This is due to the indole's extended π-conjugation and planarity, which favor strong groove binding. The Ce(III) complexes **3** and **6**, the Dy(III) complex **9** and **12,** and the Gd(III) complexes **15** and **18** demonstrated particularly strong binding affinities (K_b in the order of 10^5 M^{-1}), indicating their potential as effective DNA-binding agents. In contrast, the aroylhydrazones, H_2salbh and H_2salnh and their respective complexes displayed significantly lower binding constants, suggesting weaker groove-binding interactions. The incorporation of N-donor pyridine rings in H_2salnh marginally improved DNA affinity compared to H_2salbh. Overall, the findings underscore the potential of Hindbh-derived lanthanide complexes, especially those of Ce(III), Dy(III), and Gd(III), as promising scaffolds for further development in DNA-targeted drug design and metallopharmaceutical research.

References

1. Pages, B.J., Ang, D.L., Wright, E.P. and Aldrich-Wright, J.R., 2015. Metal complex interactions with DNA. *Dalton Transactions*, 44(8), pp. 3505–3526.

2. Keene, F.R., Smith, J.A. and Collins, J.G., 2009. Metal complexes as structure-selective binding agents for nucleic acids. *Coordination Chemistry Reviews*, 253(15–16), pp. 2021–2035.

3. Azimi, S.G., Shakour, N., Bagherzade, G., Saberi, M.R., Azimi, H. and Moosavi, F.M., 2025. A comprehensive review of the biological activities of medicinal metal complexes synthesized from quinoline scaffolds. *Bioinorganic Chemistry and Applications*, 2025(1), p. 3133615.

4. Zaki, M., Arjmand, F. and Tabassum, S., 2016. Current and future potential of metallo drugs: revisiting DNA-binding of metal-containing molecules and their diverse mechanism of action. *Inorganica Chimica Acta*, 444, pp. 1–22.

5. D'Anna, L., Marretta, L., Froux, A., Rubino, S., Butera, V., Spinello, A., Bonsignore, R., Terenzi, A. and Barone, G., 2025. DNA Binding Activity of Functionalized Schiff Base Metal Complexes. *European Journal of Inorganic Chemistry*, *28*(6), p.e202400705.

6. Mvelase, S.T., Benson, S.O., Omondi, R.O., Kumah, R.T., Fatokun, A.A. and Ojwach, S.O., 2025. Structural, DNA/BSA binding interactions and cytotoxicity studies of carboxamide (pyridyl) pyrazine palladium(II) complexes. *Journal of Molecular Structure*, 1322, p. 140267.

7. Murugappan, S., Dastari, S., Jungare, K., Barve, N.M. and Shankaraiah, N., 2024. Hydrazide-hydrazone/hydrazone as enabling linkers in anti-cancer drug discovery: a comprehensive review. *Journal of Molecular Structure*, 1307, p. 138012.

8. Kargar, H., Fallah-Mehrjardi, M. and Munawar, K.S., 2024. Metal complexes incorporating tridentate ONO pyridyl hydrazone Schiff base ligands: crystal structure, characterization and applications. *Coordination Chemistry Reviews*, 501, p. 215587.

9. Deepa, S., Mathangi, N., Mudavath, R., Shekhar, I., Aparna, A.V. and Devi, C.S., 2025. Heteroleptic complexes of hydrazone scaffold

of picolinoyl N-oxide and 2,4-dihydroxy phenyl moieties; evaluation of antioxidant activity, DNA and protein binding properties and in vitro antiproliferation studies. *Inorganica Chimica Acta*, 574, p. 122391.

10. Tolan, D.A., Kashar, T.I., Yoshizawa, K. and El-Nahas, A.M., 2021. Synthesis, spectral characterization, density functional theory studies, and biological screening of some transition metal complexes of a novel hydrazide–hydrazone ligand of isonicotinic acid. *Applied Organometallic Chemistry*, 35(6), p.e6205.

11. Khalid, R.O., Al-Janabi, A.S., Al-Bayati, A.A. and Alheety, M., 2025. Bivalent metal complexes of N'-(4-chlorobenzylidene) isonicotinohydrazide: synthesis, characterization, biological, DFT and hydrogen storage studies. *Journal of Molecular Structure*, 1323, p. 140721.

12. Yasrebi, S.A., Mobasheri, H., Sheikhshoaie, I. and Rahban, M., 2013. DNA-binding studies of two dioxomolybdenum(VI) complexes of salicylaldehyde benzoylhydrazone ligands. *Inorganica Chimica Acta*, 400, pp. 222–227.

13. Reshma, P.R., Tom, L., Dhanya, N.P., Hussan, K.S., Raphael, V.P., Bhagyesh, V.B. and Joseph, B., 2025. Two novel aroyl hydrazones from 4-methoxybenzhydrazide: comprehensive study including synthesis, X-ray crystallography, DFT analysis, antibacterial activity and molecular docking. *Journal of Molecular Structure*, 1335, p. 141866.

14. Moreira, J.M., Rodrigues, R., Trindade, M.A.G., dos Santos, K.C., da Silva, M.M., Tirloni, B., Brandl, C.A., Paveglio, G.C., Roman, D. and de Carvalho, C.T., 2025. Characterization (XRD/TGA-DSC) and assessment of calf thymus DNA interaction with single-crystalline novel complexes from Schiff base ligands. *Inorganica Chimica Acta*, 575, p. 122443.

15. Kiwaan, H.A., El-Mowafy, A.S. and El-Bindary, A.A., 2021. Synthesis, spectral characterization, DNA binding, catalytic and in vitro cytotoxicity of some metal complexes. *Journal of Molecular Liquids*, 326, p. 115381.

16. Anjana, T.M., Manoj, E., Naseera, C.M., Liyakhath, F.M., Thayyullathil, A., Naduparambath, S., Sheeja, S.R. and Kurup, M.P., 2025. Photophysical properties, DFT calculations and DNA binding

studies of a series of deep blue emitting cerium(III) complexes. *Journal of Molecular Structure*, 1327, p.141186.

17. Chundawat, N.S., Jadoun, S., Zarrintaj, P. and Chauhan, N.P.S., 2021. Lanthanide complexes as anticancer agents: a review. *Polyhedron*, 207, p. 115387.

18. Jiang, B., Wang, M., Li, C. and Xie, J., 2013. DNA-binding and hydrolytic cleavage promoted by tetraazamacycle La(III) and Ce(III) complexes. *Medicinal Chemistry Research*, 22(7), pp. 3398–3404.

19. Sheta, S.M., Akl, M.A., Saad, H.E. and El-Gharkawy, E.S.R., 2020. A novel cerium(III)–isatin Schiff base complex: spectrofluorometric and DFT studies and application as a kidney biomarker for ultrasensitive detection of human creatinine. *RSC Advances*, 10(10), pp. 5853–5863.

20. Andrezálová, L. and Országhová, Z., 2021. Covalent and noncovalent interactions of coordination compounds with DNA: an overview. *Journal of Inorganic Biochemistry*, 225, p. 111624.

21. Biebricher, A.S., Heller, I., Roijmans, R.F., Hoekstra, T.P., Peterman, E.J. and Wuite, G.J., 2015. The impact of DNA intercalators on DNA and DNA-processing enzymes elucidated through force-dependent binding kinetics. *Nature Communications*, 6(1), p. 7304.

22. Barone, G., Terenzi, A., Lauria, A., Almerico, A.M., Leal, J.M., Busto, N. and Garcia, B., 2013. DNA-binding of nickel(II), copper(II) and zinc(II) complexes: structure–affinity relationships. *Coordination Chemistry Reviews*, 257(19–20), pp. 2848–2862.

23. Kellett, A., Molphy, Z., Slator, C., McKee, V. and Farrell, N.P., 2019. Molecular methods for assessment of non-covalent metallodrug–DNA interactions. *Chemical Society Reviews*, 48(4), pp. 971–988.

24. Elsayed, S.A., El-Gharabawy, H.M., Butler, I.S. and Atlam, F.M., 2020. Novel metal complexes of 3-acetylcoumarin-2-hydrazinobenzothiazole Schiff base: Design, structural characterizations, DNA binding, DFT calculations, molecular docking and biological studies. *Applied Organometallic Chemistry*, *34*(6), p.e5643

25. Hashemi, S., Karami, K., Saberi Dehkordi, Z., Momtazi-Borojeni, A.A. and Esmaeili, S.A., 2022. Novel P, C-orthopalladated complexes containing histidine and phenylalanine amino acids: synthesis, DNA and BSA interactions, *in vitro* antitumoral activity and molecular docking approach. *Journal of Biomolecular Structure and Dynamics*, *40*(11), pp.5000-5015.

26. Santhiya, S. and Daniel, S., 2022. DNA binding and cleavage study of novel ruthenium(II)-polypyridine-5-(3-pyridyl)-4H-1,2,4-triazole-3-thiol complex on Escherichia coli genomic DNA. *Biomedical and Biotechnology Research Journal (BBRJ)*, 6(2), pp. 208–215.

27. Matesanz, A.I., Albacete, P., Perles, J. and Souza, P., 2015. A structural and biological study on the new 3,5-diacetyl-1,2,4-triazol bis(p-chlorophenylthiosemicarbazone) ligand and its bimetallic complexes. *Inorganic Chemistry Frontiers*, 2(1), pp. 75–84.

28. Turgut, E., Gungor, O., Kirpik, H., Kose, A., Gungor, S.A. and Kose, M., 2021. Benzimidazole ligands with allyl, propargyl or allene groups, DNA binding properties, and molecular docking studies. *Applied Organometallic Chemistry*, 35(9), p. e6323.

29. Vuradi, R.K., Putta, V.R., Nancherla, D. and Sirasani, S., 2016. Luminescent behavior of Ru(II) polypyridyl morpholine complexes: synthesis, characterization, DNA, protein binding, sensor effect of ions/solvents and docking studies. *Journal of Fluorescence*, 26(2), pp. 689–701.

30. Ishaniya, W. and Ganeshpandian, M., 2022. Mixed ligand copper(II) complexes of diimine co-ligands: synthesis, characterization, DNA binding and DNA cleavage activity. *Materials Today: Proceedings*, 50, pp. 358–364.

31. Anbu, S., Kamalraj, S., Varghese, B., Muthumary, J. and Kandaswamy, M., 2012. A series of oxyimine-based macrocyclic dinuclear zinc(II) complexes enhances phosphate ester hydrolysis, DNA binding, DNA hydrolysis, and lactate dehydrogenase inhibition and induces apoptosis. *Inorganic Chemistry*, 51(10), pp. 5580–5592.

32. Kumar, P., Gorai, S., Santra, M.K., Mondal, B. and Manna, D., 2012. DNA binding, nuclease activity and cytotoxicity studies of Cu(II) complexes of tridentate ligands. *Dalton Transactions*, 41(25), pp. 7573–7581.

33. Skyrianou, K.C., Raptopoulou, C.P., Psycharis, V., Kessissoglou, D.P. and Psomas, G., 2009. Structure, cyclic voltammetry and DNA-binding properties of the bis(pyridine)bis(sparfloxacinato)nickel(II) complex. *Polyhedron*, 28(15), pp. 3265–3271.

34. Kumar, P. and Nath, M., 2024. Synthesis, structural characterization, and DNA binding/cleavage studies of diorganotin(IV) carboxylates and their complexes with 1,10-phenanthroline: X-ray structures of $[Me_8Sn_4(p\text{-}FC_6H_4CO_2)4O_2]$, $[Bu_2Sn(p\text{-}NO_2C_6H_4CO_2)_2.phen]$, and DFT studies. *Journal of Molecular Structure*, 1300, p. 137250.

CHAPTER 8

GENERAL CONCLUSIONS

This thesis, entitled **Lanthanide(III) complexes of aroylhydrazones: DNA binding and fluorescence studies**, is organized into nine chapters. Each chapter systematically addresses a distinct facet of the research, collectively providing a comprehensive understanding of the subject. A brief summary of the content and focus of each chapter is outlined below.

Chapter 1

This chapter provides a detailed introduction to the chemistry of aroylhydrazones and their coordination complexes with lanthanide ions, specifically cerium(III), dysprosium(III), and gadolinium(III) ions. The chapter begins with a foundational overview of coordination chemistry, tracing its historical evolution and emphasizing the significance of Schiff bases and aroylhydrazone in metal coordination. The synthesis, structural aspects, and versatile applications of aroylhydrazones and their lanthanide complexes are systematically outlined, with particular focus on their photoluminescent and DNA-binding properties. The chapter further elucidates the individual characteristics of Ce(III), Dy(III), and Gd(III) ions, highlighting their luminescent and biomedical relevance. A critical outlook on recent advancements in the utilization of these complexes in sensing, imaging, and therapeutic contexts is presented to establish the scientific context of the study.

Chapter 2

A systematic study has been carried out on the synthesis and characterisation of three aroylhydrazones salicylaldehyde benzoylhydrazone (H_2salbh), salicylaldehyde nicotinoylhydrazone (H_2salnh), and indole-3-carbaldehyde benzoylhydrazone (Hindbh) *via* condensation reactions. These aroylhydrazones were selected due to their potential as multidentate chelators and their diverse structural features.

Various characterization techniques, such as elemental analysis, ESI-MS, FT-IR, UV-vis, NMR, and single-crystal X-ray diffraction were employed to confirm their successful formation. Elemental analysis validated the expected stoichiometry, while mass spectrometry displayed the $[M+1]^+$ molecular ion peaks, confirming their molecular formulae. FT-IR spectra exhibited characteristic stretching frequencies of the N–H, C=N, C=O, and O–H groups, confirming the formation of hydrazone functionalities. Especially, the absence of the O–H vibrational bands in Hindbh's IR spectrum supports its non-phenolic structure. The ^{1}H NMR spectra confirmed the presence of azomethine protons across the three aroylhydrazones. Single-crystal X-ray diffraction of Hindbh further established its molecular structure. These studies also confirm that aroylhydrazones predominantly exist in the keto form and possess suitable donor atoms for metal coordination.

Chapter 3

This chapter presents the synthesis and characterisation of six Ce(III) complexes incorporating the aroylhydrazones both with and without L-histidine as a coligand. The partial elemental analysis confirmed a 1:1 metal-to-ligand ratio, while molar conductance measurements in DMF (6–15 $ohm^{-1}cm^2mol^{-1}$) indicated a non-electrolytic behaviour. FT-IR spectra exhibited shifts in the carbonyl and azomethine stretching bands upon complexation, indicating the coordination of metal ions with oxygen and nitrogen donor atoms. Additionally, the appearance of new bands confirmed the presence of Ce–O and Ce–N bonds. Monodentate coordination of nitrate groups was also evident from characteristic IR signals. Mass spectra supported the proposed molecular formulas, while UV–vis studies revealed typical intraligand charge transfer transitions ($\pi \rightarrow \pi^*$, $n \rightarrow \pi^*$) as well as ligand-to-metal charge transfer (LMCT) bands. The Ce(III) complexes of H_2salbh and H_2salnh exhibited $4f \rightarrow 5d$ transitions, with observable red shifts upon L-histidine coordination. Structurally, H_2salbh and H_2salnh functioned as tridentate ONO ligands, whereas Hindbh coordinated in a bidentate mode and L-histidine as coligand, contributed additional donor atoms, enhancing the coordination sphere.

Chapter 4

A series of investigations were carried out on the synthesis and characterization of six Dy(III) complexes derived from the aroylhydrazones, with and without the inclusion of L-histidine. The partial elemental analysis confirmed the proposed compositions of the

metal complexes. Molar conductance measurements indicated that all complexes behaved as non-electrolytes. FT-IR spectra displayed significant shifts in the C=N, C=O, and N–H regions, alongside new bands corresponding to Dy–O and Dy–N vibrations strongly suggesting coordination through both oxygen and nitrogen atoms. UV–vis spectra showed LMCT bands, reinforcing the evidence of successful coordination, and mass spectrometry confirmed the expected molecular weights. H_2salbh and H_2salnh again acted as tridentate ONO donors, while Hindbh coordinated in a bidentate fashion. L-histidine enhanced the overall coordination geometry by coordinating through the donor atoms. These findings demonstrate the adaptability of aroylhydrazones in constructing stable lanthanide complexes with potential functional applications.

Chapter 5

In this chapter, the synthesis and characterization of six Gd(III) complexes using H_2salbh, H_2salnh, and Hindbh, both with and without L-histidine, are described. FT-IR spectra confirmed coordination through azomethine nitrogen and carbonyl oxygen, evidenced by notable shifts in their stretching vibrations. Metal–ligand bonds were further supported by M–O and M–N bands. UV–vis analysis showed intraligand charge-transfer transitions indicative of ligand-metal interactions. MALDI-TOF mass spectrometry provided molecular ion peaks consistent with the predicted structures. Molar conductance values indicated that all complexes behaved as non-electrolytes. Structurally, H_2salbh and H_2salnh acted as tridentate ligands, while

Hindbh maintained its bidentate coordination pattern. L-histidine's coordination *via* its amino and carboxylate groups contributed to the overall stability and geometry of the complexes. These findings highlight the ligand's versatility and suitability for stable Gd(III) complex formation.

Chapter 6

This chapter explores the luminescent properties of the synthesized Ce(III), Dy(III), and Gd(III) complexes. It was observed that complexation with lanthanide(III) ions significantly enhanced the photoluminescence properties of all the complexes. Ce(III) complexes of H_2salbh and H_2salnh exhibited efficient $d \rightarrow f$ transitions, confirming energy transfer from the aroylhydrazones. Photoluminescence lifetime studies revealed microsecond- nano second range lifetimes, suggesting improved excited-state stability. The addition of L-histidine further elevated quantum yields, underscoring the influence of coligand architecture. These complexes demonstrate promising attributes for blue-emitting OLED materials. Dy(III) complexes showed strong fluorescence enhancement upon coordination, attributed to the suppression of PET and the activation of CHEF mechanisms. One of the Dy(III) complexes also proved effective in bioimaging, highlighting its dual role as a luminescent sensor and imaging agent. Similarly, Gd(III) complexes displayed improved emission intensity, primarily due to structural rigidification and increased conjugation. The suppression of PET and enhanced radiative decay pathways contributed to the observed luminescence. These findings emphasize

the importance of ligand design in tuning luminescent behaviour for practical applications in sensing, imaging, and optoelectronics.

Chapter 7

This final working chapter investigates the DNA-binding capabilities of the synthesized aroylhydrazones and their corresponding Ce(III), Dy(III), and Gd(III) complexes using UV–vis spectroscopic methods. Incremental addition of DNA led to hyperchromism across all compounds, suggesting an external groove-binding mode. Metal coordination was found to significantly enhance the binding affinity of the aroylhydrazones. Among them, Hindbh and its metal complexes exhibited the highest binding constants, with K_b values in the range of 10^{-5} M^{-1}. This is attributed to the planarity and extended π-conjugation of the indole ring, indicating their potential as scaffolds for DNA-targeted therapies and bioinorganic applications. H_2salnh and the corresponding complexes showed moderate DNA interaction due to its pyridine ring, while H_2salbh and its complexes displayed lower affinities. These results reveal the influence of ligand structure and metal coordination on DNA-binding ability. Hindbh-based lanthanide complexes, in particular, show potential as scaffolds for DNA-targeted therapies and bioinorganic applications.

Chapter 8

This chapter deals with the general conclusions.

CHAPTER 9

RECOMMENDATIONS

The future scope of the work encompasses

- To study the electroluminescence properties of the synthesized complexes.

  Future research could explore the electroluminescence behaviour of the synthesized complexes to evaluate their suitability for use in light-emitting devices and display technologies. Understanding their electroluminescent efficiency and stability would pave the way for potential applications in organic electronics and photonic materials.

- To study the magnetic properties of the complexes.

  Investigating the magnetic properties of these complexes could reveal valuable information about their spin states, magnetic anisotropy, and potential uses in magnetic sensors or data storage. Such studies may also contribute to the development of new materials with multifunctional magnetic and luminescent characteristics.

- To synthesize the complexes using different amino acids.

  Synthesizing complexes with different amino acids could help in tailoring their structural and functional properties, potentially enhancing their biological compatibility and activity. This approach may also result in novel complexes with improved stability, diverse coordination modes, and applications in medicinal and catalytic fields.

PUBLICATION

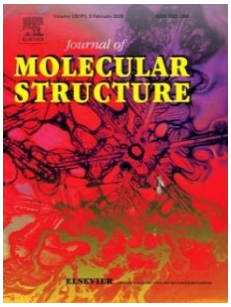

T.M. Anjana, E. Manoj, C.M. Naseera, F.M. Liyakhath, A. Thayyullathil, S. Naduparambath, S.R. Sheeja, M.R.P. Kurup, Photophysical properties, DFT calculations and DNA binding studies of a series of deep blue emitting cerium(III) complexes, *J. Mol. Struct.* 1327 (2025) 141186. DOI:10.1016/j.molstruc.2024.141186

CONFERENCE PRESENTATIONS

- Presented a paper "DNA Binding Studies and Characterization of a Luminescent Cerium(III) Schiff Base Complex'' in International conference on materials for the millennium conducted by Dept. of Applied Chemistry, CUSAT 12-14th January 2023

- Presented a paper ''Photophysical properties and DNA Binding Studies of Dysprosium(III) - Schiff Base Complex" in International conference on Emerging Frontiers in Chemical Sciences (EFCS), conducted by Dept. of Chemistry, Farook College, 19-21 December 2023.

- Presented a paper "DNA Binding Studies and Characterization of a Luminescent Gadolinium(III) - Schiff Base Complex" in National Seminar on New Developments in Chemical Sciences conducted by Dept. of Chemistry, Govt. College Madappally, 16-17 November 2023.